




MSU
LIBRARIES

This is to certify that the
thesis entitled
Diffusion and Reaction of Small Molecules
in Thin Polymer Films

presented by
Janice Lisa Tardiff

has been accepted towards fulfillment
of the requirements for
M.S. degree in Chemical Engineering


Major professor

Date July 30, 1993

PLACE IN RETURN BOX to remove this checkout from your record.
TO AVOID FINES return on or before date due.

DATE DUE	DATE DUE	DATE DUE
MAR 06 1998		
OCT 20 2001		
NOV 01 2003		
DEC 03 2003		

MSU is An Affirmative Action/Equal Opportunity Institution
c:\civ\dtd\due.pm3-p.1

1948 30 00
1949 30 00

**DIFFUSION AND REACTION OF SMALL MOLECULES
IN THIN POLYMER FILMS**

by

Janice Lisa Tardiff

A THESIS

Submitted to Michigan State University
in partial fulfillment of the requirements
for the degree of

MASTER OF SCIENCE

Department of Chemical Engineering
1993

stud

coe

pol

dur

spr

inf

tre

in

th

na

ep

we

co

sy

ex

ABSTRACT

DIFFUSION AND REACTION OF SMALL MOLECULES IN THIN POLYMER FILMS

By

Janice Lisa Tardiff

Diffusion and reaction in thin polymer films was studied for two different systems. The diffusion coefficient and kinetic rate constant for the sulfonation of polystyrene was estimated using the weight gain in the film during sulfonation, as measured by the extension of a quartz spring. Auger and FTIR analysis provided additional information about sulfonation, such as the required post-treatment of sulfonated material and the reaction mechanism in films such as polypropylene.

In an epoxy/diamine system the diffusion coefficient of the diamine was estimated by the diffusion of a similar material, m-xylene, as determined by the weight gain in epoxy using an electrobalance. The kinetic rate constants were then estimated from extent of reaction data.

The determined diffusion coefficients and rate constants provided the information required to model both systems. Results of the mathematical model were compared to experimental data to determine the accuracy of the model.

the
I
pat
Coa
hel
gy
the

Com
an
Aug
I a
te:
to
are

fu
ti
th
co
in

Ko
lo
en

ar
do
tr
th

ACKNOWLEDGEMENTS

There are many people who I wish to thank for both their help and support in completing this project. Firstly, I would like to thank my advisor, Dr. Eric Grulke, for his patience and helpful advice. I would also like to thank Coalition Technologies Ltd., in particular Bill Walles, for helping the sulfonation graduate students with the technology and for being more than willing to answer questions about the process.

I must say a very big thank you to the staff at the Composite Materials and Structures Center. Dan Hook spent an incredible amount of time working with me to get the Auger analysis technique to work on sulfonated material, and I am extremely grateful. Mike Rich was very helpful in teaching me different analysis techniques and was very easy to work with. Brian Rook always had helpful advice. They are truly a professional staff.

Several people provided other support which I am grateful for. I thank Dr. Alec Scranton for many good conversations and suggestions. Rod Andrews was a tremendous help in the lab and it is doubtful that this project would have been completed at this time without his aid. Adam Havey was instrumental in the design of the sulfonation apparatus.

I must also thank my parents, Richard and Florence Koehler, for their love and support. They have never allowed me to say "I can't" and have been behind me in every endeavor that I have undertaken.

Finally, I thank my husband Joe for his love, patience, and support. He has had to deal with me through the ups and downs of this project and is probably even more relieved than I about its completion. But he has been wonderful through it all and I must sincerely thank him.

TABLE OF CONTENTS

List of Tables	v
List of Figures	vi
I. Introduction	1
II. Gas Reacting with Polymeric Surfaces	
A. Theory	4
1. Fluorination	4
2. Chlorination	7
3. Sulfonation	9
B. General Mathematical Model	15
1. Theory	15
2. Model for Sulfonation	27
D. Experimental Methods	32
1. Experimental Setup	32
2. Results of Experiments	37
3. Determination of Diffusion Coefficients and Rate Constants	51
4. Further Studies	59
E. Analysis of Sulfonated Material	62
1. Auger Analysis	62
a. Theory	62
b. Sample Preparation	65
c. Method Development	69
2. FT-IR Analysis	86
a. Theory	86
b. Experimental Results	87
III. Liquid Polymerization in a Thin Surface Film	93
A. Analysis of an Epoxy-Diamine System	93
B. Mechanisms for the Epoxy/Diamine Coupling	98
C. Equations Describing the System	101
D. Determination of the Solubility of Diamine	103
E. Determination of the Diffusion Coefficient	114
F. Determination of the Kinetic Rate Constant	119
IV. Appendices	131
A. Appendix A - Basic Program for Modelling Diffusion	132
B. Appendix B - Basic Program to Model Sulfonation	134
C. Appendix C - Weight Gain from Sulfonation	138
D. Appendix D - Basic Program to Model Curing of an Epoxy	141
V. References	146

1

a

a

List of Tables

Table 4.1 - Dimensions of samples for sulfonation	38
Table 4.2 - Results of experiments with kinetic apparatus	48
Table 4.3 - Experimentally determined diffusivity and rate constant	58
Table 6.1 - Experimental solubility of xylene in epoxy	109
Table 6.2 - Comparison of Least Squares Error for Constant and Exponentially Dependent Diffusivities	114

Fig

Fig

Fig

Fig

Fig

Fig

Fig

Fig

Fig

Fig

Fig

Fig

Fig

Fig

Table of Figures

Figure 3.1 -	Grid for solving partial differential equation explicitly.	18
Figure 3.2a -	Concentration of diffusing species vs. time at a position of 1 micron from the interface.	22
Figure 3.2b -	Concentration of diffusing species vs. time at a position of 1 micron from the interface.	23
Figure 3.2c -	Concentration of diffusing species vs. time at a position 15 microns from the interface.	24
Figure 3.3a -	Concentration of diffusing species vs. time at a position of 1 micron from the interface.	25
Figure 3.3b -	Concentration of diffusing species vs. time at a position of 1 micron from the interface.	26
Figure 3.4 -	Schematic of the sulfonation reaction	28
Figure 4.1 -	Schematic of quartz spring experiment	33
Figure 4.2a -	Mass uptake in polystyrene vs. time for run #1	39
Figure 4.2b -	Mass uptake in polypropylene vs. time for run #1	40
Figure 4.3a -	Mass uptake in polystyrene vs. time for run #2	41
Figure 4.3b -	Mass uptake in polypropylene vs. time for run #2	42
Figure 4.4a -	Mass uptake in polystyrene vs. time for run #3	43
Figure 4.4b -	Mass uptake in polypropylene vs. time for run #3	44
Figure 4.5a -	Mass uptake in polystyrene vs. time for run #4	45

Fig

Fig

Fig

Fig

Fig

Fig

Fig

Fig

Fig

Fig

Fig

Fig

Fig

Fig

Figure 4.5b -	Mass uptake in polypropylene vs. time for run #4	46
Figure 4.6 -	Comparison of model to experimental results for the sulfonation of polystyrene in run #1	55
Figure 4.7 -	Comparison of model to experimental results for the sulfonation of polystyrene in run #2	56
Figure 4.8 -	Comparison of model to experimental results for the sulfonation of polystyrene in run #4	57
Figure 4.9 -	Comparison of model to Auger line scan	60
Figure 5.1 -	Result of interaction of electron beam with surface electrons in Auger analysis	63
Figure 5.2 -	Schematic of how sample block is to be trimmed for Auger analysis	67
Figure 5.3a -	Low magnification of sulfonated polystyrene embedded in epoxy	71
Figure 5.3b -	High magnification of sulfonated polystyrene embedded in epoxy	71
Figure 5.4a -	Sulfonated, unneutralized HDPE embedded in epoxy	74
Figure 5.4b -	Sulfonated, unneutralized PP embedded in epoxy	74
Figure 5.4c -	Sulfonated, unneutralized PS embedded in epoxy	75
Figure 5.5a -	Low magnification of sulfonated, unneutralized PP embedded in acrylic	78
Figure 5.5b -	High magnification of sulfonated, unneutralized PP embedded in acrylic	78
Figure 5.5c -	Low magnification of sulfonated, unneutralized PS embedded in acrylic	79
Figure 5.5d -	High magnification of sulfonated, unneutralized PS embedded in acrylic	79

i

i

i

i

P

P

P

P

P

P

P

P

P

P

P

Figure 5.6a -	Low magnification of sulfonated, neutralized PP embedded in acrylic	81
Figure 5.6b -	High magnification of sulfonated, neutralized PP embedded in acrylic	81
Figure 5.6c -	Low magnification of sulfonated, neutralized HDPE embedded in acrylic	82
Figure 5.6d -	High magnification of sulfonated, neutralized HDPE embedded in acrylic	82
Figure 5.6e -	Sulfonated, neutralized PS embedded in acrylic	83
Figure 5.7 -	Comparison of IR spectrums of unsulfonated and sulfonated polypropylene	89
Figure 5.8 -	Comparison of IR spectrums of unsulfonated and sulfonated HDPE	90
Figure 5.9 -	Comparison of IR spectrums of unsulfonated and sulfonated polystyrene	92
Figure 6.1 -	Schematics of epoxy system	94
Figure 6.2 -	Reactants in epoxy system	96
Figure 6.3 -	Reactions occurring during the cure of the epoxy	97
Figure 6.4 -	Structure of m-xylene	105
Figure 6.5 -	Schematic of electrobalance equipment	106
Figure 6.6a -	Weight gain with time for run #1 using the electrobalance	110
Figure 6.6b -	Weight gain with time for run #2 using the electrobalance	111
Figure 6.6c -	Weight gain with time for run #3 using the electrobalance	112
Figure 6.7a -	Comparison of experimental results to model results for run #1	116
Figure 6.7b -	Comparison of experimental results to model results for run #3	117

Figure 6.8 -	Experimental extent of reaction	123
Figure 6.9 -	Comparison of model to experimental extent of reaction	125
Figure 6.10 -	Determination of k_0 and E_a	126
Figure 6.11 -	Predicted concentration gradient of primary amine after two hours at 75° C	128
Figure 6.12 -	Predicted concentration gradient of secondary amine after two hours at 75° C	129
Figure 6.13 -	Predicted concentration gradient of tertiary amine after two hours at 75° C	130

Introduc

The

films is

literatur

carbon di

is not we

in isolat

process.

many ind

reaction

attempt

and reac

and the

Su.

of poly

diffuse

groups

layer i

molecul

been us

emissio

techniq

differe

polar g

Chapter 1

Introduction

The diffusion of small molecules into thin polymer films is a process which is well characterized in the literature. Examples include the diffusion of oxygen or carbon dioxide into polymer films. Diffusion with reaction is not well characterized, however, due to the difficulties in isolating the diffusion process from the reaction process. This is an interesting phenomenon since there are many industrial processes which depend on the diffusion and reaction of small molecules within polymer films. An attempt is made in this thesis to characterize two diffusion and reaction problems; the sulfonation of thin polymer films and the cure of an epoxy/diamine system.

Sulfonation is a technique which modifies the surface of polymeric films using sulfur trioxide vapor. The vapor diffuses into the films and reacts to provide sulfonic acid groups within a thin surface layer of the film. This thin layer is polar and reduces the permeation of many nonpolar molecules through the polymer. For example, sulfonation has been used on the inside of plastic fuel tanks to reduce the emission of organic vapors into the atmosphere. The technique may also be used to recycle plastics by making different plastics miscible through the interaction of the polar groups on the surface of the films.

Sul

which re

with a me

completel

barrier c

changing

Use

does not

allows th

which re

Walles,

in the u

helped t

However,

been we

provide

In

epoxy,

epoxy a

coating

epoxy c

interfa

To dete

coeffic

be char

importa

Sulfonation can also be followed by metallization, which replaces the hydrogen atom of the sulfonic acid group with a metal ion. This provides the polymer film with completely different surface properties. Potentially, the barrier can be modified to provide specific properties by changing the counter-ion of the sulfonic acid group.

Use of sulfonation to modify the surface properties does not alter the properties of the bulk polymer. It allows the polymer to be used in particular applications which requires it to have specific barrier properties. Bill Walles, of Coalition Technologies Ltd., has been a pioneer in the use of sulfur trioxide vapor for sulfonation. He has helped to promote the use of this technology in industry. However, the diffusion and reaction of sulfonation has not been well characterized. It is hoped that this thesis will provide a better understanding of the sulfonation process.

In the epoxy/diamine system, a fiber is coated with the epoxy, which is then exposed to a stoichiometric mixture of epoxy and the diamine. The diamine diffuses into the epoxy coating and eventually cures the coating. Ideally, the epoxy coating around the fiber is cured to the fiber interface, to provide protection and strength to the fiber. To determine the extent of cure of the epoxy, the diffusion coefficient and rate constants for the curing reactions must be characterized. A technology such as this has many important applications. It is hoped that a model of this

system w

the cure

coating.

Both

concentra

temperatu

determine

technique

measure t

balance,

cathetom

to the d

but the

which pr

these sy

system will provide enough information to help to optimize the cure cycle and provide complete cure of the epoxy coating.

Both systems will be characterized in terms of their concentration- dependent diffusion coefficients and their temperature-dependent rate constants. Methods used to determine these variables include an electrobalance technique, using a similar, but non-reactive species, to measure the diffusion coefficient, and a quartz spring balance, which measures the weight gain with time using a cathetometer. These techniques only provide approximations to the diffusion coefficients and reaction rate constants, but the approximations allow the systems to be modeled, which provides a better understanding of what occurs within these systems.

Gas Reac

Theory

A c

film is

has been

chlorine

chlorine

the mai

the met

to fluc

fluorine

sulfone

literat

further

Fluorine

F

has be

surfac

tanks

organi

from u

is due

backbo

Chapter 2

Gas Reaction with a Polymeric Surface

Theory

A common method of modifying the surface of a polymeric film is to expose the film to a reactive gas. This method has been used in processes such as fluorination, chlorination, and sulfonation, which use fluorine gas, chlorine gas, and sulfur trioxide, respectively. Although the main interest of this thesis is the sulfonation process, the methods used to model this process can also be applied to fluorination and chlorination. Present knowledge of fluorination and chlorination can also be used to understand sulfonation. Therefore, it is important to review the literature of these surface modification techniques before further research is conducted.

Fluorination

Fluorination is a surface modification technique which has been used to improve the barrier properties of plastic surfaces. It has been shown that fluorinated plastic fuel tanks on automobiles reduce the emissions of volatile organics from the fuel system, as compared to the emissions from untreated plastic fuel tanks. The barrier improvement is due to the addition of fluorine radicals on the polymer backbone, which increases the polarity of the polymer.

These po

fuel. T

and has

Fluor

a mixture

diffuses

fluorine

propertie

material,

microns,

times.

because

almost n

The

with the

backbone

the carb

amount o

oxifluor

$-\text{CH}_2$

where F*

surface

fluorina

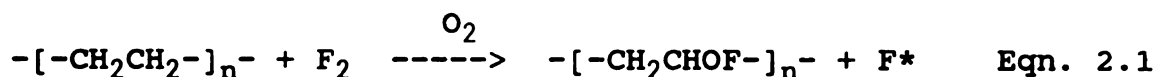
usually

the syst

These polar groups repel nonpolar organic compounds in the fuel. The fluorination process has been well characterized and has found a significant amount of use in industry.¹

Fluorination occurs by exposure of polymer surfaces to a mixture of fluorine gas and an inert gas. The mixture diffuses into a thin layer of the polymer surface and the fluorine reacts with the surface to provide modified surface properties. To modify the barrier properties of a polymeric material, only a thin surface layer, on the order of 10 microns, must be treated. This requires short exposure times. Longer exposure times are generally ineffective because the improvement in barrier with longer times is almost negligible.²

The fluorine gas initiates a free radical reaction² with the polymer to abstract a hydrogen from the carbon backbone of the polymer or from a substituent located off the carbon backbone. It has been determined that if a small amount of oxygen is present during fluorination, oxifluorination occurs.



where F^* is the fluorine radical. The oxyfluorinated surface provides better barrier properties than the fluorinated surface and is the preferred treatment. It is usually very difficult to prohibit the presence of oxygen in the system, particularly in a manufacturing atmosphere, as

it is likely to be present as an impurity in the gas, as residue in the reactor, or absorbed in the polymer.³

Surface property modifications as a result of fluorination include a lower dispersion energy, a lower polar energy, and a higher hydrogen-bonding energy. A lower surface energy is expected since fluorocarbons have lower surface energies than hydrocarbons, but the increase in hydrogen-bonding energy is unexpected. The change in the hydrogen-bonding energy is most likely due to the presence of oxygen in the modified surface as a result of oxifluorination. Hydrocarbon solvents are retained within the fluorinated surface even though they may wet the surface because of these property modifications. Aromatic solvents, however, are not well retained because they are more polar.

Fluorination of plastic fuel tanks and bottles is usually conducted during the blow-molding process. Fluorine gas, or another fluorine containing gas, is introduced during the expansion stage of the blow-molding operation at a recommended concentration from 0.1-20% by volume in the gas. The precise fluorine concentration depends on the desired surface modifications and the material being used, but for polyethylene, a concentration of 3.5% by weight is usually sufficient.⁴

Chlorina

Chlorina

technique

liquid, s

found wi

limitati

gas usua

particul

problem

light o

centers

number

indust

W

been i

chlori

uptake

much

The f

amorp

attri

amorp

since

there

gas c

Since

Chlorination

Chlorination is another polymer surface modification technique that uses chlorine gas or a chlorine containing liquid, such as sulphuryl chloride. The technique has not found widespread application, however, due to its many limitations. Exposure of the polymer surface to chlorine gas usually does not result in a high level of chlorination, particularly for crystalline materials.⁵ To overcome this problem the polymer surface must be treated using ultraviolet light or electron beam irradiation to produce free radical centers before exposure to chlorine gas. This presents a number of problems when the technique is used on an industrial scale.

When chlorine gas is exposed to surfaces which have not been irradiated or exposed to ultraviolet light, some chlorination has been found to occur in polyethylene. The uptake of chlorine is fast in the first 5-10 minutes and much slower for further exposure times up to 120 minutes. The fast chlorine uptake is attributed to reaction in the amorphous regions of polyethylene, while the slow uptake is attributed to reaction in the crystalline regions. In the amorphous region the density of the polymer is much less since there is not an ordered crystal lattice structure as there is in the crystalline region. Therefore, the chlorine gas can diffuse more quickly through the amorphous region.⁶ Since the chlorination reaction occurs quickly, the greatest

limitat

region

into the

To

sample i

irradiat

which res

polymer.

some of t

radical c

chlorinat

where Cl

reaction

sites ap

irradiat

larger c

larger a

decrease

chlorine

A m

slow to

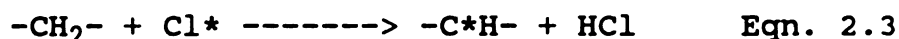
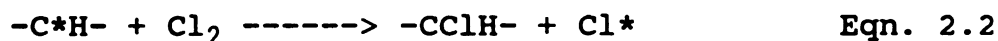
of the i

hazardou

methods

limitation to the chlorination reaction in the amorphous region is the extent to which the chlorine gas can diffuse into the sample.

To enlarge the amorphous region of the polymer, the sample is treated by ultraviolet light or electron beam irradiation. These techniques produce free radical centers, which results in damage to the crystal structure of the polymer. The change in the crystal structure will affect some of the properties of the polymer. Once the free radical centers are produced, the propagation of chlorination occurs via;



where Cl^* is the chlorine radical. Termination of the reaction occurs when the number of available chlorination sites approaches zero.⁶ As expected, higher doses of irradiation result in a greater uptake of chlorine due to a larger crystalline area which is damaged and, hence, a larger amorphous region. The level of chlorination decreases with decreasing temperature due to the lower chlorine gas diffusivity at lower temperatures.

A major problem with the technique is that it is too slow to be of practical value. Another problem is that both of the irradiation and ultraviolet light methods are hazardous due to the production of hydrochloric acid. The methods are also impractical for use in industry due to the

difficult

ultraviolet

chlorine

also requires

polymer

azobisisobutyronitrile

chlorine

The radiation

backbone

The chain

Unfortunately

this reaction

and environmental

techniques

use.

Sulfonation

Much

solution

swelling

method

gas molecular

the bulk

efficiency

however

difficulty in exposing the entire surface area to ultraviolet light or the electron beam.

Chlorination using a liquid such as sulphuryl chloride also requires the production of a free radical center on the polymer chain.⁷ In this case an initiator, such as azobisisobutyronitrile (ABIN), is used to abstract a chlorine atom to produce the sulphuryl chloride radical. The radical then abstracts a hydrogen atom from the polymer backbone to produce a radical site on the polymer chain. The chain is then chlorinated using sulphuryl chloride. Unfortunately, hydrochloric acid is also a side product in this reaction, as well as sulfur dioxide, which are health and environment problems. Therefore, the use of this technique for chlorination has also not found widespread use.

Sulfonation

Much work has been done on solution sulfonation, but solution sulfonation causes problems such as polymer swelling and solvent contamination. A gaseous sulfonation method is preferred, using sulfur trioxide gas. The small gas molecule can diffuse farther into a polymer sample than the bulky liquid group, resulting in a more thorough and efficient surface modification. Sulfur trioxide gas is, however, difficult to use due to its high affinity for

water.

gaseous

The

which me

oxygen a

double b

oxygen a

and the

with a

where

polyme

sulfur

proto

Since

found

SO_3SO

the

one

grou

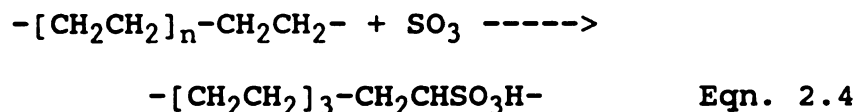
and

for

wate

water. Much of the work that has been done to characterize gaseous sulfonation has been conducted by Walles.

The sulfur trioxide molecule is a resonance hybrid, which means that the oxygen atoms are equivalent. The oxygen atoms are strongly bound, with a large degree of double bond character. Due to the binding nature of the oxygen atoms, the sulfur atom is strongly electron-deficient and the oxygen atoms are electron-rich.⁸ A typical reaction with a polymer is;



where the sulfonic acid group ($-\text{SO}_3\text{H}$) is added to the polymer chain. Therefore, in reactions with polymers, the sulfur atom attacks the electron-rich sites, abstracts a proton, and the oxygen atoms accept the acidic protons. Since sulfur trioxide often exists as a complex, it has been found that the modified surface group may initially exist as $\text{SO}_3\text{SO}_3\text{H}$, with one SO_3 group being more strongly bound than the other. With a water wash after sulfonation, however, one SO_3 group is removed as H_2SO_4 , thus producing the SO_3H group on the polymer chain.⁹

The sulfonation reaction has a small negative enthalpy and is a reversible reaction. Due to its strong affinity for water, the sulfonic acid group may be removed with water, producing sulfuric acid.¹⁰ To prevent the loss of

the sulf

neutral:

The neut

complex

due to

and the

T

unneut

polyme

the r

a goo

appli

furt

ions

call

poly

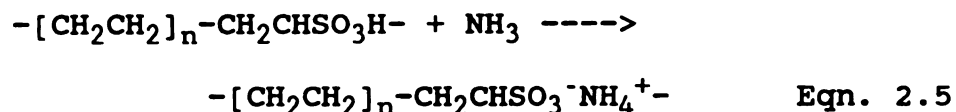
rea

pol

for

for

the sulfonic acid group, the sulfonated material is neutralized with ammonia or ammonium hydroxide;



The neutralized sulfonic acid group ($\text{SO}_3^-\text{NH}_4^+$) is stable complex which resists the attack of solvents such as water due to the strong attraction between the sulfonic acid ion and the ammonium ion.

The neutralized sulfonic acid group, as well as the unneutralized sulfonic acid group, is polar, thus making the polymer water wettable. Water-wettability is important for the recycling of plastic materials. The group also provides a good barrier to nonpolar solvents and gases for use in applications such as sulfonated plastic fuel tanks. To further change the surface properties of plastics, metal ions can be exchanged for the ammonium ion in a process called reductive metallization.¹¹

Reports by Ihata¹² indicate that during sulfonation a polymer radical is produced. The polymer radical may then react with the sulfonic acid group to produce the sulfonated polymer, or the elimination of a hydrogen atom may occur to form an unsaturated bond within the chain, with the formation of sulfurous acid.

The form

accompan

yellow-

unsatur

and po

This i

sulfur

argume

Appli

publ

mate

the

sulf

of p

et.

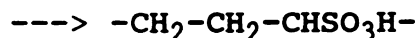
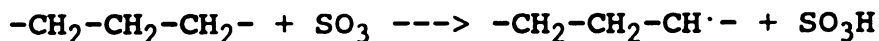
poly

impre

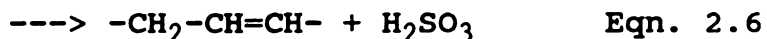
compa

inter

and t



or



The formation of the unsaturated bond within the chain is accompanied by a color change for clear materials to yellow-brown and then brown. This side reaction to form the unsaturated bond occurs in materials such as polyethylene and polypropylene, but not in materials such as polystyrene. This indicates that the side reaction only occurs when sulfur trioxide attacks the polymer backbone. A stronger argument for this will be given later in this thesis.

Applications of Sulfonated Polymers

Several studies of sulfonated polymers have been published which indicate the usefulness of sulfonated material due to the modified surface properties. Many of the studies to be cited use material which has been sulfonated using solution methods, but they show the types of potential applications for sulfonation materials. Wang et. al.¹³ have used sulfonated polystyrene in blends with poly(ethyl acrylate 4 vinyl pyridine) (P(EA-co-VP)) to improve the compatibility of the materials. The enhanced compatibility of the materials is due to the ionic interactions between the negatively charged sulfonate groups and the protonated nitrogen atoms on the P(EA-co-VP) chains.

Hara et.

exhibite

whether

solvents

attract

enhance

polar s

The pol

ion cor

enhanc

were e

verifi

W

betwee

found

of su

LisPS

more

since

tempe

impro

and p

unmod

to al

polys

Hara et. al.¹⁴ showed that sulfonated polystyrene ionomers exhibited different solution properties depending upon whether polar or nonpolar solvents were used. In nonpolar solvents the ionomers tended to form aggregates because of attraction between the ion pairs. The aggregation was enhanced by increasing the ion content of the ionomer. In polar solvents the ionomers showed polyelectrolyte behavior. The polyelectrolyte behavior was enhanced with increasing ion content. Therefore, the intramolecular attraction was enhanced by nonpolar solvents and the intermolecular forces were enhanced by polar solvents. Hara's results are verified by the results of MacKnight and Lundberg.¹⁵

Weiss et. al.¹⁶ studied the improvement in miscibility between sulfonated polystyrene and Nylon 6 blends. They found that Nylon 6 was completely miscible with metal salts of sulfonated polystyrene, with miscibility improving by $\text{LiSPS} < \text{ZnSPS} < \text{MnSPS}$. Transition metal salts were found to be more effective at improving the miscibility with Nylon 6, since phase separation occurred for the lithium salt at temperatures of 250° C. The authors expect miscibility improvements with other polar polymers such as polycarbonate and poly(ethylene terephthalate).

Armstrong et. al.¹⁷ mixed sulfonated polystyrene with unmodified polystyrene in an attempt to improve the adhesion to aluminum. For low molecular weight functionalized polystyrene (10,000 MW) the adhesive strength improved with

a use of

blends.

addition

for the

blend is

absorbs

then bor

polymer

functio

region

weight

highest

decrea

functi

functi

unmodi

levels

adhes.

a use of 10-20 wt. % of sulfonated polystyrene in the blends. The adhesive strength decreases with further addition of sulfonated material in the blend. The reason for the optimum amount of sulfonated polystyrene in the blend is that only a small amount of functionalized polymer absorbs on the aluminum surface. The functionalized polymer then bonds to the higher molecular weight unfunctionalized polymer by van der Waal's forces. As the amount of functionalized polymer increases, a thicker interphase region builds up which is not as strong. High molecular weight functionalized polystyrene (60,000 MW) has the highest adhesive strength at 35 wt. % sulfonated polymer. A decrease in the adhesive properties with higher levels of functionalized polymer does not occur since the functionalized polymer has the same molecular weight as the unmodified polymer. It is noted, however, that higher levels of sulfonated polymer in the blend does not improve adhesion.

Chapter 3

General Mathematical Model

Theory

Mathematical modelling of engineering processes has become a common technique used to predict the outcomes of experimental or industrial procedures. A model can predict additional properties of the system from the properties already determined by experimental methods, or it can predict outcomes based upon data found in the literature. Industry is becoming more reliant upon mathematical models, as demonstrated by the increasing use of computer-aided engineering (CAE), and is finding CAE to be a very powerful tool. It is therefore logical that this study should begin with the development of a mathematical model of the sulfonation process so that additional information can be obtained about the process.

Since the systems being considered are polymer films, the model will consider unsteady state diffusion in a plane sheet. According to Crank¹⁸, the theory of diffusion is based on the assumption that the rate of transfer of the diffusing substance through a unit area of a section is proportional to the concentration gradient normal to the section. Therefore,

$$F = -D \frac{\delta C}{\delta X} \quad \text{Eqn. 3.1}$$

where F is the rate of transfer per unit section, D is the diffusion coefficient, C is the concentration of the diffusing substance and x is the coordinate normal to the plane of the sample. An unsteady state balance around a slab results in;

$$\frac{\delta C}{\delta t} + \frac{\delta F_x}{\delta x} + \frac{\delta F_y}{\delta y} + \frac{\delta F_z}{\delta z} = 0 \quad \text{Eqn. 3.2}$$

If it is assumed that the slab is sufficiently thin, the rate of transfer in the y and z directions is negligible and the above equation becomes;

$$\frac{\delta C}{\delta t} = D \frac{\delta^2 C}{\delta x^2} \quad \text{Eqn. 3.3}$$

This equation assumes that the diffusion coefficient is not dependent upon concentration. Equation 3.3 is the basis of the model for diffusion of sulfur trioxide into polymer thin films.

The system being considered is sulfur trioxide gas diffusing into a thin polymer film. It is assumed that one side of the film is exposed to a constant concentration of the gas and the other side does not see any gas. In other words, the polymer is a semi-infinite medium. The initial condition and boundary conditions for this system are;

$$\begin{aligned}
 \text{I.C.:} \quad & \text{At } t = 0, C = C_0 = 0 \\
 \text{B.C. 1:} \quad & \text{At } x = 0, C = C_1 \\
 \text{B.C. 2:} \quad & \text{At } x = \infty, C = C_2 = 0
 \end{aligned}$$

Solving the differential equation using the above initial and boundary conditions through Laplace transforms results in the following solution;

$$C = C_1 \operatorname{erfc} \frac{x}{2\sqrt{Dt}} \quad \text{Eqn. 3.4}$$

Therefore, the results of the model can be verified by comparing it to the results found using the error function.¹⁹

To solve the above partial differential equation, a computer program was written using a finite difference technique. Finite difference techniques require the use of a network of grid points. For the problem under consideration, the network is two dimensional, with each dimension representing an independent variables, the x-coordinate and time.²⁰ The grid spacings are therefore Δx and Δt . The subscripts i and n are used in the computer program to denote the space points, with i referring to position and n referring to time, as shown in Figure 3.1.

Consider the problem of;

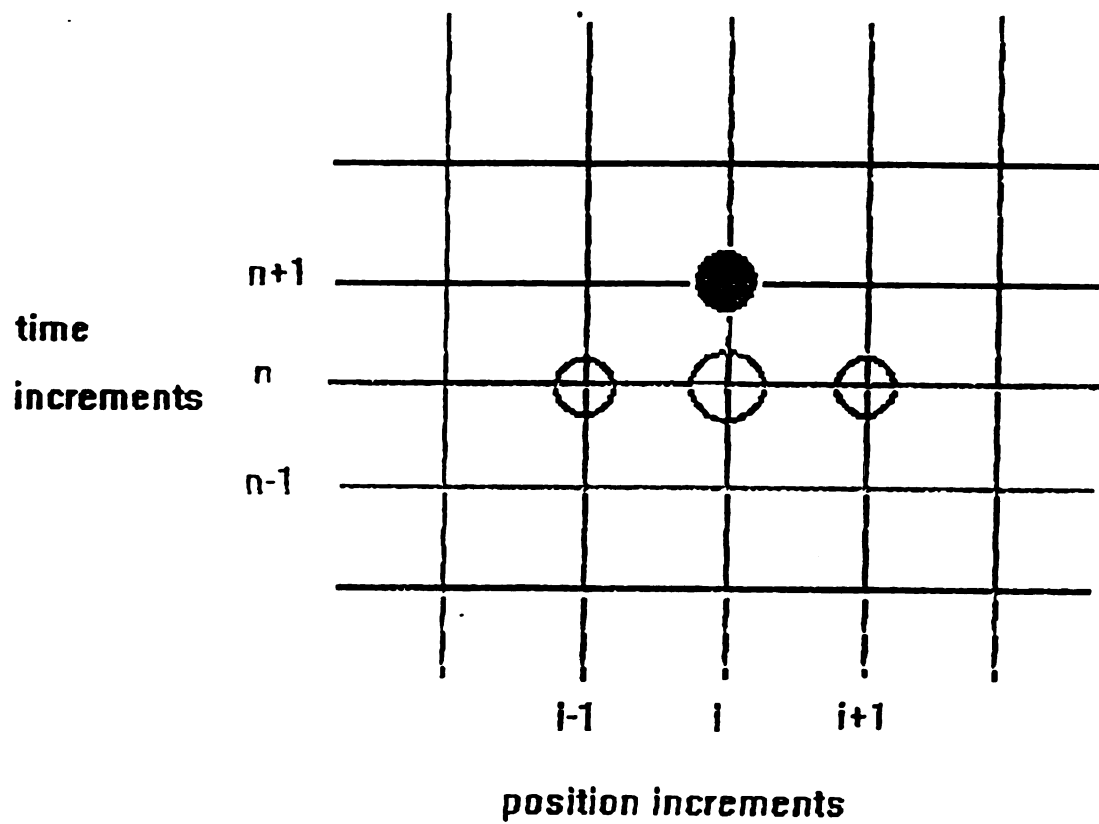


Figure 3.1 - Grid for solving partial differential equations explicitly

$$\frac{\delta v}{\delta t} = \frac{\delta^2 v}{\delta x^2} \quad \text{Eqn. 3.5}$$

where v is the concentration of the diffusing species.

Using the network of grid points, the problem may be solved using the explicit form of the differential equation or the implicit form. The explicit form involves finding solutions to the problem at different grid points based upon knowledge of solutions at previous time steps, or n coordinates. The explicit form is easy to use, but has the limitation of λ less than or equal to zero. This limitation provides some difficulties in certain applications, particularly at long times.²¹

The implicit method is somewhat more complicated, but overcomes the limitations of the explicit method. In the implicit method, solutions at time coordinate n are determined by writing the differential equations in terms of time coordinate $n+1$ and solving the resulting equations simultaneously. The problem consists of $M-1$ simultaneous equations with $M-1$ unknowns. Since this method introduced several complications into the computer program, the explicit method was chosen for use in the research presented in this paper.

The finite-difference method chosen for use in this thesis to model diffusion into a polymer film was a modification of the Saul'yev method.²¹ Although it is an

explicit method, it is an unconditionally stable method, which means that it is free of the limitation of λ less than or equal to 0.5. A brief comparison was made between the modified Saul'yev method and the Crank-Nicholson method (an implicit method), which indicated that there was no loss of accuracy when the modified Saul'yev method was used.

The modified Saul'yev method is an alternating-direction procedure which computes two intermediate values at a particular time level and then takes the average of the intermediate values as the final value. The intermediate value p was calculated in the positive x -direction from the surface exposed to the gas, while the intermediate value q is calculated in the negative x -direction, from the semi-infinite region to the gas/polymer interface. It is noted that in a model of mass transfer, the v in the above equations, as well as p and q , are the concentration of the diffusing species. The formulas used in the calculation were;

$$\frac{(p_{i,n+1} - v_{i,n})}{\Delta t} = D \frac{(p_{i-1,n+1} - p_{i,n+1} - v_{i,n} + v_{i+1,n})}{\Delta x^2} \quad \text{Eqn. 3.8}$$

$$\frac{(q_{i,n+1} - v_{i,n})}{\Delta t} = D \frac{(v_{i-1,n} - v_{i,n} - q_{i,n+1} + q_{i+1,n+1})}{\Delta x^2} \quad \text{Eqn. 3.9}$$

$$v_{i,n+1} = 0.5(p_{i,n+1} + q_{i,n+1}) \quad \text{Eqn. 3.10}$$

Equations 3.8 and 3.9 are solved for $p_{i,n+1}$ and $q_{i,n+1}$, respectively, and the results are used to calculate $v_{i,n+1}$. Thus, the output of the mathematical model was the concentration of the diffusing species. It is noted that in solving for $q_{i,n+1}$, the equation is first solved at the extreme distance of the semi-infinite medium, which is denoted as $q_{\text{index},n+1}$.

The initial conditions for the system were;

$$\begin{aligned} \text{At } t = 0: \quad p_{i,0} &= 0 \\ q_{i,0} &= 0 \\ v_{i,0} &= 0 \end{aligned}$$

This means that at $t = 0$ there was no gas in the system.

The boundary conditions were;

$$\begin{aligned} \text{At } x = 0: \quad p_{0,n} &= C_1 \\ q_{0,n} &= C_1 \\ v_{0,n} &= C_1 \end{aligned}$$

$$\begin{aligned} \text{At } x = \text{index}: \quad p_{\text{index},n} &= 0 \\ q_{\text{index},n} &= 0 \\ v_{\text{index},n} &= 0 \end{aligned}$$

To determine the how well the model fits the error function solution, several values for the variables were arbitrarily selected. In the first comparison, $\Delta t = 30$ sec, $\Delta x = 10^{-6}$ m, $C_1 = 3$ mol/L and $D = 10^{-14}$ m²/sec. The value for index was specified to be 20 so that the thickness of the slab was 2×10^{-5} m. Figures 3.2a, b and c show the results of the model for these values. The model corresponds to the error

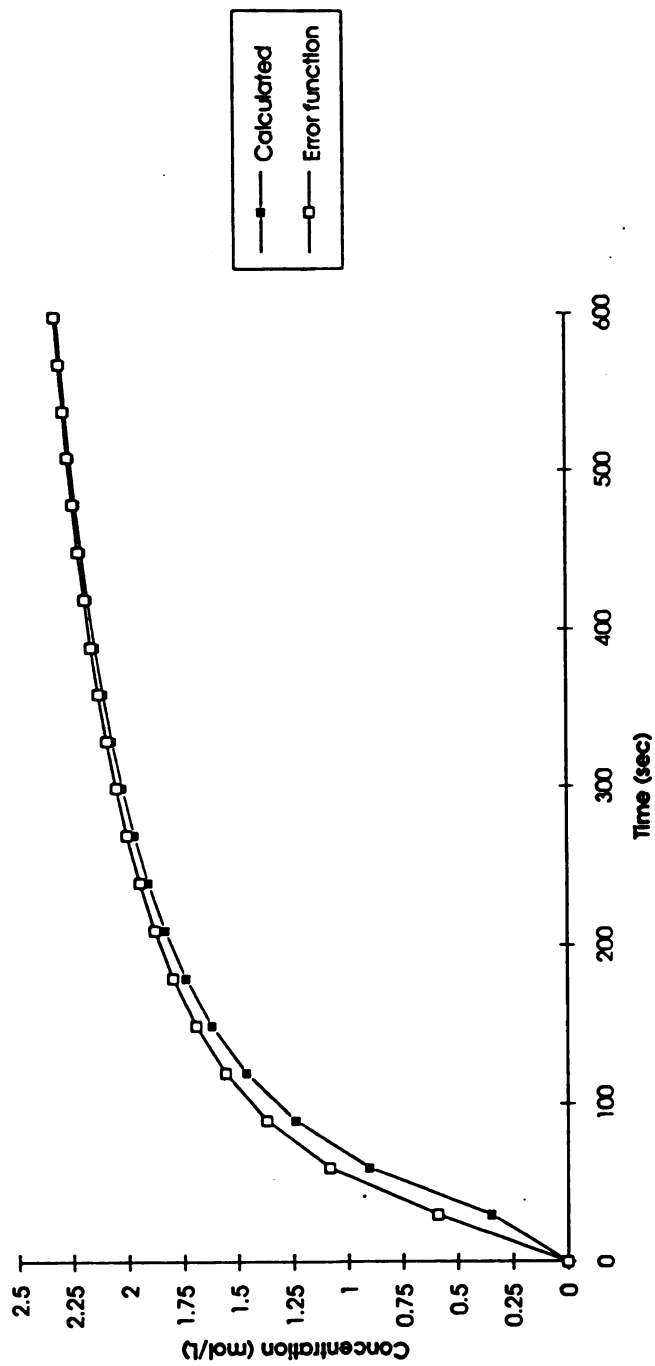


Figure 3.2a - Concentration of diffusing specie vs. time at a position 1 micron from the interface:
Comparison of the model to the error function for $\lambda=0.3$

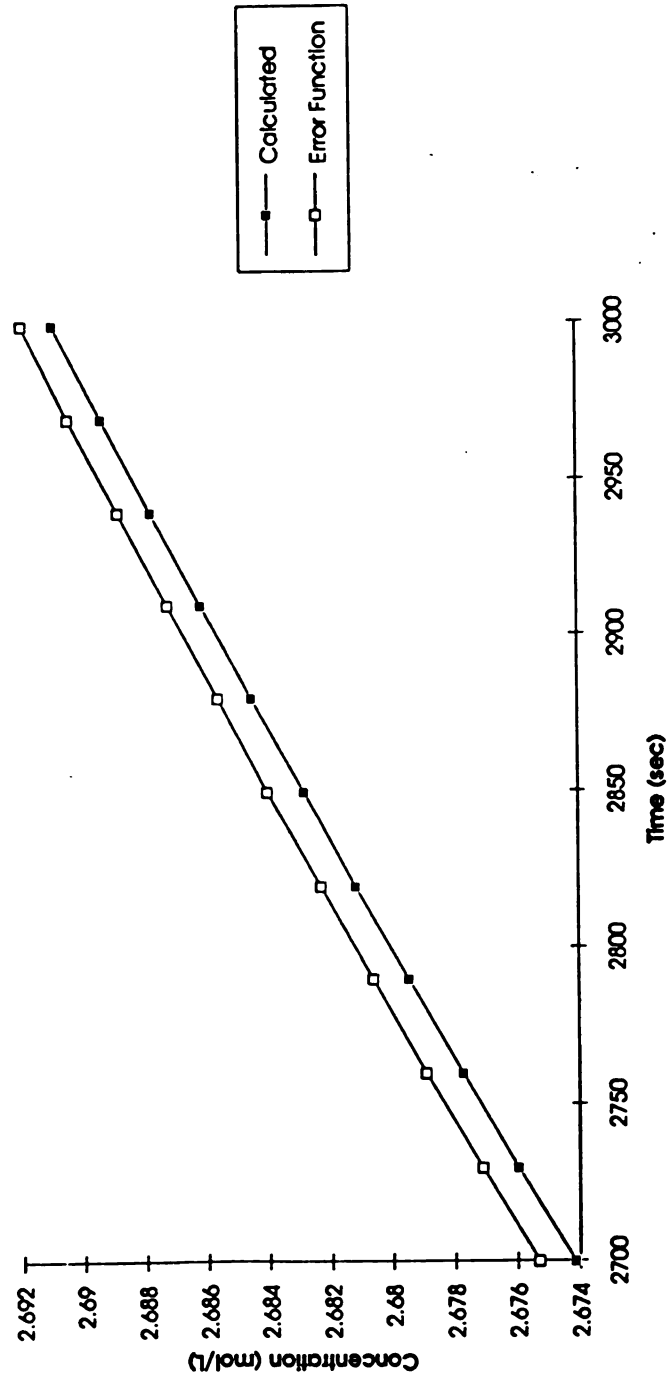


Figure 3.2b - Concentration of diffusing specie vs. time at a position 1 micron from the interface:
Comparison of the model to the error function for $\lambda=0.3$

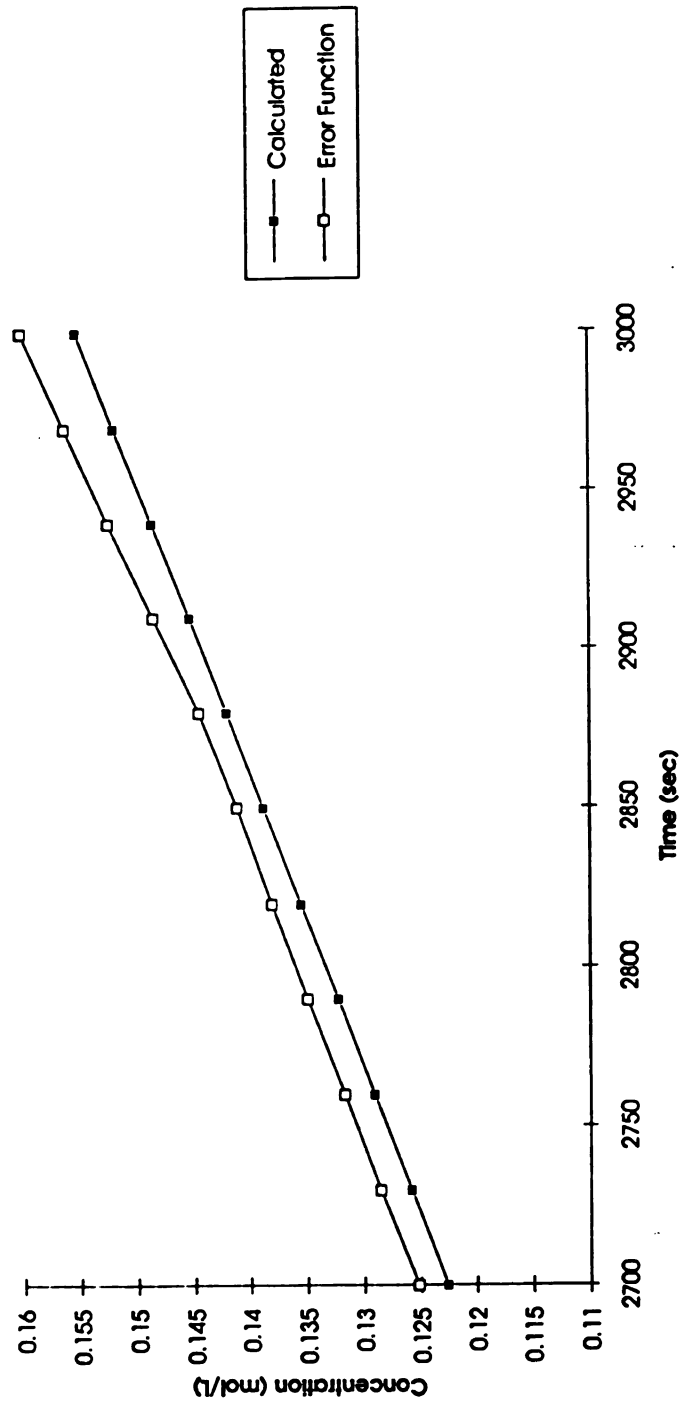


Figure 3.2c - Concentration of diffusing specie vs. time at a position 15 microns from the interface:
Comparison of the model to the error function for $\lambda=0.3$

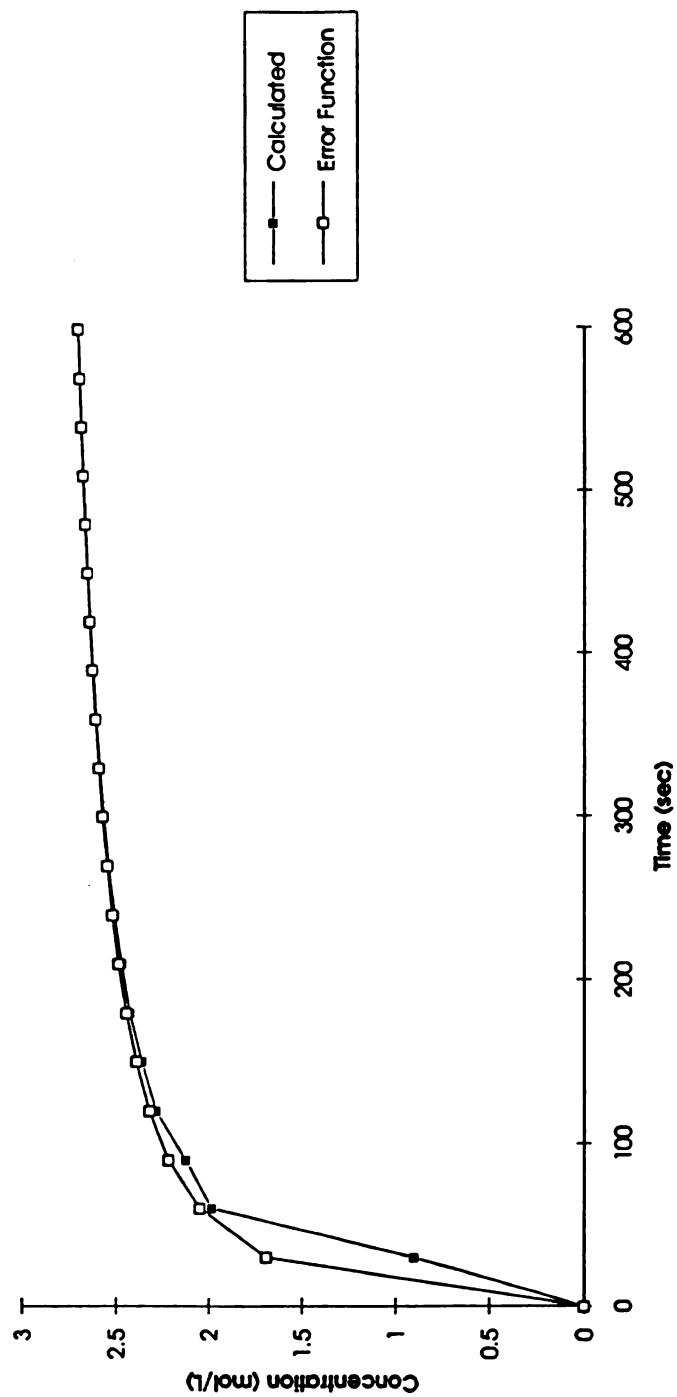


Figure 3.3a - Concentration of diffusing specie vs. time at a position 1 micron from the interface:
Comparison of the model to the error function for $\lambda > 0.3$

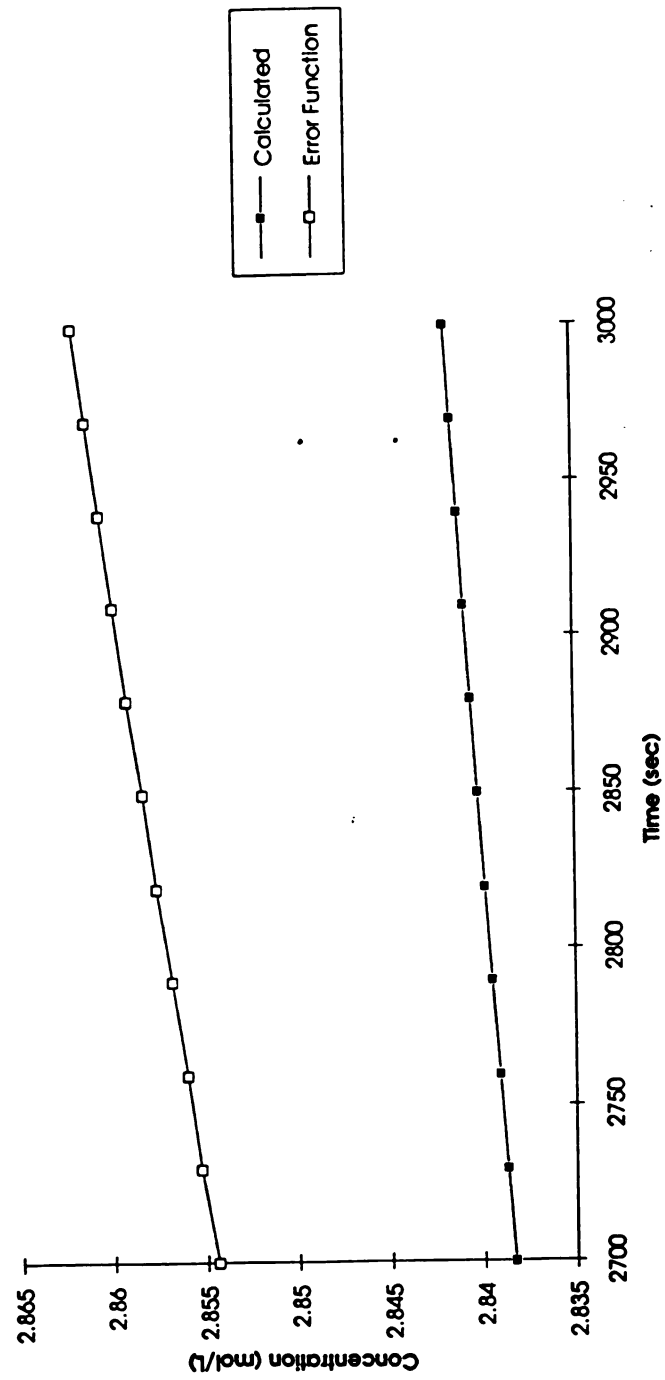


Figure 3.3b - Concentration of diffusing specie vs. time at a position 1 micron from the interface:
Comparison of the model to the error function for $\lambda)0.3$

function values quite well. It is noted that the value for λ for this case was 0.3, which met the stipulations for a typical explicit method. It was desired to know if the model corresponded to the error function for $\lambda > 0.5$. For this comparison, $D = 5.5 \times 10^{-18} \text{ m}^2/\text{sec}$, $\Delta t = 30 \text{ sec}$, and $\Delta x = 1 \times 10^{-8} \text{ m}$. The results for this case are shown in Figures 3.3a and b. It was found that at long times the calculated results diverge from the error function values and continue to grow larger for longer times. This appears to be a concern, but the level of divergence is small enough to be negligible. At 100 minutes, it was found that the difference between the model values and the error function values were less than one percent. Therefore, because of the good correlation between the model and the error function, the model was expanded to include the reaction.

Model for Sulfonation

The model of sulfonation was somewhat more complicated than the above model due to the fact that the diffusion coefficient of sulfur trioxide was dependent upon concentration and the chemical reaction was included. There are three species whose concentrations changed during the reaction: sulfur trioxide (SO_3), unsulfonated polymer (UP), and sulfonated polymer (SP). Figure 3.4 is a schematic of the sulfonation reaction. The model had to include finite difference methods to calculate the changing concentration

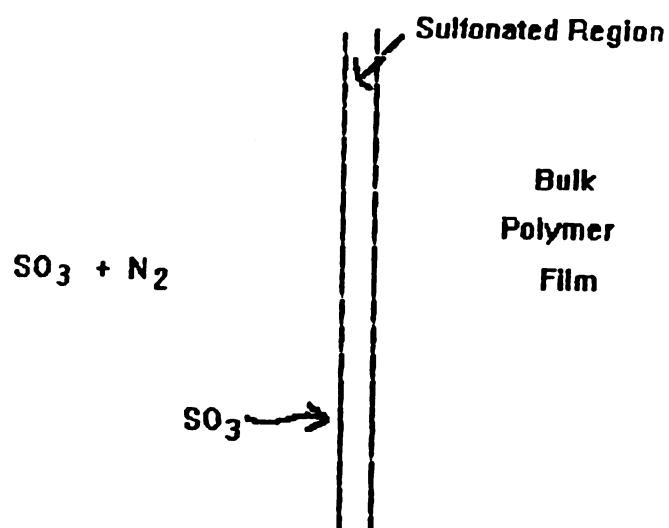
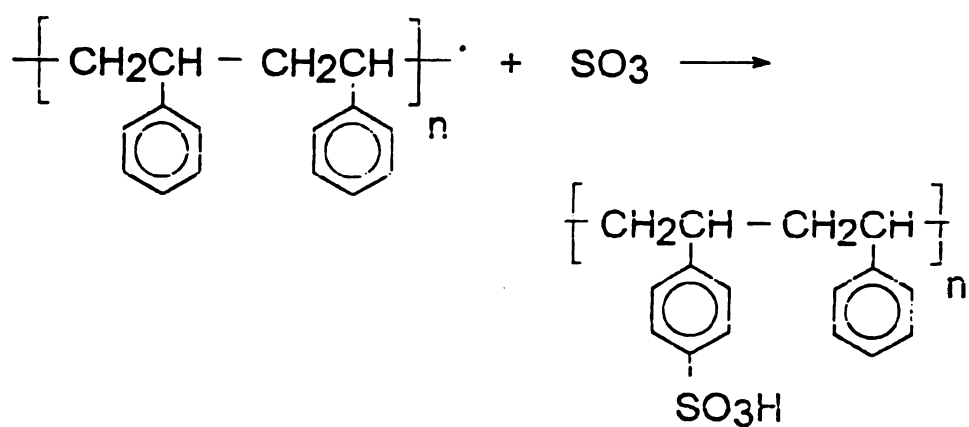
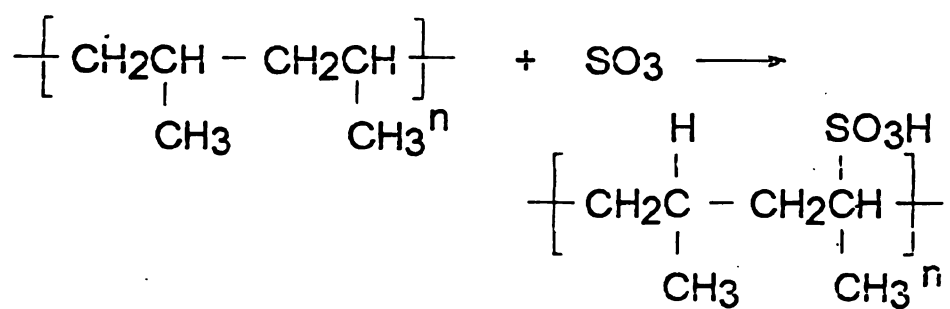


Figure 3.4 - Schematic of the sulfonation reaction

of each of the species. Assuming that the sulfonation reaction is a first order reaction, the rate equations for each of the species are;

$$\frac{\delta C_{SO_3}}{\delta t} = \frac{\delta}{\delta x} D_{SO_3} \frac{\delta C_{SO_3}}{\delta x} - k C_{SO_3} C_{UP} \quad \text{Eqn. 3.11}$$

$$\frac{\delta C_{UP}}{\delta t} = \frac{\delta}{\delta x} D_{UP} \frac{\delta C_{UP}}{\delta x} - k C_{SO_3} C_{UP} \quad \text{Eqn. 3.12}$$

$$\frac{\delta C_{SP}}{\delta t} = \frac{\delta}{\delta x} D_{SP} \frac{\delta C_{SP}}{\delta x} + k C_{SO_3} C_{UP} \quad \text{Eqn. 3.13}$$

However, since the unsulfonated polymer and sulfonated polymer have diffusion coefficients which are approximately zero, due to the large size of these species, the last two rate equations reduce to;

$$\frac{\delta C_{UP}}{\delta t} = -k C_{SO_3} C_{UP} \quad \text{Eqn. 3.14}$$

$$\frac{\delta C_{SP}}{\delta t} = +k C_{SO_3} C_{UP} \quad \text{Eqn. 3.15}$$

The rate equation for each species was written in the grid

form of the Saul'yev method, as described in the opening paragraphs.

The initial conditions for the system are as follows;

$$\begin{aligned} \text{At } t = 0; \quad C_{\text{SO}_3} &= C_{\text{SO}_3}^0 = 0 \\ C_{\text{UP}} &= C_{\text{UP}}^0 \\ C_{\text{SP}} &= C_{\text{SP}}^0 = 0 \end{aligned}$$

In other words, at time zero, there is no sulfur trioxide gas present in the system and therefore, no sulfonated polymer. The concentration of the unsulfonated polymer is the mass of the polymer divided by its molecular weight and its volume. Boundary conditions are not required for the unsulfonated and sulfonated polymer because there is no coordinate dependency on its concentration, but are required for sulfur trioxide, the diffusing species. The SO_3 boundary conditions are;

$$\begin{aligned} \text{At } x = 0, \quad C_{\text{SO}_3} &= C_1 \\ \text{At } x = \infty, \quad C_{\text{SO}_3} &= C_2 = 0 \end{aligned}$$

The second boundary condition is a result of the semi-infinite media assumption in the system. In the first boundary condition, C_1 is equal to the solubility of the diffusing species (in this case SO_3) in the polymer. In the previous example, C_1 was assumed to be 3 mol/L. The actual value of the solubility of SO_3 in any particular polymer is difficult to determine and was one of the objectives of this work. If the SO_3 vapor does not condense on the surface of

the film, the SO_3 solubility should be the concentration of SO_3 in the gas phase.

Since there is no data in the literature on the diffusion coefficient of SO_3 in polymers or on the rate constants for the reaction, these parameters must be experimentally determined before the system can be modelled. The following section describes the method for determining these parameters. The results of the mathematical model are then discussed.

Chapter 4

Experimental Methods for Sulfonation

Experimental Setup

To obtain experimental data for the determination of the diffusion coefficient of sulfur trioxide and rate constant for sulfonation, a quartz spring balance and cathetometer technique was used. Although other techniques, such as the use of electrobalance, may have been preferable to obtain precise data, use of such a method was impossible due to the corrosive nature of the reactant. A diagram of the experimental system is shown in Figure 4.1. As shown in Figure 4.1, the polymeric film was suspended in the sample chamber using a quartz spring. An important step before beginning the experiment was to ensure that the chamber was tightly sealed. This was important not only for the safety of the researchers, but to prevent a leak in the system which would cause the vapor to condense on the film and result in false data. As the polymeric film was exposed to sulfur trioxide vapor, the quartz spring extended, and the extension was measured using a cathetometer. Recordings of the extension using the cathetometer were somewhat crude because of the flow rate of vapor through the sample chamber caused the sample to bounce and resulted in errors in the extension measurement.

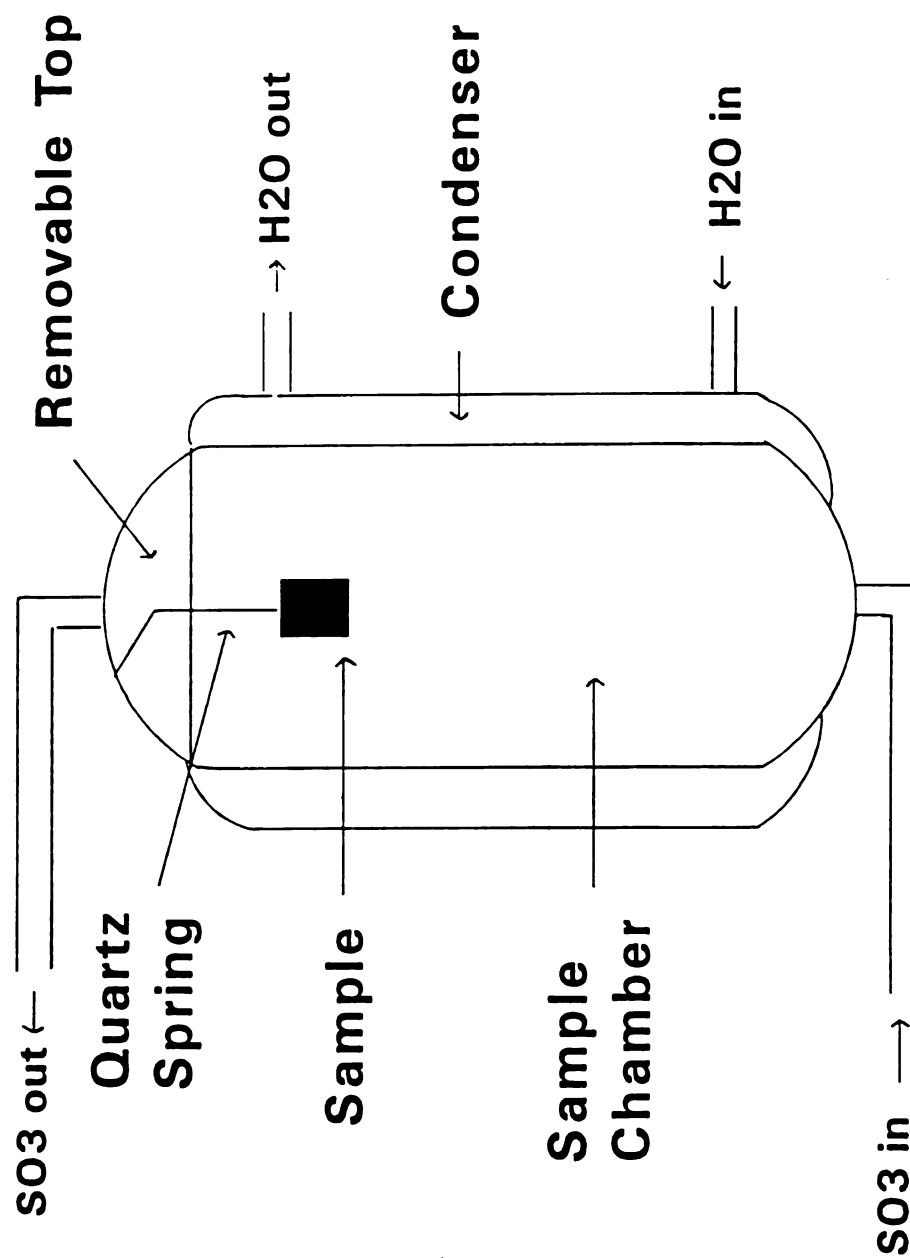


Figure 4.1 - Schematic of quartz spring experiment

Since the cathetometer measured the extension of the quartz spring, in centimeters, the weight gain in the sample due to sulfonation was determined using the spring constant. The spring constant, with units of milligram per millimeter, was multiplied by the spring extension, resulting in mass gained.

The source of the SO_3 was an SO_3 generator obtained from Coalition Technologies Ltd.²³ The SO_3 generator consisted of a reactor containing oleum which was internally circulated with a liquid pump when not in use. During use, a gas pump was used to externally circulate the gas through the experimental system. The experimental system, in this case, consisted of a kinetic test chamber in the form of a condenser, as shown in Figure 4.1. The sample chamber was made of glass to allow the viewing of the quartz spring and polymer sample. Water in the condenser portion of the sample chamber was kept at a constant temperature using a refrigerated water bath.

Rates of reaction are usually highly dependent upon temperature. Therefore, in an effort to isolate the diffusion process from the reaction, low temperature experiments were used. These low temperature experiments were used to estimate the diffusion coefficient, without reaction, of SO_3 in the polymeric films. An assumption was made that only diffusion occurred in these experiments, although, in reality, some reaction did occur. Once the

diffusion coefficient was determined, higher temperature experiments, where both diffusion and reaction occurred, were used to identify the reaction rate constant.

To prepare for an experiment, the chamber was tightly sealed and purged with nitrogen gas to remove any volatiles that might have been present in the system. Exit gases from this purge went through a gas scrubber containing sodium hydroxide to neutralize any acid vapors before being released to the atmosphere. The valves on the inlet and exit lines were then closed and a vacuum was pulled on the system. This step was important for the removal of any condensed liquids on the film, sides of the sample chamber, or in the stainless steel lines of the system. Failure to pull a vacuum on the system would result in condensation of liquid on the film surface and an exaggerated weight gain. After the vacuum step, the pressure of the system was increased to atmospheric pressure using nitrogen gas. In the meantime, the gas pump was turned on and the SO_3 generator was left on internal circulation until that system equilibrated, as set by a timer built into the system.

To begin an experiment, a measurement of the polymer sample height was made using the cathetometer before SO_3 was introduced into the sample chamber. The SO_3 generator was then switched to external circulation and readings of the extension of the quartz spring were taken using the

cathetometer every 30 seconds. Typical experimental times were ten minutes.

An attempt was made to determine the vapor concentration in the sample chamber by taking a vapor sample, mixing it with water, and then titrating the liquid solution. This technique was not, however, reproducible and therefore not reliable. Problems occurred with use of this technique, such as leakage of vapor from the syringe, leakage of vapor from the sample port, and condensation of water vapor or residual acid within the syringe which gave false measurements. Thus, to determine the concentration of SO_3 at the sample interface, or the boundary condition of the problem, the solubility was determined using the weight gain data from the quartz spring and cathetometer experiment.

In the experiment, the mass uptake with time was determined. To determine the concentration of SO_3 at the interface, the mass uptake was divided by the molecular weight of SO_3 to determine the number of moles within the polymer film. The volume of the polymer film was determined by multiplying the thickness of the sulfonated layer within the film by two times the surface area of the film. The two is included in the equation since two faces of the film are exposed to the vapor. Figure 4.9 shows that the thickness of the sulfonated layer is approximately six microns. An in-depth discussion of this figure is postponed until latter

in this thesis. Thus, the concentration at the gas-solid interface was the moles of SO_3 divided by the volume of polymer. An assumption was made that the volume change of the sample with sulfonation was negligible. This method was used for all experimental conditions, since the concentration of SO_3 at the interface changed with gas phase concentration and reaction temperature.

Results of Experiments

Two polymer films, polystyrene and polypropylene, were sulfonated using the quartz spring balance technique. The polystyrene samples had dimensions 2 cm x 4 cm and the polypropylene samples were about 28 mm x 40 mm. The thickness of the samples were determined using a microscope and a micron scale. A sample of each polymer was run at four different sulfonating conditions. A summary of the dimensions and weight of the samples is given in Table 4.1.

The samples were prepared for sulfonation by washing with ethanol to remove any surface contaminants. A 1/16 inch hole was punched in each sample to allow room for the hook on the quartz spring. A sample was then loaded into the sample chamber and the run began as described above.

Figures 4.2a and b show the results of run #1, which is the weight gain in polystyrene and polypropylene, respectively, with time. In run #1, the reactor temperature was 90° F (32.2° C) and the temperature in the sample

chamber was 11° C. Figures 4.3a and b show the results of run #2, which again the weight gain of PS and PP with time. Run #2 differs from run #1 only in the chamber temperature of 20° C during the experiment. Figures 4.4a and b show the results of run #3. In run #3, the reactor temperature was 110° F (43.3° C) and the chamber temperature was 11° C. Figures 4.5a and b show the results of run #4, which differs from run #3 only in the chamber temperature, which is 20° C in this case. Different reactor temperatures resulted in different vapor phase concentrations of SO₃. At higher reactor temperatures, it was expected that the concentration of SO₃ in the vapor phase was higher.

Sample	Length (mm)	Width (mm)	Thickness (microns)	Volume (L x 10 ⁷)	Mass (g)
Run #1- PS	40	20	54.26	4.3408	0.0463
Run #1- PP	40	26	53.62	5.5765	0.0501
Run #2- PS	40	20	54.26	4.3408	0.0464
Run #2- PP	40	27.5	53.62	5.8982	0.0499
Run #3- PS	40	20	54.26	4.3408	0.0456
Run #3- PP	40	28	53.62	6.0054	0.0510
Run #4- PS	40	20	54.26	4.3408	0.0445
Run #4- PP	40	28	53.26	6.0054	0.0490

Table 4.1 - Dimensions of samples for sulfonation.

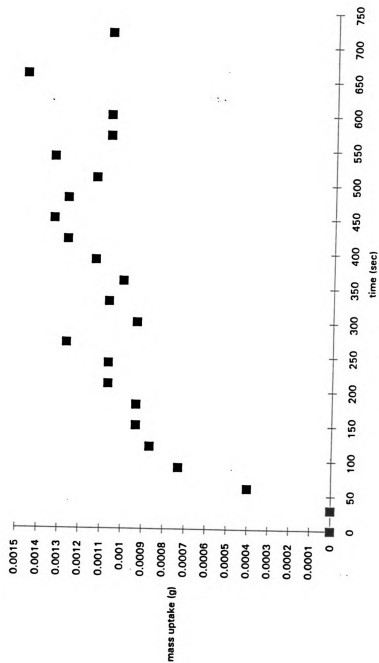


Figure 4.2a - Mass uptake in polystyrene vs. time for run #1

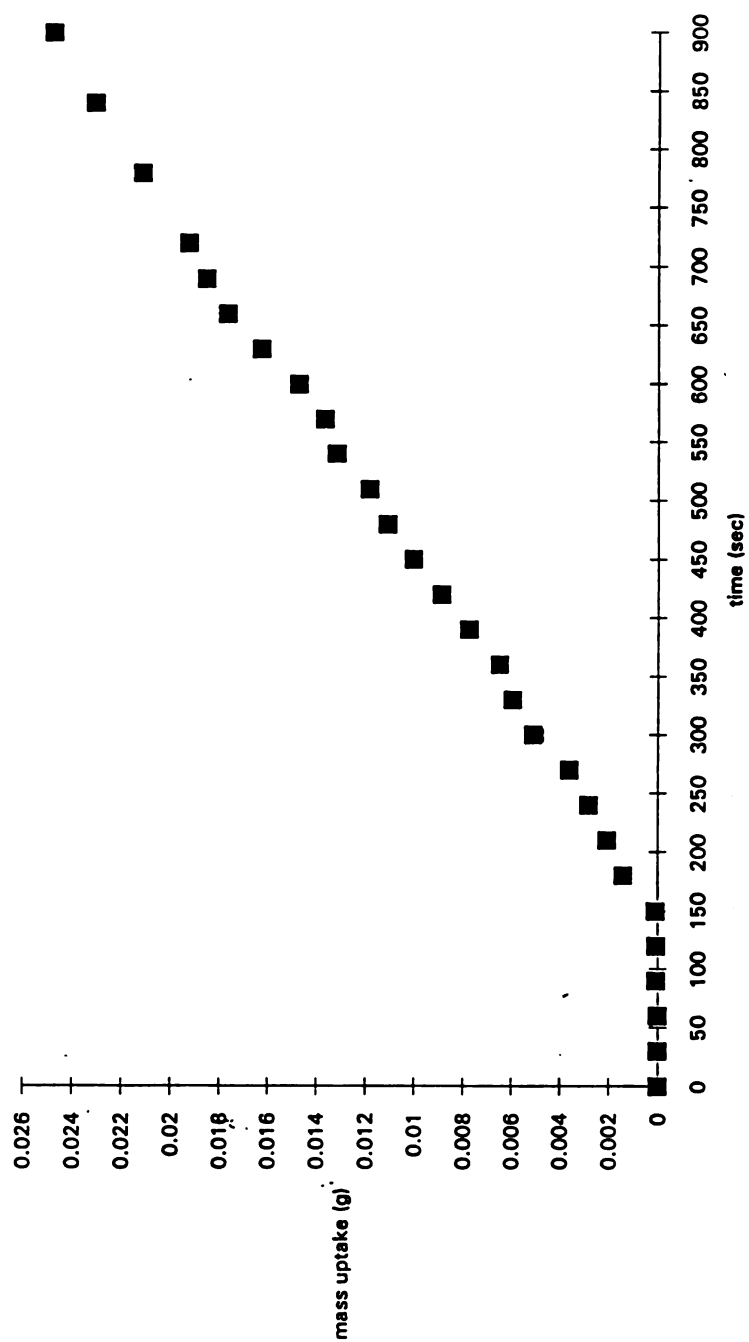


Figure 4.2b - Mass uptake in polypropylene vs. time for run #1

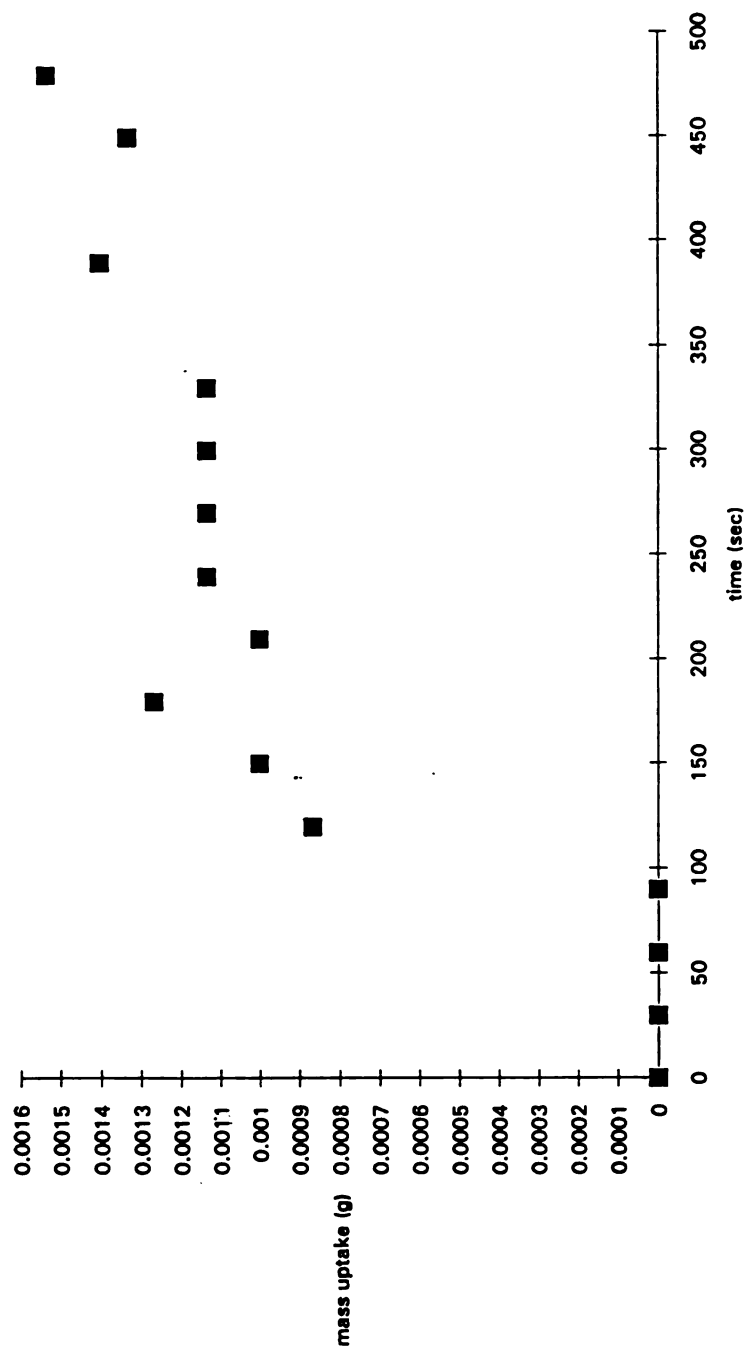


Figure 4.3a - Mass uptake in polystyrene vs. time
for run #2

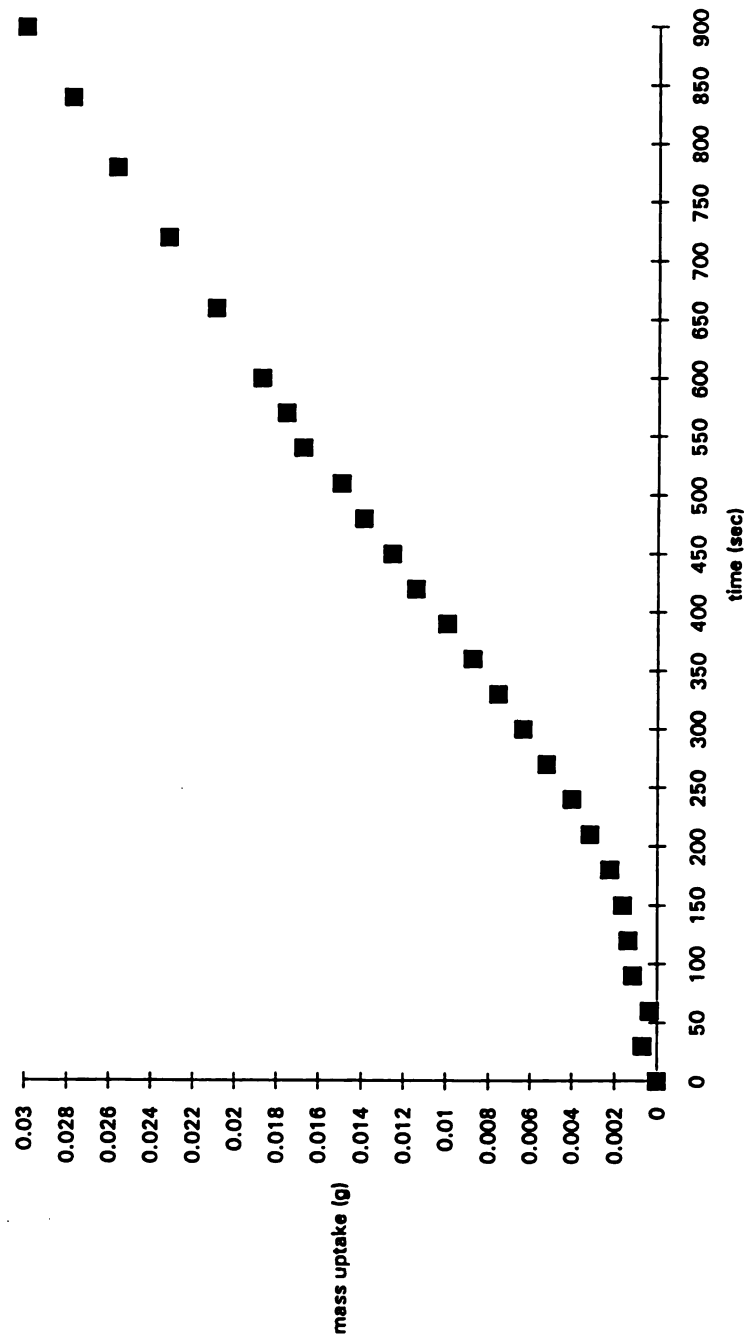


Figure 4.3b - Mass uptake in polypropylene vs. time for run #2

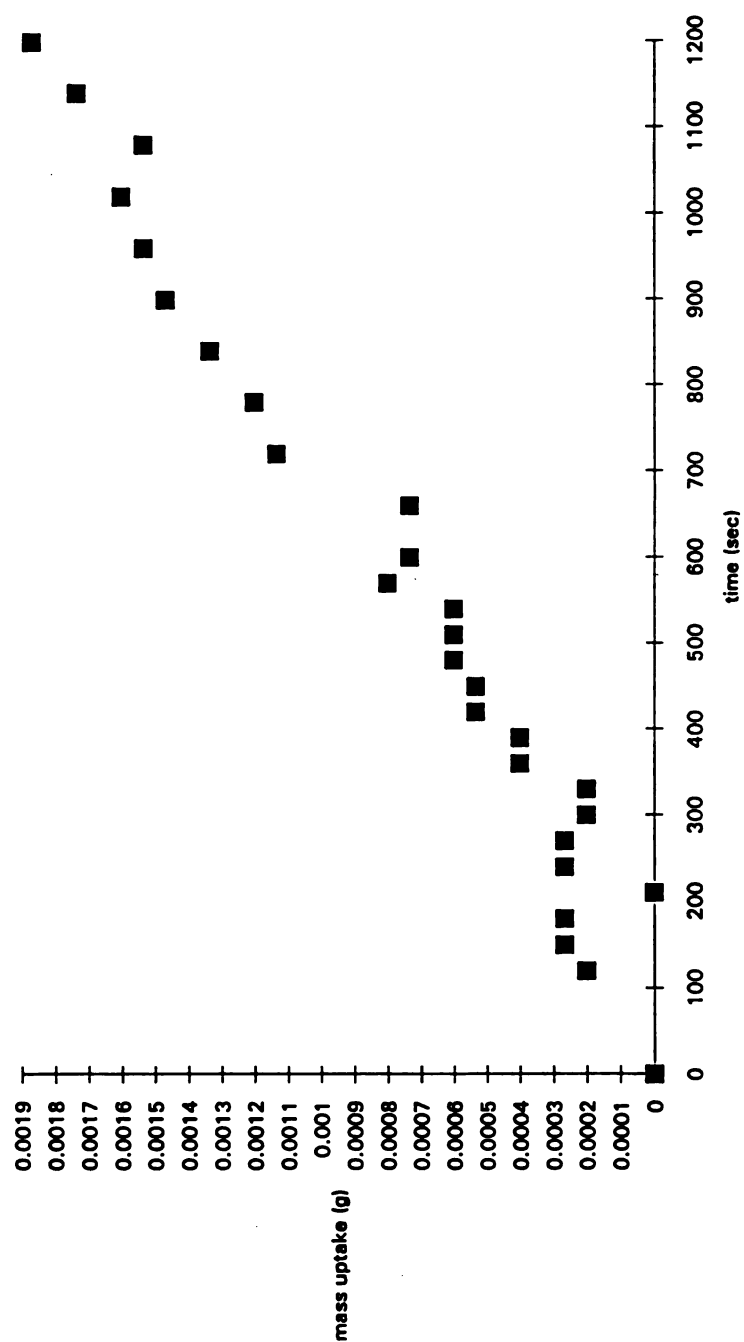


Figure 4.4a - Mass uptake in polystyrene vs. time
for run #3

1

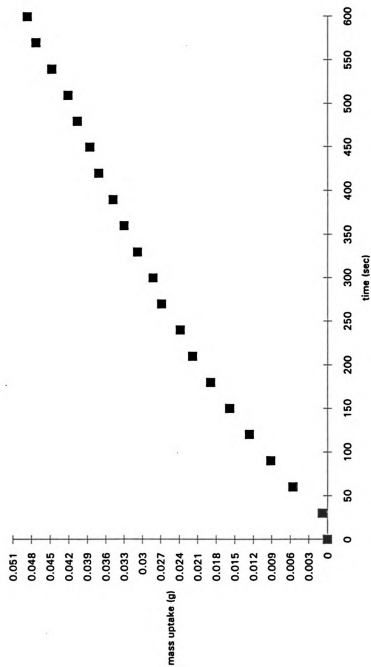


Figure 4.4b - Mass uptake in polypropylene vs. time for run #3

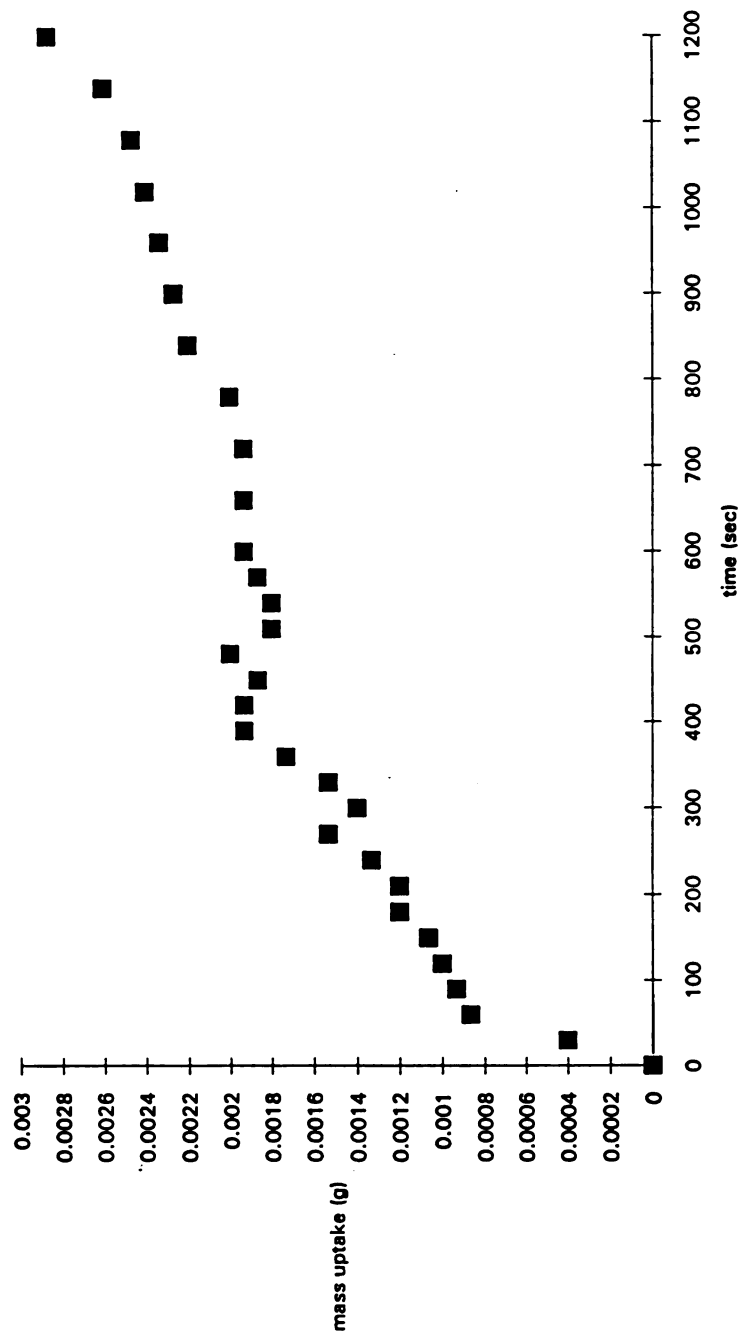


Figure 4.5a - Mass uptake in polystyrene vs. time for run #4

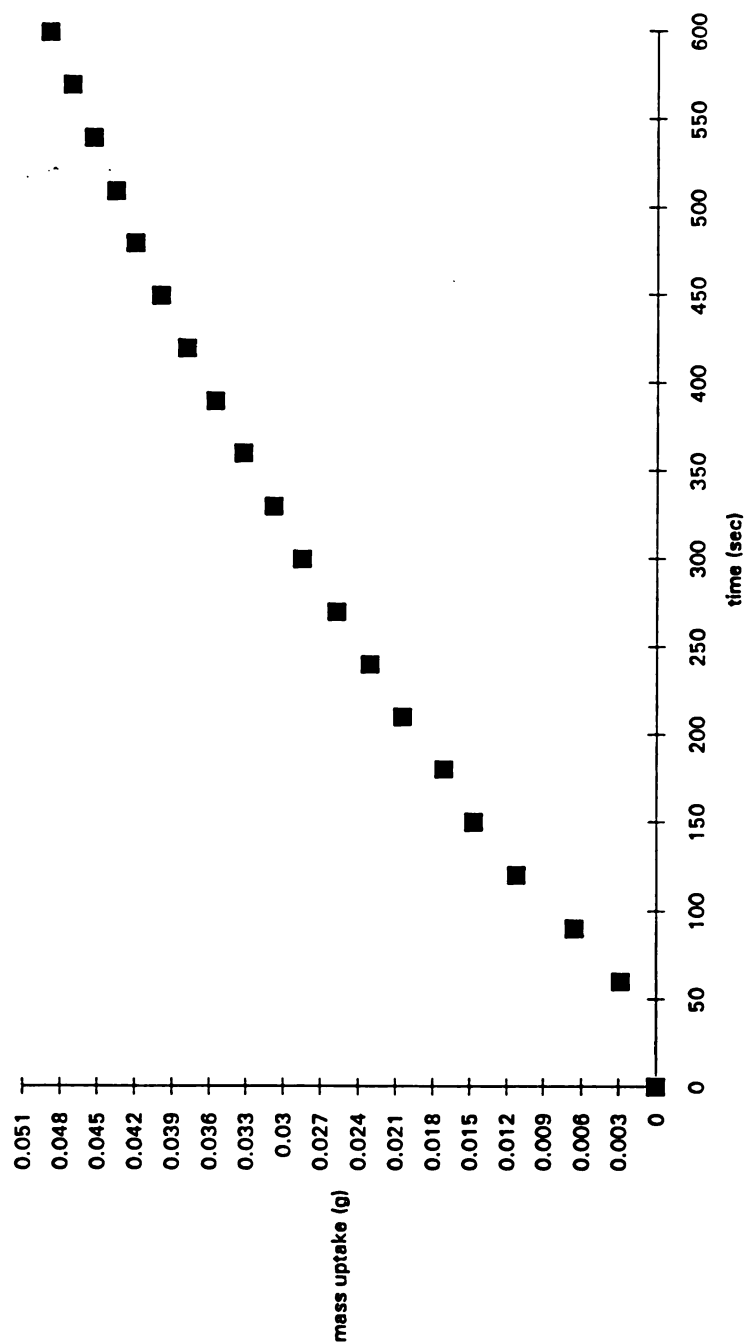


Figure 4.5b - Mass uptake in polypropylene vs. time for run #4

A temperature of 11° C was the lower temperature limit of the water bath, since lower temperatures caused the sample chamber to frost, making sample viewing impossible. It was hoped that runs #1 and #3 would isolate the diffusion process fairly well from the reaction and that runs #2 and #4 would give an indication of the kinetics of the process.

There was a concern about condensation on the polymer film sample during the sulfonation process. To determine if this was the case, a teflon sample was suspended from the quartz spring and the weight gain with time was measured. Teflon was used since SO_3 does not react with the material or diffuse into the material. Therefore, any weight gain on the teflon would be due only to condensation. Teflon samples with the dimensions of 6.75 mm x 5.64 mm, a thickness of 1.46 mm, and a weight of 0.1122 g were suspended in the sample chamber with the same quartz spring, which had a spring constant of 300 mg/450 mm. It was found that after ten minutes there was no weight gain on the teflon. Therefore, it was concluded that condensation on the polymer film was not a factor in this experiment.

Using the weight gain of SO_3 in polystyrene for each sulfonation condition, the concentrations of SO_3 at the gas-solid interface were estimated for each case. It is noted that in Figure 4.2a, 4.3a, 4.4a, and 4.5a, the weight gain in polystyrene appears to have reached a steady state value.

Therefore, the concentration of SO_3 at the interface can be determined by the method described above with great confidence. These values are reported in Table 4.2.

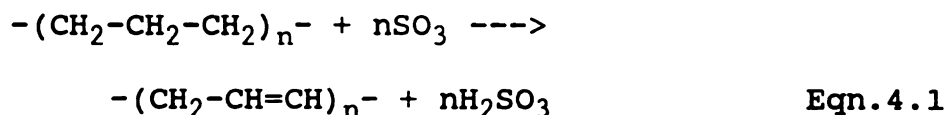
Run #	Percent Mass Uptake	Concentration of SO_3 at the interface (mol/L)
1 - PS	2.74%	1.6485
1 - PP	48.56%	NA
2 - PS	3.30%	1.9946
2 - PP	58.81%	NA
3 - PS	4.09%	2.4287
3 - PP	79.35%	NA
4 - PS	6.44%	2.6022
4 - PP	85.81%	NA

Table 4.2 - Results of experiments with kinetic apparatus

In Figures 4.2b, 4.3b, 4.4b, and 4.5b, for the sulfonation of polypropylene, it is noted that at the end of the experimental run the weight gain within the polymer film has not reached steady state. The sulfonation reaction for polypropylene is much more complicated than that for polystyrene, due mainly to side reactions which occur. Therefore, only crude estimates can be made about the sulfonation of polypropylene in this thesis. It would have been nice to have continued the experiment until steady state conditions were obtained, but the weight gain due to sulfonation was beyond the limit of the quartz spring. Further measurements would have resulted in failure of the spring. A spring constant with a higher spring constant

could have been used, but would not have been sensitive to the weight gain at low times. Therefore, the concentration of SO_3 at the gas-solid interface for polypropylene could not be determined with any accuracy.

An interesting observation in the literature was that some polymer samples changed color from transparent to dark brown during sulfonation.¹¹ This observation was also made when polyethylene samples were sulfonated by this author. It is believed that this color change was due to a side reaction which occurred during sulfonation. This reaction is;



The sulfurous acid produces the color change of the samples and such reactions has been reported by Ihata.¹² The presence of the conjugated bond in the polymer backbone for sulfonated polyethylene and polypropylene has also been supported by FT-IR experiments, as reported in Chapter 6 of this thesis. With long reaction times, the color change will worsen and a layer of the sulfonated film will eventually slough off when rinsed with water. Therefore, a degradation of the polymer surface occurs when these samples are sulfonated. This is an important observation because the color change occurred within one to two minutes of sulfonation at low SO_3 concentrations for polyethylene and

polypropylene. These results are also supported by the high percent mass uptake in polypropylene reported in Table 4.2 and the linear relationship of mass uptake in polypropylene versus time shown in Figure 4.2b, 4.3b, 4.4b, and 4.5b. In run #4, the percent mass uptake for polypropylene was 85% after 8 minutes. It is unlikely that such a high mass uptake is due strictly to the diffusion of SO_3 and the reaction to form sulfonated polymer. It is more likely that the sulfurous acid formed by the side reaction condenses on the film to produce the large weight gain. Therefore, the reaction mechanism for sulfonation in polypropylene is much more complicated than originally expected.

As noted in Table 4.2, the percent mass uptake for the polystyrene after twenty minutes was much smaller than that for polypropylene. There was also no color change for PS upon sulfonation. A possible explanation for this lack of color change is that SO_3 preferentially attacks at the para position of the benzene ring of PS.²⁴ Only at very long sulfonation times is it possible that the SO_3 may attack the polymer backbone. Therefore, the formation of sulfurous acid in the sulfonation of PS is not important in normal exposure times and the side reaction does not need to be included in the mathematical model for polystyrene.

Determination of the Diffusion Coefficients and Rate Constants

To determine the diffusion coefficients and rate constants for the sulfonation process, the mathematical model must predict the experimental curves of mass uptake versus time shown in Figures 4.2a, 4.3a, 4.4a, and 4.5a. An analysis of sulfonation in polypropylene will not be made since there the mechanism is more complicated than expected and therefore requires a more in-depth analysis to be completely understood. It is believed that the side reaction plays an important role in the sulfonation of polypropylene, but a precise determination of the reaction mechanism is beyond the scope of this thesis. Any determination of the diffusion coefficient and reaction rate constant for the sulfonation of polypropylene based upon the data presented above would certainly be false.

To predict the experimental curves, Equations 3.11, 3.14, and 3.15 were solved using the mathematical model. As a reminder, these equations are;

$$\frac{\delta C_{SO_3}}{\delta t} = \frac{\delta}{\delta x} D_{SO_3} \frac{\delta C_{SO_3}}{\delta x} - k C_{SO_3} C_{UP} \quad \text{Eqn. 4.2}$$

$$\frac{\delta C_{UP}}{\delta t} = -k C_{SO_3} C_{UP} \quad \text{Eqn. 4.3}$$

$$\frac{\delta C_{SP}}{\delta t} = +kC_{SO_3}C_{UP} \quad \text{Eqn. 4.4}$$

The sulfonated polymer (SP) was taken to mean polymer which has sulfonic acid groups present, while UP is the unsulfonated polymer.

It should be noted that the diffusion coefficient for sulfur trioxide in equation 4.2 is differentiated with respect to x , which is the distance within the polymer slab. Inclusion of the diffusion coefficient within the derivative is necessary since it is dependent upon concentration. Crank notes that the concentration dependence of the diffusion coefficient of vapors in high-polymer substances is a marked, characteristic feature.¹⁹ A commonly used form of D is;

$$D = D_0 \exp^{aC} \quad \text{Eqn. 4.5}$$

where D_0 is the diffusion coefficient in the limit of zero concentration and a is a variable determined empirically. This form of the diffusion coefficient is used in the model in this thesis, since it provides the best fit for the experimental data.

Using the mathematical model developed in this thesis, a constant diffusion coefficient was first found which fit the curve in Figure 4.2a. Another constant diffusion

coefficient was found which fit the curve in Figure 4.3a. Values for D_0 and a were then chosen which provided diffusion coefficients similar to the constant diffusivities previously determined. The values for D_0 and a which best fit the experimental curves of Figures 4.2a and 4.3a were;

$$\begin{aligned} D_0 &= 1.37 \times 10^{-14} \text{ m}^2/\text{sec} \pm 0.3 \times 10^{-14} \\ a &= 0.41 \pm 0.09 \end{aligned}$$

Remembering that Figures 4.2a and 4.3a are the curves for runs #1 and #2, which were at different temperatures, D_0 also includes whatever temperature effects which may have been present. In other words, the form of D_0 is actually;

$$D_0 = D_{\infty} \exp \frac{-E_a}{RT} \quad \text{Eqn. 4.6}$$

Although the sample chamber temperature was the same for run #3, the experimental data for run #3, as shown in Figure 4.4a, is not characteristic of the other polystyrene experiments. Since there is a question about the reliability of the data shown in Figure 4.4a, it was left out of this analysis.

In the next step of the model, the kinetic rate constant was determined. In Table 4.2, the mass uptake in polystyrene for run #4 was twice as much as for runs #1 and #2 for the same experimental time, indicating that reaction probably played a greater role. Therefore, using the diffusion coefficient determined above, the kinetic rate

constant was determined by fitting the model results to Figure 4.5a. The kinetic rate constant was of the form;

$$k = k_0 \exp \frac{-E_a}{RT} \quad \text{Eqn. 4.7}$$

The kinetic activation energy was estimated to be 10 kcal/mol. Therefore, to determine the rate constant for the sulfonation reaction, k_0 was varied in the model until the theoretical results fit the experimental data. The resulting value for k_0 was;

$$k_0 = 2.22 \text{ L/mol} \pm 0.09$$

This value for k_0 provided reaction rate constants on the order of 7.7×10^{-8} L/mol. A comparison of the theoretical results to the experimental results for polystyrene runs 1, 2, and 4 are given in Figure 4.6, 4.7, and 4.8, respectively. It is noted that in all three figures the reaction is probably complete after about 300 seconds and there is little weight gain due to diffusion at longer times.

To summarize, the determined parameters for the diffusion coefficient and the rate constant are;

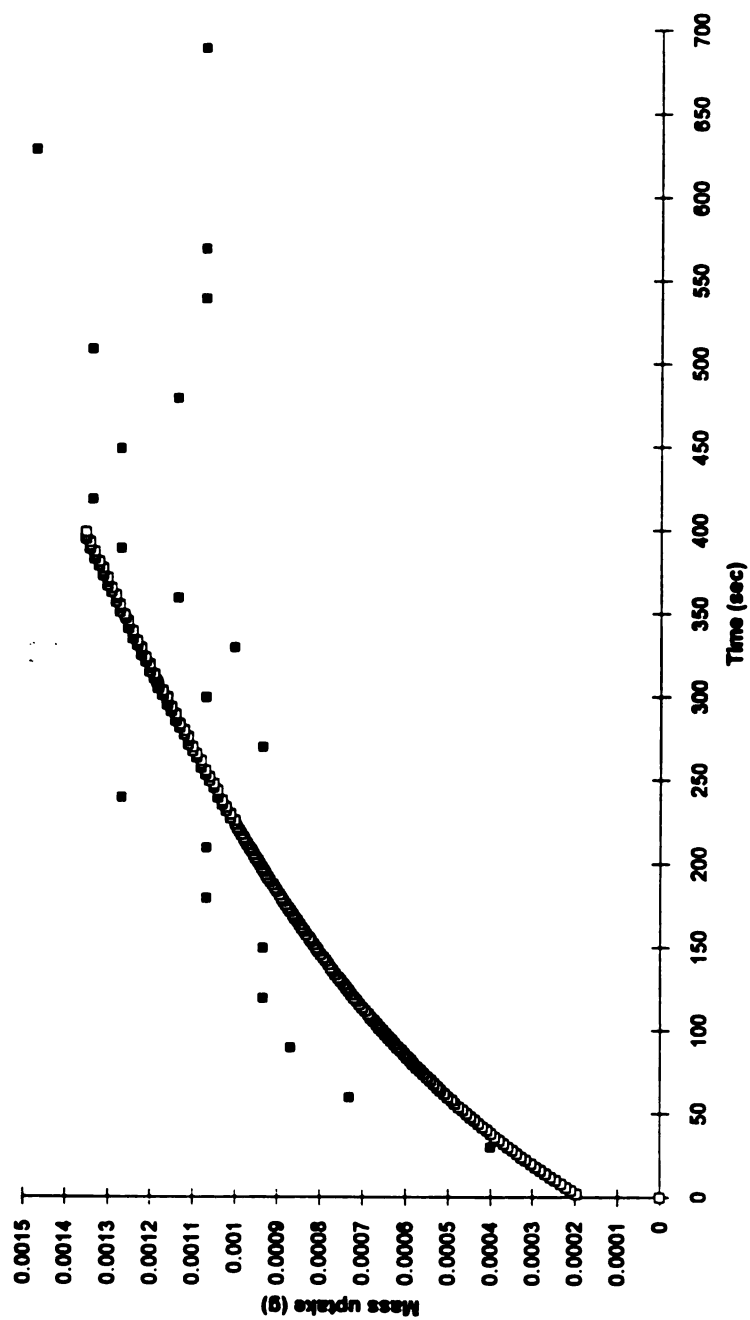


Figure 4.6 - Comparison of model to experimental results
for the sulfonation of polystyrene in run #1

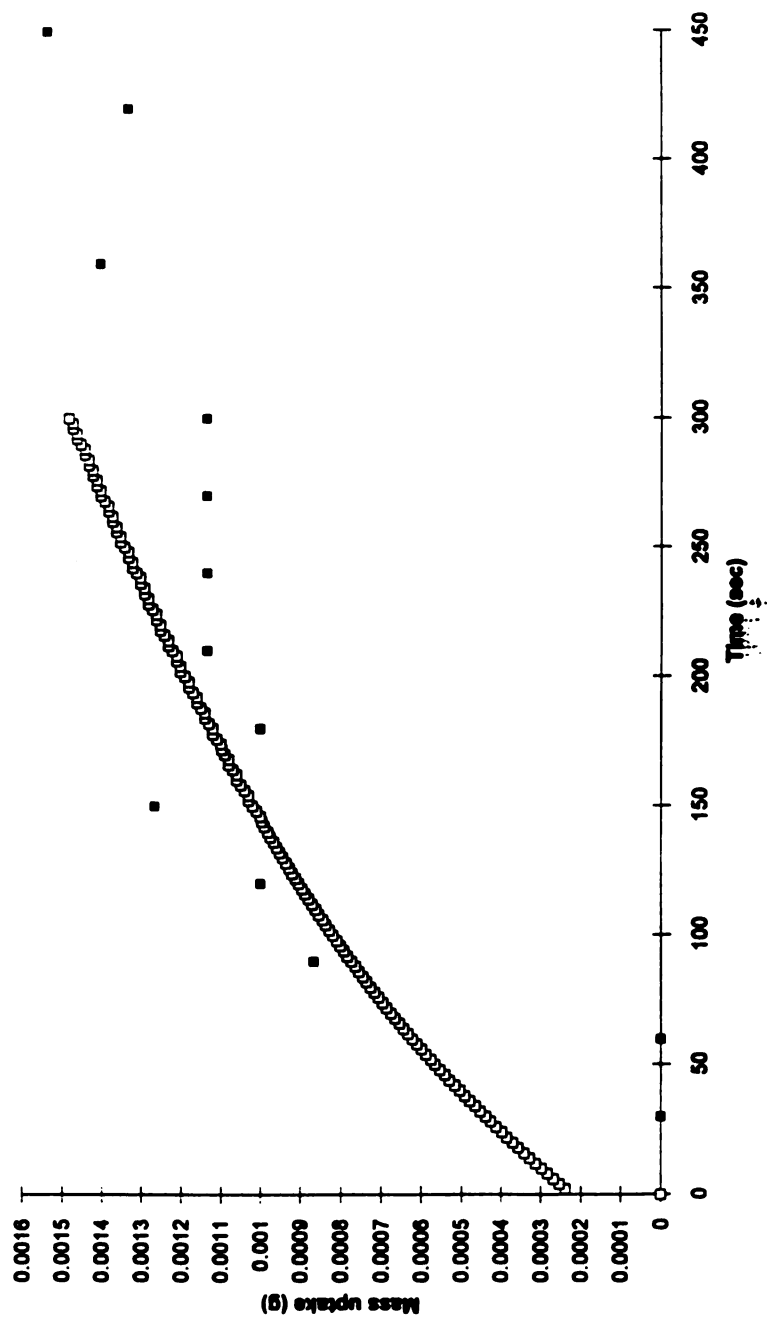


Figure 4.7 - Comparison of model to experimental results for the sulfonation of polystyrene in run #2

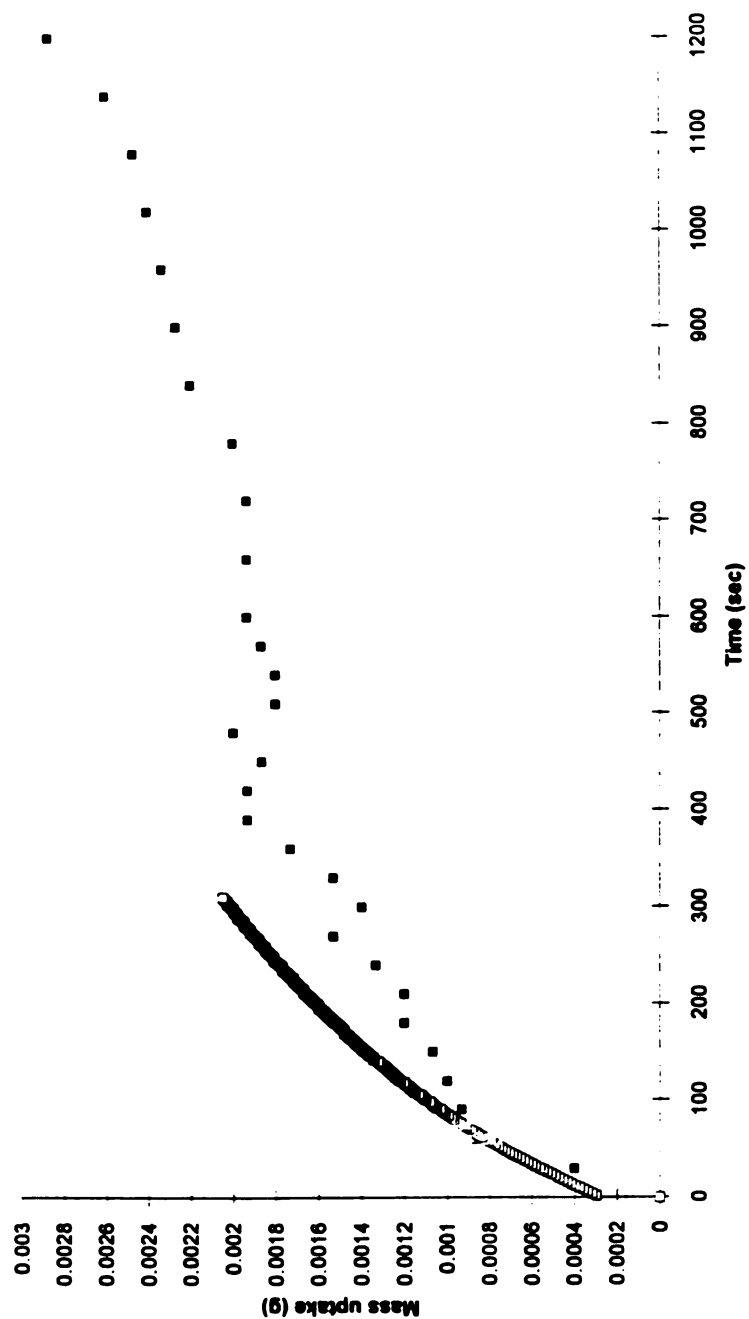


Figure 4.8 - Comparison of model to experimental results for the sulfonation of polystyrene in run #4

D_o	a	k_o
1.37×10^{-14} m^2/sec $\pm 0.3 \times 10^{-14}$	$0.41 \pm$ 0.09	2.22 L/mol ± 0.09

Table 4.3 - Experimentally determined diffusivity and rate constant

To further test the accuracy of the mathematical model, the model was used to predict the results of an Auger analysis line scan across the cross-section of the polystyrene film. The Auger line scan produced a concentration profile for sulfur into the film, indicating the thickness of the sulfonated layer. When the model was used with the parameters determined above, it was found that the predicted thickness of the sulfonated region in the film was greater than that shown by the Auger line scan.

However, the sulfonated polystyrene had been rinsed and neutralized with ammonium hydroxide before the Auger analysis. As noted previously¹⁰, studies had indicated that the sulfur trioxide vapor sulfonated the film in the form of a dimer ($\text{SO}_3\text{SO}_3\text{H}$). Sulfonation by means of the dimer had been observed in the weight gains studies with the quartz spring and cathetometer. Thus, the diffusion coefficient and rate constant reported above are based upon sulfonation by the dimer. However, with water washing and neutralization, it has been indicated that the second SO_3 group is removed, leaving only the sulfonic acid group on the polymer. Therefore, the amount of sulfur trioxide

observed in the Auger line scan is most likely about half the amount observed in the quartz spring studies. Thus, the mathematical model must be modified to provide a fair comparison to the Auger line scan by halving the concentration at the vapor-solid interface. In other words, the boundary condition was modified.

The film analyzed by the Auger line scan had been sulfonated under the conditions of run #2. To predict the results of the line scan with the model, the concentration at the interface, or the boundary condition at $x = 0$, was reduced to half the value reported in Table 4.2. Thus, the boundary condition was;

$$\text{At } x = 0, C_{\text{SO}_3} = 0.9973 \text{ mol/L}$$

This alteration provided a good fit to the Auger line scan data. A comparison with the Auger line scan is given in Figure 4.9. Since the model results fit well with the Auger line scan, it can be concluded that the diffusion and reaction mechanism for the sulfonation of polystyrene has been well characterized.

Further Studies

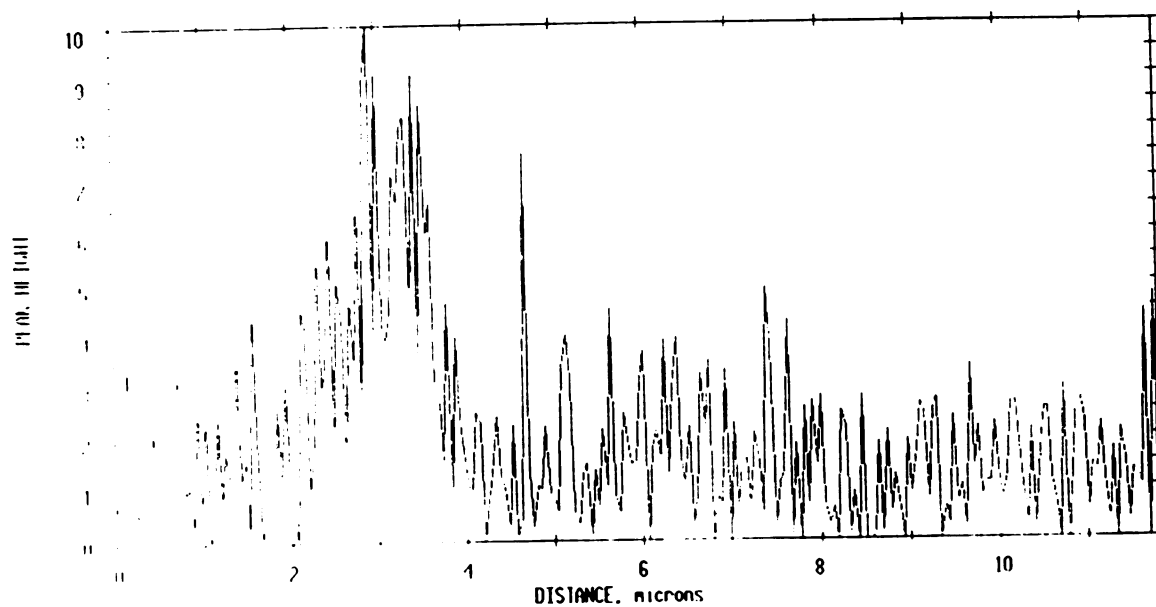
Although the concentration dependent diffusion coefficient and the kinetic rate constant have been estimated for polystyrene in this thesis, it is believed by this author that further studies are required to provide a better understanding of the sulfonation process.

ANALYST: P.C. 12/18/92 EL=51 REG 1 LINE 1 ACO TIME=15.36 MIN.

FILE: ps2/3 Sulfonated ps / 110F

SCALE FACTOR= 0.245 k c/s. OFFSET= 0.000 k c/s

BV=3.00kV BI=0.0000uA



Concentration profile

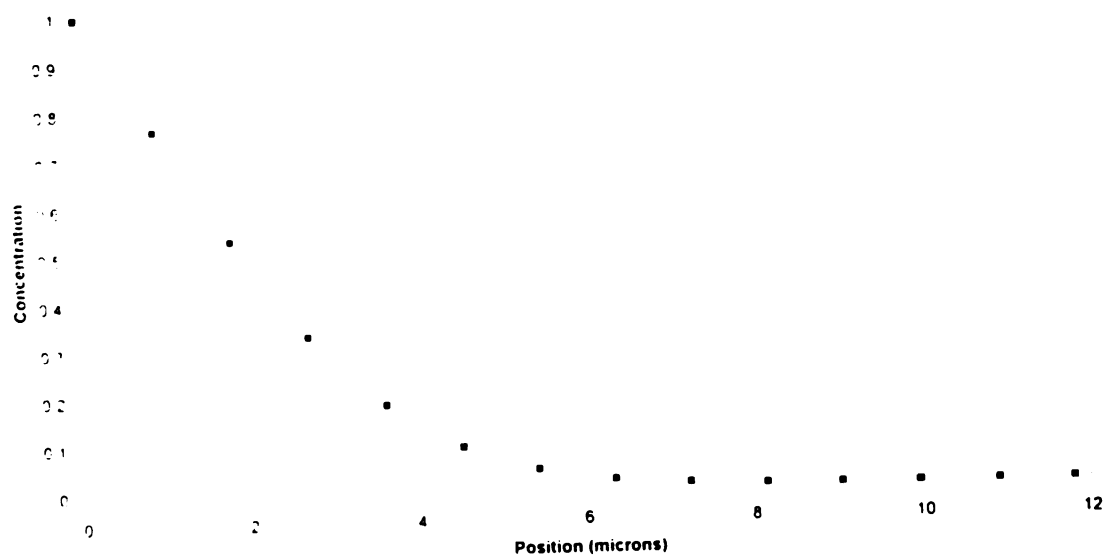


Figure 4.9 - Comparison of model to Auger line scan

Sulfonation was found to be much more complex than originally believed, particularly for polypropylene and HDPE. A more controlled experimental setup is required for sulfonation of those materials, and a more in-depth kinetic study is needed to understand the reaction mechanisms. In particular, the effect of neutralization on the reaction rate expression still needs to be characterized.

It is also believed that the desorption studies are necessary to determine the amount of SO_3 which remains reacted in the polymer. Use of a vacuum would provide a convenient desorption method in a reasonable time frame. Desorption is important since it will remove the second SO_3 group of the dimer and show the actual weight gain within the film after rinsing and neutralization.

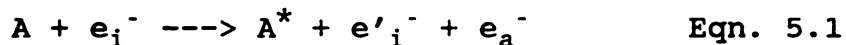
Chapter 5

Analysis of Sulfonated Materials

Auger Analysis

Theory:

Auger electron spectroscopy (AES) is a surface analytical technique which uses an electron beam to excite the sample. Electrons from the electron beam interact with electrons on the surface of the sample being analyzed and force the formation of the electronically excited electron A^* by a transfer of energy to the sample. The mechanism for this process is;



where e_i^- is the incident electron from the source, $e_i'^-$ is the same electron after it has interacted with A and lost energy, and e_a^- is the electron which has been ejected from an inner orbital of A.²⁴ When an electron is ejected from an inner shell, an electron from an outer shell fills the resultant vacancy. Figure 5.1 shows a schematic of this process. The Auger electron, e_a^- , has a kinetic energy E_k which is independent of the energy of the electron which originally created the vacancy in the inner orbital of A. The kinetic energy of the Auger electron is the difference

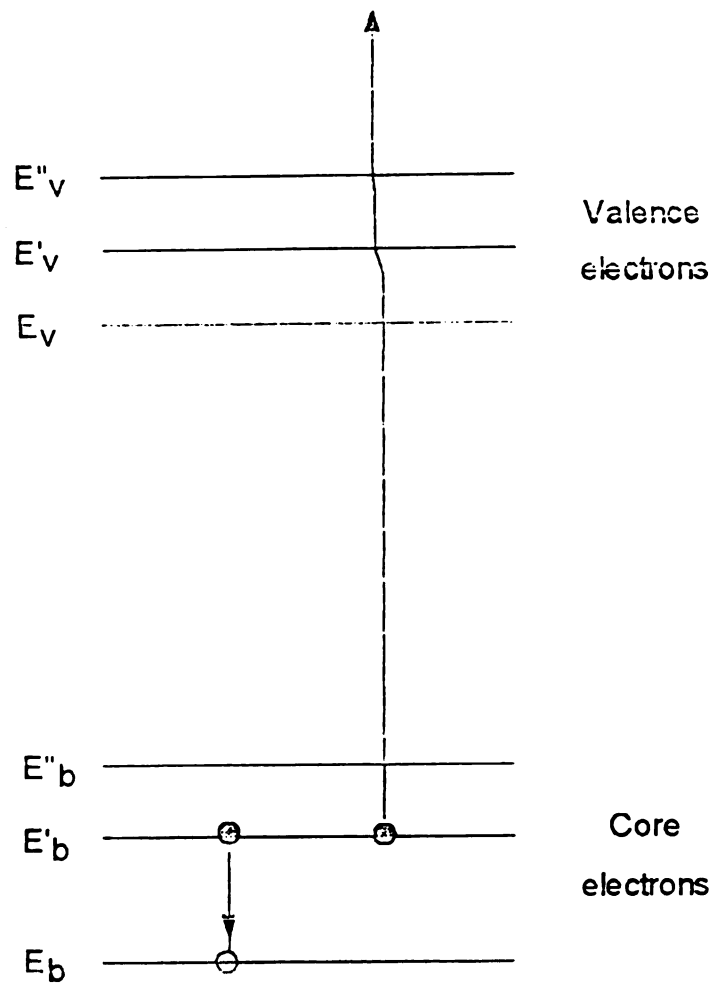


Figure 5.1 - Result of interaction of electron beam
with surface electrons in Auger analysis

between the energy released in the relaxation of the excited electron ($E_b - E_b'$) and the energy required to remove the second electron from its orbital (E_b').²⁴ Therefore;

$$E_k = (E_b - E_b') - (E_b') = E_b - 2E_b' \quad \text{Eqn. 5.2}$$

The electron beam is scattered upon entering the sample and will either back-scatter to the surface or proceed to the inner orbital of the sample. After incident electrons reach the inner orbital of the sample, the resulting Auger electrons lose energy as they travel through the solid by inelastic collisions with bound electrons. However, if Auger electrons are released close to the surface, they can escape with little energy loss and be detected by an electron spectrometer. An Auger spectrum, therefore, produces information on back-scattered electrons and Auger electrons. Output from the spectrometer produce peaks due to the Auger electrons which are superimposed on a background of back-scattered electrons. It is important to note that the Auger electrons are very sensitive to the state of the surface and to its topography.²⁵ Therefore, the sample surface must be as smooth as possible and a careful sample preparation technique is necessary.

The exciting electron beam voltage is chosen to provide an adequate excitation of the Auger electrons and to produce a desired spatial resolution. Usually the beam voltage is

chosen between 5 and 10 eV. However, in this analysis the beam voltage was lowered to reduce charging effects.

Charging is a problem when insulating materials, such as polymers, are analyzed. It results when the total current reaching the specimen is greater than that leaving through back-scattering and Auger electron emission. To overcome charging problems, the sample can be rotated so that the incident beam is at a glancing incidence and the primary beam energy can be reduced. Both of these methods were used in this analysis.

The primary components of the Auger electron spectroscopy system are the electron gun, an electron spectrometer, an electron detector, and an ion gun. The ion gun can be used for specimen cleaning and depth profiling. During specimen cleaning, the ion gun is typically an argon beam which erodes a small area of the specimen.

Sample preparation:

Cross-sections of polymer films which were sulfonated for up to 10 minutes in a gas mixture of up to 10% by volume SO_3 in nitrogen were analyzed by Auger analysis to determine the concentration gradient of SO_3 through the film. Since these films were quite thin, on the order of 50 microns thick, an extensive preparation technique was

necessary before the analysis could be conducted. This technique was developed by Kalantar²⁶ for analysis of the fiber-matrix interphase in polymer composites and is a modification of the standard Transmission Electron Microscopy microtoming technique.²⁷

Sulfonated films were first embedded in an epoxy matrix, which was allowed to cure. The type of epoxy used in the analysis was critical and will be discussed later. There must be enough epoxy around the film to allow the sample block to be trimmed with a razor blade. The epoxy around the sample was trimmed at an angle so that a trapezoid containing the film and a small amount of epoxy stands above the rest of the sample block. An example of how the sample was trimmed is shown in Figure 5.2.

Caution must be taken when trimming the sample block so that the adhesion between the epoxy and the polymer film is not disturbed because a disturbance results in a loss of adhesion between the materials and cause a gap between the film and the epoxy. This prevents trimming the epoxy very close to the film. The purpose of the Auger analysis is to scan the film for sulfur from the side which has been sulfonated to the center of the film. The result is a concentration profile for sulfur across a cross-section of the sulfonated film. If a gap between the epoxy and the

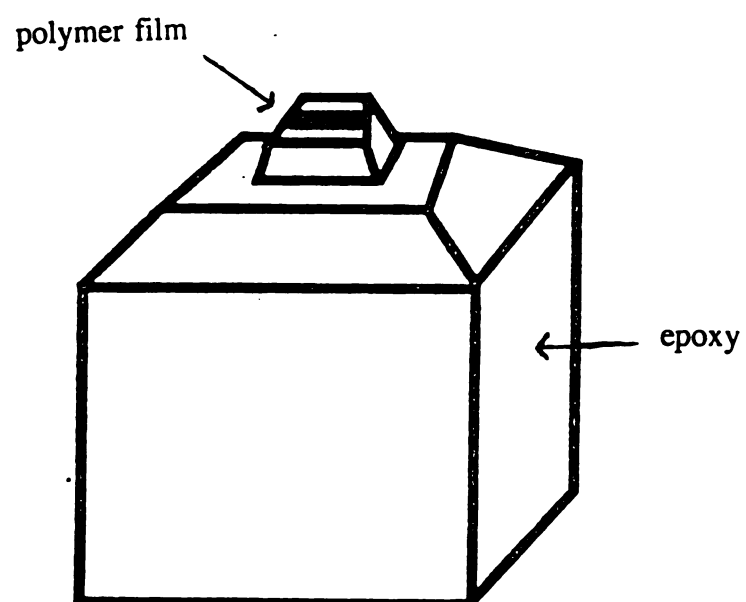


Figure 5.2 - Schematic of how sample block is to be trimmed for Auger analysis

film appears, the sample cannot be analyzed due to charging problems in the area of the gap, which distorts the image on the sulfonated side of the film. The gap distorts the smoothness of the surface and probably causes Auger electrons and backscattered electrons to be released in the gap in various directions, rather than towards the spectrometer.

The sample block was then microtomed using a glass knife to provide a smooth surface. Microtoming will probably be necessary before the sample block is trimmed with the razor blade so that the embedded polymer sample can be easily identified. The purpose of the microtoming procedure is not to section the sample, but to provide a smooth surface for analysis by the electron beam. Once a reasonably smooth surface has been obtained, the sample block is removed from the microtome specimen grip and placed in a gold plasma coater, with the microtomed side facing up. A thick gold coating (approximately 100 nm) is placed upon the sample block to alleviate charging on the sample surface. The gold coated sample block is then returned to the microtome for a final trimming by the glass knife to remove gold from the surface being analyzed and to provide a smooth surface. The surface being analyzed was, however, surrounded by a region of gold, which reduced the problem of charging.

Method Development:

After preparing the sample as described above, the sample was placed on the sample stage in the spectrometer and exposed to a vacuum overnight. Pumping the sample for such a long period of time was necessary to remove volatiles from the sample, such as unreacted curing agent from the epoxy. Once the sample was ready for analysis, the beam voltage was set at 3 eV and the electron gun was turned on. It was immediately apparent on all of the samples which were analyzed that charging was still a problem even though the samples were sputtered with a thick coat of gold and the incident beam was rotated to a 30 degree glancing incidence. Therefore, it was necessary to sputter the sample with argon from the ion beam. This technique carbonized the sample surface, which means that carbon atoms were placed on the surface. These carbon atoms aided the transfer of energy so that the charging effect was significantly reduced. An attempt was made to skip this sputtering step by mixing carbon black with the epoxy as the sample was embedded, but it was found that this method had little effect on the charging problem.

The main problem with sputtering the sample with argon was that not much else other than carbon and sulfur could be detected because Auger electrons for other elements did not possess enough energy to be detected. For example, it would

have been nice to have identified nitrogen to determine if all of the sulfur trioxide groups were with ammonium hydroxide. However, the energy of the nitrogen Auger electrons was so low compared to that of the back-scattered electrons that there was no indication that nitrogen was present. The technique also made it difficult to detect sulfur, but with persistence the sulfur peak was identified.

Upon viewing the sample through the scanning electron microscope (SEM) portion of the Auger electron spectrometer, it was apparent where the bulk of the sulfonic acid groups lay within the sulfonated polymer film. A bright line along the interphase of the film and the epoxy matrix was seen, which contained sulfonic acid groups. This line was brighter than the rest of the sample block due in part to the higher electron density of this region, because of the sulfur and oxygen atoms. Figure 5.3 shows this effect at several magnifications using the scanning electron microscope. The material in the figure is sulfonated polystyrene, which had not been neutralized. Figure 5.3a is the sample at a lower magnification, with the bright region between the unsulfonated film and the epoxy readily apparent. The epoxy is on the left side and the film on the right. Figure 5.3b is the sample at a higher magnification. The thin strip through the center of the sample is the sulfonated region. An interesting observation is this

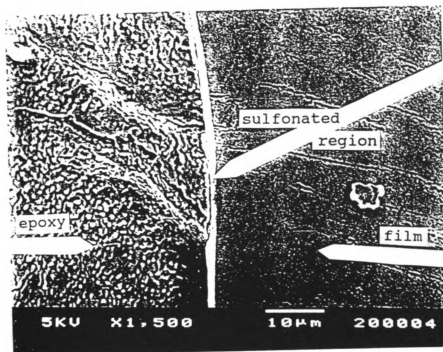


Figure 5.3a - Low magnification of sulfonated polystyrene embedded in epoxy. Epoxy on the left, film on the right.

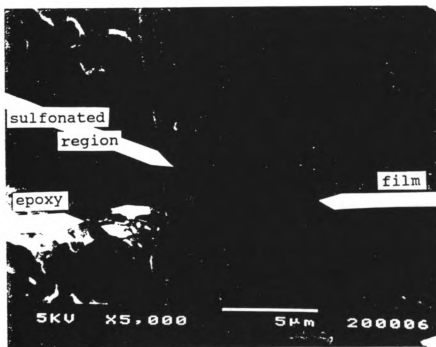


Figure 5.3b - High magnification of sulfonated polystyrene embedded in epoxy.

figure is that there appears to be two interfaces. One is between the epoxy and the sulfonated region of the film and the other is between the sulfonated region and the unsulfonated region of the film. Based upon the scale given in Figure 5.3b, the sulfonated region appears to be about 1.4 microns thick and is a uniform thickness through the sample. Before sulfonation the thickness of the polymer film was about 54 microns, indicating that only a very small layer of the polymer was sulfonated in approximately 10 minutes. Obviously, the surface properties of the sulfonated layer is much different than that of either the epoxy or the bulk polymer film.

A point analysis was conducted with the Auger electron microscope within the bright region of the sample to ensure that sulfur was present. A test acquisition for sulfur was then made to determine the maximum energy of the sulfur Auger electrons compared to the energy of the back-scattered electrons. This test acquisition was done as precisely as possible to get the best signal-to-noise ratio. The sample was then magnified to the appropriate level, which depended upon the thickness of the polymer film. A line scan for sulfur was conducted to get the concentration gradient of sulfur trioxide through the sample.

Figure 5.4a,b, and c show the results of the line scan for sulfur in sulfonated high density polyethylene,

polypropylene, and polystyrene. These samples were unneutralized and embedded in a commercial epoxy. In Figure 5.4a, the interface is at approximately the center of the photograph, with the epoxy on the left side and the polyethylene film on the right. The line scan for sulfur peaks at the interface, with sulfur found on each side of the interface. This result was quite different than the expected gradient which is at a maximum at the interface and decreases at distances toward the center of the film. The only practical explanation for why sulfur is observed in the epoxy is due to diffusion of sulfur trioxide out of the film and into the epoxy.

Figure 5.4b is sulfonated polypropylene embedded in epoxy, with the polymer film on the left side and the epoxy on the right. The peak concentration of sulfur is at the interface of the epoxy and the film, but there is a gradient of sulfur into the epoxy, indicating diffusion of the sulfonic acid groups into the epoxy.

Figure 5.4c is sulfonated polystyrene embedded in epoxy with the film on the left and the epoxy on the right. Again, the sulfonic acid groups appear to be diffusing out of the sample since the peak in the sulfur peak is at the interface of the film and the epoxy. These results were somewhat perplexing, so another commercial epoxy was used, but the same results were obtained. These results suggest

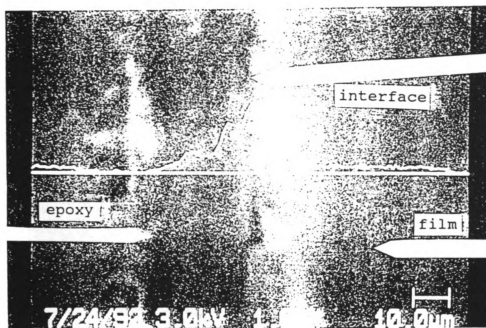


Figure 5.4a - Sulfonated, unneutralized HDPE embedded in epoxy. Epoxy on the left, HDPE film on the right.

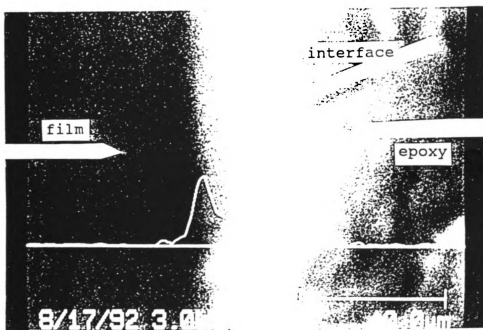


Figure 5.4b - Sulfonated, unneutralized PP in epoxy. Epoxy on the right, film on the left.

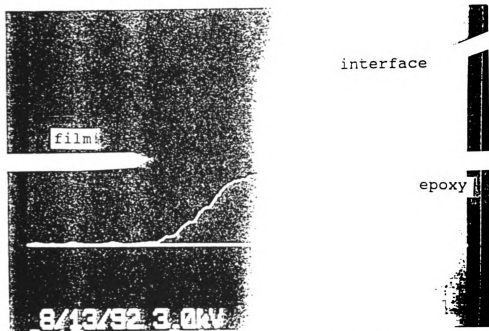


Figure 5.4c - Sulfonated, unneutralized PS embedded in epoxy. Film on the left, epoxy on the right.

that the sulfonic acid groups are not strongly bound to the polymer films, regardless of the type of polymer used. Upon investigation it was found that both of the commercial epoxies used were mercaptan based. Several hypotheses were then made concerning the diffusion of the sulfonic acid groups out of the polymer films. It is possible that the mercaptan groups in the epoxy were attracting the sulfonic acid groups. It is also possible that there was excess amine in the epoxy which attracted the sulfonic acid groups, in the same way as a neutralizing agent such as ammonium hydroxide readily reacts with the sulfonic acid groups.

Both of these hypotheses indicated that the sulfonic acid groups are not strongly bound to the polymer, which is a concern if one considers the applications of the sulfonation technology. It was also suggested that the local temperature of the sample may have risen during the Auger analysis and maybe forced the reverse reaction to occur. This possibility is not likely to be the sole reason for the observations. First, not all of the samples showed beam damage, but all of them showed indications of sulfur trioxide diffusion into the epoxy. Therefore, the rise in the local temperature is not a solid reason for the observations. Secondly, for the reverse reaction to occur, there are indications that it is necessary for water to be present. Since the sample was exposed to a vacuum overnight

to remove the volatiles, including water, it is unlikely that any water was present in the system. Therefore, a different explanation must be given for the diffusion of the sulfonic acid groups out of the polymer film.

Unneutralized, sulfonated samples were next embedded in an acrylic based epoxy to see if the mercaptan groups in the commercial epoxy were causing the problem of the sulfonic acid groups diffusing out of the polymer film. Figure 5.5a, b, c and d show the results of the Auger analysis. Figure 5.5a is sulfonated polypropylene embedded in acrylic, with the entire polypropylene film running through the center of the photograph. Figure 5.5b is the same sample at a higher magnification with the sulfur line scan. The acrylic is on the left side and the film is on the right. Once again, the peak sulfur concentration is at the interface of the acrylic and the film, but there is a concentration gradient to the left of the peak, out of the film and into the acrylic. Figure 5.5c is sulfonated polystyrene embedded in the acrylic, with the polymer film on the left and the acrylic on the right.

The line scan for sulfur is shown in Figure 5.5d. Again, the peak concentration is at the interface, but there is a concentration gradient of sulfur into the acrylic. In this case there are no mercaptan groups present to attract the sulfuric acid groups. Therefore, it appears that the

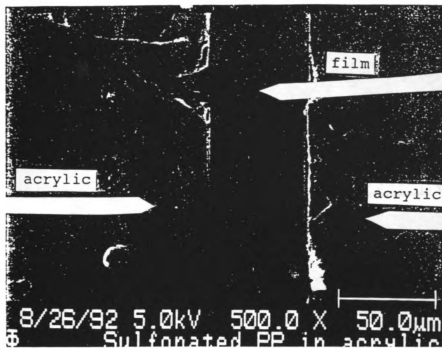


Figure 5.5a - Low magnification of sulfonated, unneutralized PP embedded in acrylic.

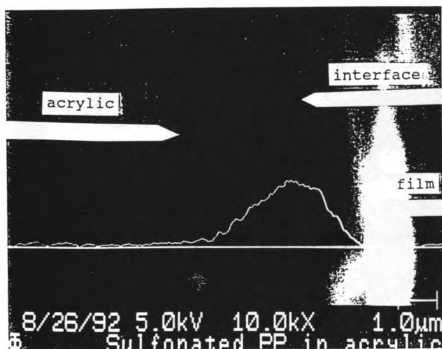


Figure 5.5b - High magnification of sulfonated, unneutralized PP in acrylic. Acrylic on the left, film on the right.

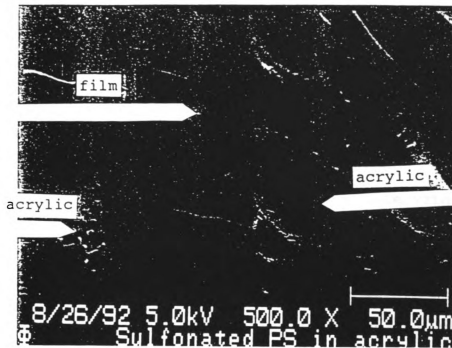


Figure 5.5c - Low magnification of sulfonated, unneutralized PS embedded in acrylic.

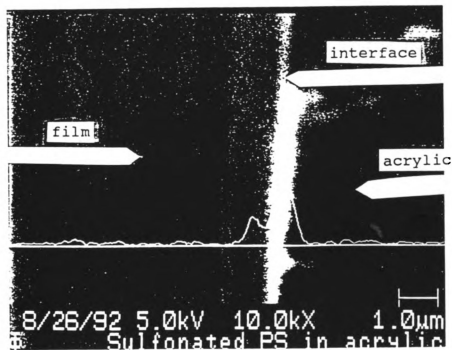


Figure 5.5d - High magnification of sulfonated, unneutralized PS embedded in acrylic. Film on the left, acrylic on the right.

sulfonic acid groups are diffusing out of the film to react with excess amine groups within the epoxy. This is a strong indication that the sulfonic acid groups are not strongly bound to the polymer film. It is clear that the unneutralized sulfonic acid groups are not stable within the polymer film.

The obvious question is whether neutralization of the sulfonic acid groups stabilizes these groups within the polymer film. Polystyrene, HDPE, and polypropylene were all sulfonated and then neutralized in ammonium hydroxide for approximately 24 hours. They were then embedded in the acrylic based epoxy and analyzed in the same manner as the other samples. The results of the line scans for sulfur for these samples are shown in Figure 5.6a, b, c, d, and e. In these cases, the bright area where sulfonation has taken place is still quite clear, but there is a distinct boundary between the epoxy and the polymer film. Figure 5.6a and b are sulfonated and neutralized polypropylene at low and high magnifications, respectively. In Figure 5.6b, with the acrylic on the left and the film on the right, all of the sulfur is contained within the sulfonated region of the film. There are no concentration gradients into the acrylic. However, for this sample, the peak sulfur concentration is not at the acrylic/film interface. Instead, the peak is halfway into the sulfonated region.

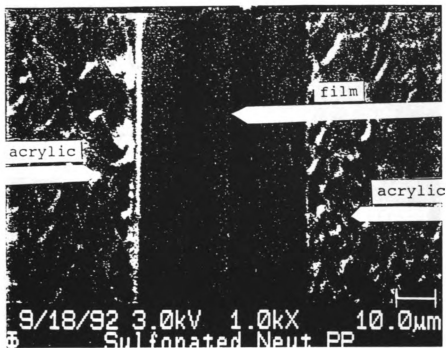


Figure 5.6a - Low magnification of sulfonated, neutralized PP embedded in acrylic.

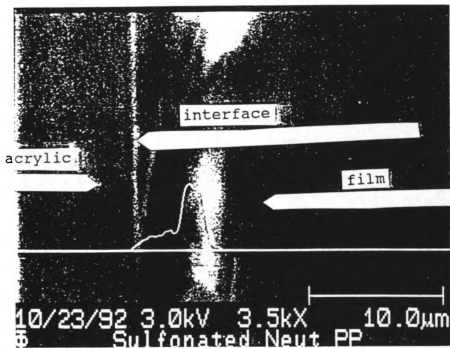


Figure 5.6b - High magnification of sulfonated, neutralized PP in acrylic. Acrylic on the left, film on the right.

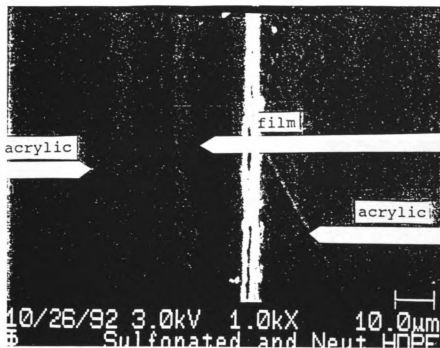


Figure 5.6c - Low magnification of sulfonated, neutralized HDPE embedded in acrylic.

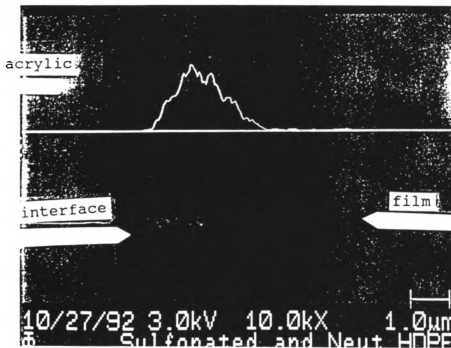


Figure 5.6d - High magnification of sulfonated, neutralized HDPE embedded in acrylic.

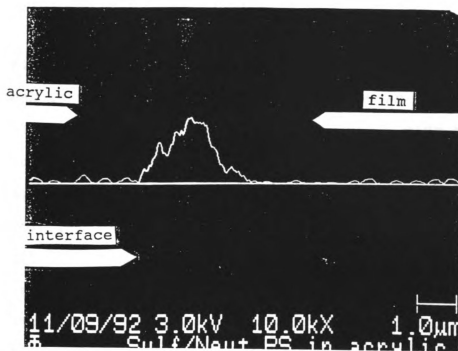


Figure 5.6e - Sulfonated, neutralized PS embedded in acrylic. Acrylic on the left, film on the right.

The initial low concentration region from the interface to the peak concentration can be attributed to an oversulfonation of the film, resulting in the side reaction of carbon double bond formation in the backbone of the polymer. This side reaction was indicated by the change in color of the sample from clear to black. Even though double bond formation occurred, some sulfonic acid groups were still present since the side reaction had not gone to completion.

Figure 5.6c and d show sulfonated and neutralized HDPE. The entire film, embedded in acrylic, is shown in Figure 5.6c. The very bright region on the right side of the film seems to be caused by a separation of the film from the acrylic since attempts at analyzing this region were futile due to charging problems. The interface on the left side appears to have two boundaries, which is the sulfonated region of the film.

Figure 5.6d show the results of the line scan for sulfur in this region. Once again, all of the sulfur was contained within these two boundaries, with no indication of the sulfonic acid groups diffusing out of the sample into the acrylic. The fact that the peak sulfur concentration is not at the interface may be again due to the side reaction which was indicated by a slight color change in the sample.

Figure 5.6e shows sulfonated and neutralized polystyrene. The acrylic is on the left and the film is on the right. Again, all of the sulfonic acid groups are contained within the sulfonated region of the film. In this sample there were indications of beam damage on the sample. However, this beam damage did not result in sulfonic acid groups diffusing out of the sulfonated region, indicating that neutralization fixes the sulfonic acid groups within the film, at least for the short times of the Auger analysis. A reason for the shift in the peak sulfur concentration away from the interface is not understood at this time, since there was no indication of the side reaction by a color change.

These results make clear the importance of neutralization to the sulfonation process. Without neutralization, the sulfonic acid groups can be attracted out of the sulfonated material and the sulfonated layer may eventually be lost. Possible neutralizing agents include ammonia gas and ammonium hydroxide.

The question at this point is whether the bond between the sulfonic acid group and the polymer film actually exists, and if so, how strong is it? According to the CRC Handbook²⁸, the bond strengths of polyatomic molecules, the C-S bond in $C_6H_5CH_2-SCH_3$ is about 59.4 kcal/mol, while the

C-H bond in $\text{H-CH}(\text{CH}_3)\text{CH}_2$ is about 83 kcal/mol. C-H bonds for other molecules are listed, with the lowest bond strength being about 70 kcal/mol. Therefore, it is possible that sulfonic acid groups could be fairly easily removed after reaction and replaced by a hydrogen atom. It is also possible that the sulfonic acid groups may be trapped within the polymer film without reaction occurring and with neutralization the bulky salt group cannot escape from the film. It is believed by the author that there is a bond between the sulfonic acid group and the polymer film, but it is weak and neutralization is absolutely necessary to hold the sulfonic acid group within the film. It may be necessary for long term studies to be conducted to determine if the neutralized groups eventually diffuse out of the polymer film.

FT-IR ANALYSIS

Theory

In infrared spectroscopy, a sample is exposed to infrared radiation, typically in the range of wavenumbers from 4000 to 400 cm^{-1} . The energy corresponding to these wavenumbers (or wavelengths) is not enough to cause electronic transitions, as in Auger spectroscopy, but they can cause groups of atoms to vibrate with respect to the

bonds that connect them. Molecules absorb energy at specific wavelengths because the vibrational transitions of the groups of atoms correspond to distinct energies.¹⁰

For a molecular vibration to be observed in the infrared spectrum, it is necessary that the dipole moment of the bond under consideration be nonzero. A bond with a zero dipole moment does not interact with the electric field of the electromagnetic wave. Therefore, there is no change in the dipole moment and, hence, no absorption of energy.¹⁰

To determine the infrared spectrum, a sample beam passes through a sample cell and a reference beam through the reference cell. A rotating mirror alternately allows light from each of the beams to enter the monochromator. The monochromator allows only one frequency of light to enter the detector at a time. The resulting signal from the detector indicates the difference between the intensity of light in the sample and reference beams.

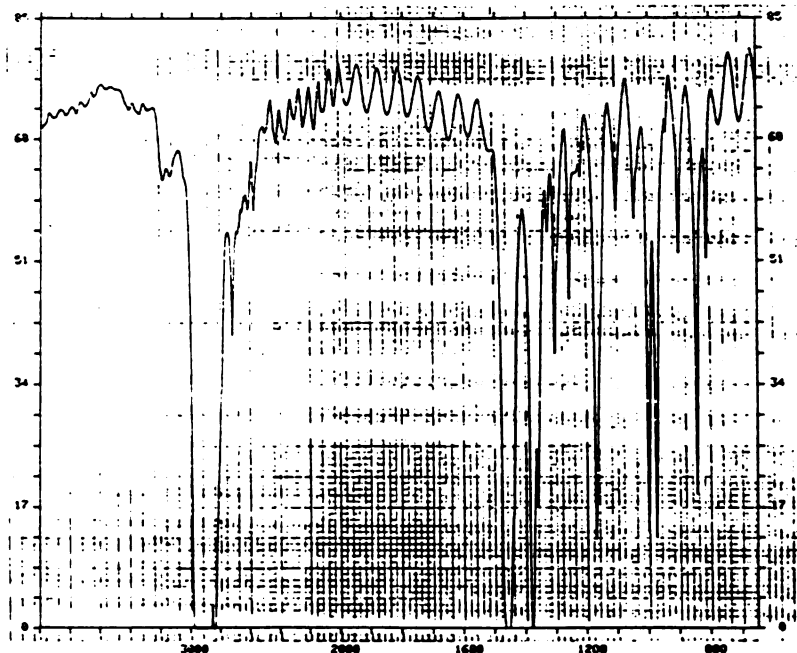
Experimental

As noted previously in this thesis, it was observed that HDPE and polypropylene films turned brown upon sulfonation, while the polystyrene film remained colorless. It was suggested by this author, based upon findings by Ihata, that a side reaction was important HDPE and

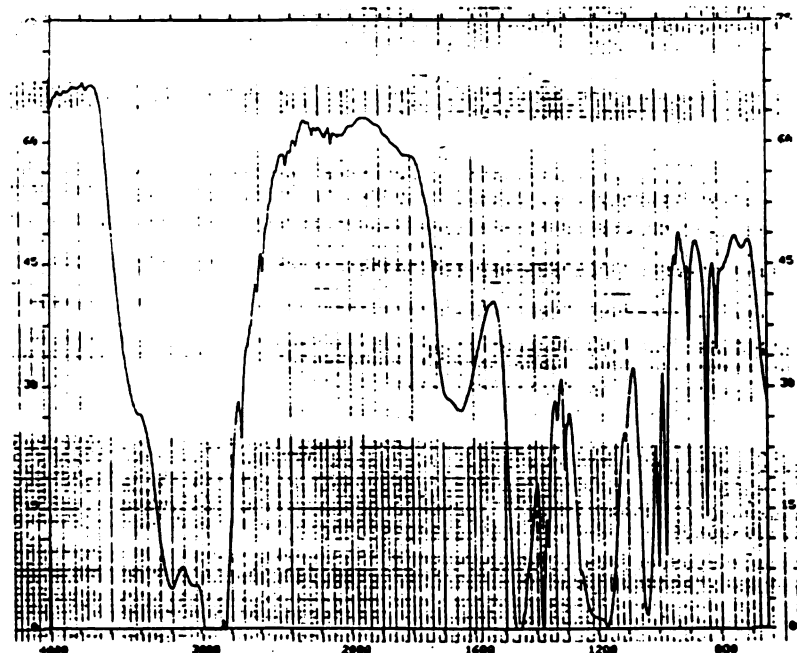
polypropylene which resulted in conjugation in the backbone of the polymer and the release of sulfurous acid. To determine if this hypothesis was in fact true, infrared spectrums were determined for both unsulfonated and sulfonated films.

Figure 5.7 compares the infrared spectrums for unsulfonated and sulfonated polypropylene. The sulfonated polypropylene sample had become dark brown through the reaction process. Sulfonated polypropylene has a much higher absorbance near 3200 cm^{-1} , indicating the presence of the hydroxyl of the sulfonic acid group. What is more interesting, however, is the high absorbance around 1680 cm^{-1} in the sulfonated polypropylene spectrum. In comparison, there is no absorbance at 1680 cm^{-1} in the unsulfonated spectrum. Absorbances at or near 1680 cm^{-1} usually indicative of a carbon double bond. Since the magnitude of the absorbance is large, these spectrum appears to give strong proof of the presence of the side reaction in the sulfonation of polypropylene.

Further proof of the presence of the side reaction is shown in the spectrums of unsulfonated and sulfonated high density polyethylene, given in Figure 5.8. In this figure, there is again strong absorbance at about 3200 cm^{-1} , indicative of the sulfonic acid groups. The strong

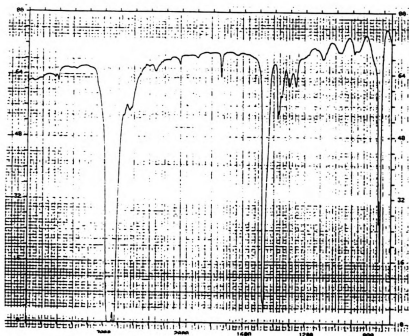


Spectrum of polypropylene film

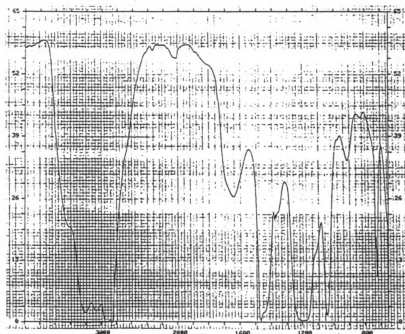


Spectrum of sulfonated polypropylene film

Figure 5.7 - Comparison the IR spectrums of unsulfonated and sulfonated polypropylene



Spectrum of HDPE film



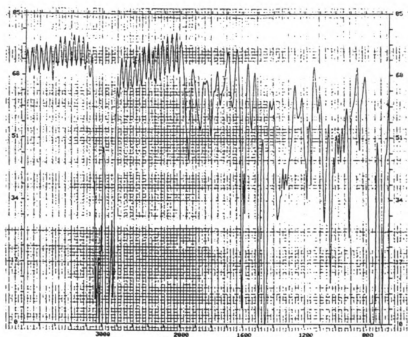
Spectrum of sulfonated HDPE film

Figure 5.8 - Comparison the IR spectra of unsulfonated and sulfonated HDPE

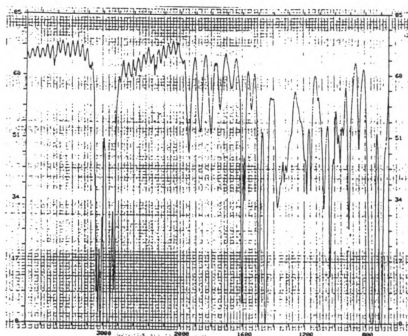
absorbance at 1200 cm^{-1} is also due to the hydroxyl groups. But more important is the -C=C- stretching frequency at 1620 cm^{-1} in the sulfonated HDPE spectrum. Once again it appears that the side reaction is an important factor in the sulfonation of this material. It is noted that the sulfonated sample in this case also had discolored after the reaction.

On the other hand, Figure 5.9 shows the spectrums of unsulfonated and sulfonated polystyrene. These samples had been sulfonated for 20 minutes at the same concentration as polypropylene and HDPE. It was observed in the kinetic experiments that polystyrene was much more difficult to sulfonate than other materials and these spectra are indicative of that. There really is no difference between the spectra. Therefore, it is likely that if the reaction is to occur, it will be the addition of sulfonic acid groups. The probability of the side reaction occurring is quite small.

It is therefore concluded that the hypothesis of the side reaction occurring for polypropylene and HDPE, but not for polystyrene, is valid. It also is likely that the side reaction will occur for other polymers in which the sulfonic acid group attacks the polymer backbone.



Spectrum of polystyrene film



Spectrum of sulfonated polystyrene film

Figure 5.9 - Comparison the IR spectrums of unsulfonated and sulfonated polystyrene

Chapter 6

Liquid Polymerization in a Thin Surface Film

Analysis of an Epoxy-Diamine System:

The system under consideration in this study is an epoxy coated fiber, as in a prepreg, which is embedded in an epoxy/diamine matrix. The matrix consists of a stoichiometric mixture of epoxy and diamine, and the fiber has an epoxy coating. The schematics of the system are shown in Figure 6.1. It is desired to know the characteristics of the diffusion of diamine into the epoxy coating and the subsequent reaction to cure the epoxy coating. In particular, it is hoped that a model of this system will shed light on the interphase region close to the fiber to determine if the epoxy is completely cured to the fiber interface or if a viscous liquid is present close to the fiber which allows movement of the fiber within the matrix. This interphase region will have properties that are different from the cured epoxy in the matrix. To adequately model this system, both the diffusion of the diamine and the kinetics of the reaction must be well understood. With a good characterization of the diffusion and reaction in the interphase region, the properties of this region can be well understood.

The epoxy used in this system is Epon 828 from Shell Chemical Company and the curing agent is metaphenylene

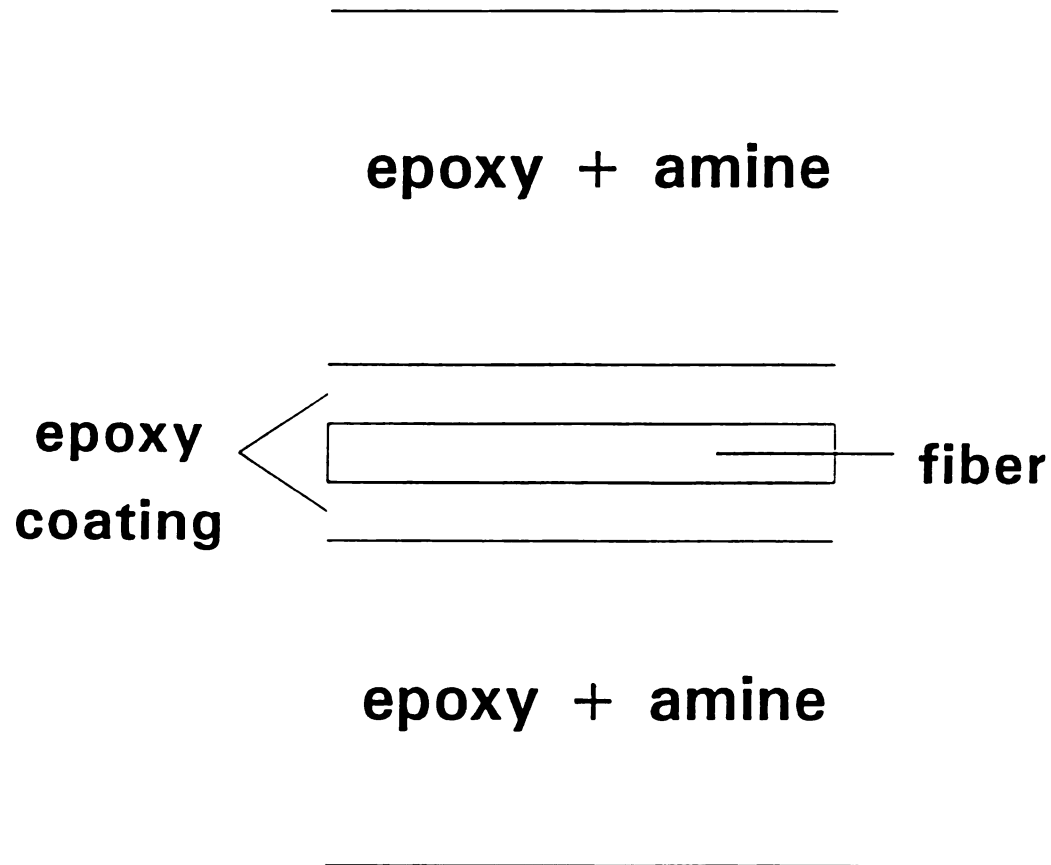


Figure 6.1 - Schematics of epoxy system

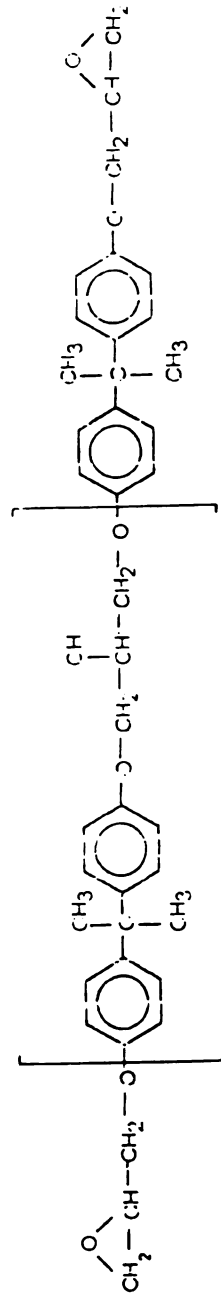
diamine. These species are shown in Figure 6.2. The reactants are mixed in stoichiometric portions and cured at 75° C for two hours, followed by curing at 125° C for two hours.²⁹ The reactions which occur during the cure of the epoxy are shown in Figure 6.3. It should be noted that both the epoxy and the diamine are tetrafunctional. In Figure 6.3, the reactions are divided between primary reactions and secondary reactions. In this study, only the primary reactions are considered because these reactions cause the crosslinking of the epoxy species and, hence, the cure. The secondary reactions do occur but are not as important in this study.

In studies of this system conducted by Rao³⁰, it was found that modification of the curing cycle was necessary since there was incomplete cure due to loss of the curing agent by diffusion at high temperatures. Rao found that a better curing cycle was;

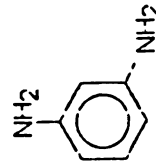
24-36 hr @ room temperature
2 hr @ 75° C
2 hr @ 125° C

In this curing cycle, it has been suggested that the room temperature step allowed some of the reaction to occur and retarded the diffusion process. Rao found that the result was that the loss of curing agent at higher temperatures was reduced by this modification of the curing cycle.

The objective of this study was to include reactant diffusion in a model for the curing process near the fiber



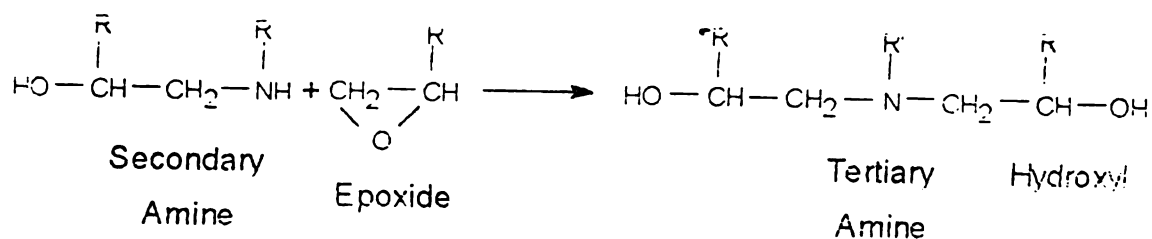
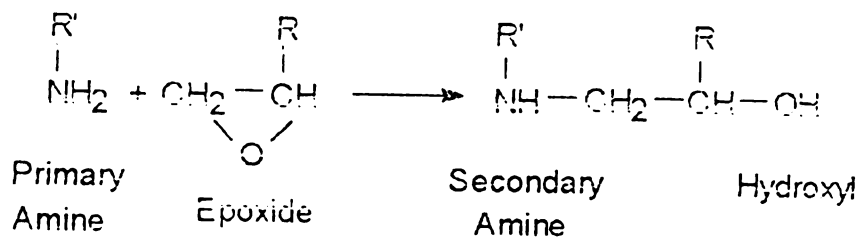
Epon 828



metaphenylene diamine (mPDA)

Figure 6.2 - Reactants in epoxy system

Main Reactions:



Secondary Reactions:

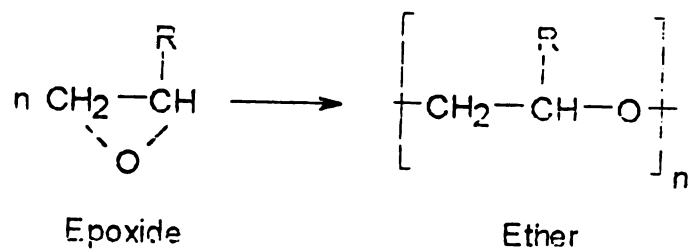
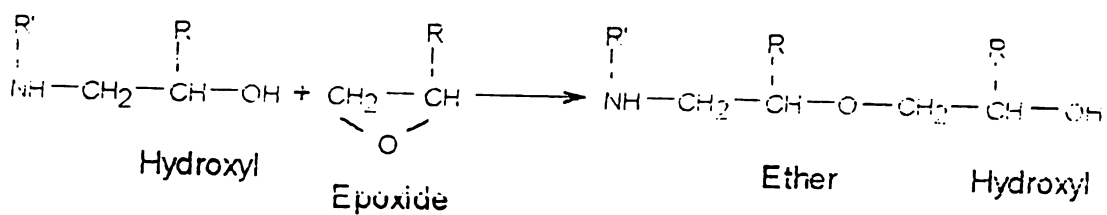


Figure 6.3 - Reactions occurring during the cure of the epoxy

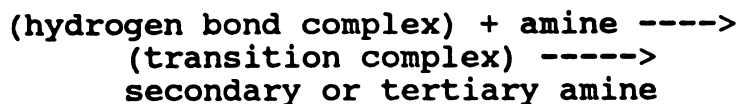
and to determine if the room temperature step is as significant as Rao suggests. Rao found that the reaction was diffusion controlled at temperatures less than 80° C. Therefore, this work focused on the low temperature step of the curing process by providing a concentration-dependent diffusion coefficient for the diamine and rate constants for the reactions which occur at these low temperatures.

Mechanisms for the Epoxy/Diamine Coupling:

There has been quite a bit of discussion in the literature about the kinetics of the epoxy/diamine system, but there is little information about the diffusion of the diamine into the epoxy. Much of the kinetic information results from studies using differential scanning calorimetry (DSC). Use of data from the DSC assumes that the heat evolved is proportional to the extent of reaction. Kenny et. al.³¹ compare their model of the processing of epoxy-based composites with DSC data. Their model describes the rheological behavior of commercial epoxy prepregs and they study the influence of different processing conditions. Tetra-Glycidyl Diamino Diphenyl Methane (TGDDM) and Diamino Diphenyl Sulfone (DDS) were the reactants in their system. They found that the temperature at the center of the laminate quickly reaches that of the external temperature, due to the thermal conductivity of the fibers, and increases due to the imbalance between the rate of heat generation and

the thermal diffusivity of the composite. Other authors, such as Williams et. al.³², have found that for systems with lower conductivity there is less heat transferred to the fiber and the reaction is activated from the epoxy/epoxy-diamine interphase and moves to the epoxy/fiber interface. Neither of the authors discussed a diffusion coefficient for the curing agent but discussed a thermal diffusivity.

Mijovic et. al.³³ discuss a mechanistic modeling of epoxy-amine kinetics. They believe that the etherification reaction between the epoxy and hydroxyl groups often occurs at high temperatures, high degrees of cure, or in the presence of a large excess of epoxy groups. An important assumption in their work was that in the absence of Lewis acid or base type accelerators, and the temperature range used employed in the study (90°-120° C), the etherification and homopolymerization reactions are negligible. They also discuss various reaction routes for the formation of secondary and tertiary amines. By comparing the reaction mechanism for the formation of secondary and tertiary amines used in this thesis with those proposed by Mijovic et. al., it is found that the mechanisms that are used to model the process are the same as those predicted to occur over the majority of the cure cycle. They find that the epoxy groups initially interact with proton donor molecules to form a hydrogen bond complex. The reaction then occurs as;



The transition complex is not explicitly included in the model used in this thesis, but implicitly the reaction to form the transition complex is included in the rate constant for the reaction.

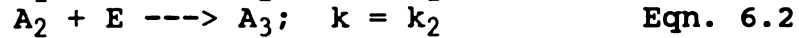
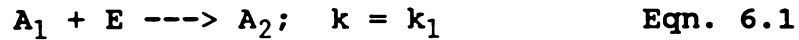
Buckley et. al.³⁴ discuss DGEBA with 2,5-dimethyl 2,5-hexane diamine (DMHDA) as the curing agent and epoxy-cresol-novolac resin. It is suggested that the primary amine hydrogens react with the epoxy at room temperature to form a linear polymer. The secondary amine does not react, however, until the sample is heated due to steric hindrance. These authors also indicate that the apparent activation energies for the curing reactions are similar, regardless of the initial condition. Their results are based upon Fourier transform infrared spectroscopy (FT-IR) and torsional braid analysis (TBA).

Based on the above literature, several assumptions are included in the model used in this thesis. The etherification reaction can be neglected for the temperature range being studied. Also, a complete cure of the system does not occur until the sample has been heated. This is indicated by the fact that the secondary amine does not react until the sample is heated. Thus, the reaction rate constants are temperature dependent. Also, the concentration of the hydrogen bond complex indicated by Mijovic et. al. is

assumed to be the same as the concentration of the epoxy coating the fiber.

Equations Describing the System:

The primary reactions which occur in this system were previously discussed. In short notation they are;



where A_1 indicates the primary amine, A_2 indicates the secondary amine, A_3 indicates the tertiary amine, and E indicates the epoxy. With the above equations, the unsteady state material balances on this system are;

$$\frac{\delta A_1}{\delta t} = \frac{\delta}{\delta x} D_{A_1} \frac{\delta A_1}{\delta x} - k_1 A_1 E \quad \text{Eqn. 6.3}$$

$$\frac{\delta A_2}{\delta t} = \frac{\delta}{\delta x} D_{A_2} \frac{\delta A_2}{\delta x} + k_1 A_1 E - k_2 A_2 E \quad \text{Eqn. 6.4}$$

$$\frac{\delta A_3}{\delta t} = \frac{\delta}{\delta x} D_{A_3} \frac{\delta A_3}{\delta x} + k_2 A_2 E \quad \text{Eqn. 6.5}$$

$$\frac{\delta E}{\delta t} = -k_1 A_1 E - k_2 A_2 E \quad \text{Eqn. 6.6}$$

The diffusion coefficients for the primary, secondary, and tertiary amine groups are concentration dependent and, therefore, included in the partial differential equation. Of great interest is the concentration of the tertiary amine, since the concentration of tertiary amine is directly

proportional to the degree of crosslinking in the system. But, of course, the tertiary amine cannot be formed until the primary and secondary amines are first formed.

The diffusivity of the secondary and tertiary amines are slower than that of the primary amine, based upon molecular weight ratios. Since the epoxy is a large group, its diffusivity can be assumed to be zero and, therefore, the epoxy concentration changes with time due to the reactions only.

Slab geometry is assumed in this model, since the problem is of diffusion in one direction only. Initially there is no diamine present in the system, so the initial conditions are;

$$\begin{aligned} \text{At } t = 0; \quad A_1 &= A_{10} = 0 \\ A_2 &= A_{20} = 0 \\ A_3 &= A_{30} = 0 \\ E &= E_0 \end{aligned} \qquad \text{Eqn. 6.7}$$

where E_0 is found from the molecular weight of the epoxy and the density. The boundary conditions are defined at $x = 0$, which is the epoxy/epoxy-diamine interphase and $x = L$, which is the epoxy/fiber interface. These boundary conditions are;

$$\text{At } x = 0; \quad A_1 = A_{11}$$

At $x = L$;

$$\frac{\delta A_1}{\delta x} = 0$$

$$\frac{\delta A_2}{\delta x} = 0$$

$$\frac{\delta A_3}{\delta x} = 0 \quad \text{Eqn. 6.8}$$

No further boundary conditions can be determined due to the reactions which are occurring. A_{11} can be determined from the molecular weight and the density of the diamine.

Determination of the Solubility of m-xylene in Epoxy:

Although there is a great deal of literature available which describes the kinetics of the epoxy/diamine system, there is very little information about the diffusion coefficient of the diamine into the epoxy. Therefore, to develop an accurate model for this system, the diffusion coefficient of the diamine was experimentally determined. Since the system is complicated because of the reaction which occurs, the diffusion coefficient was estimated by finding the diffusion coefficient of a similar material in the epoxy which does not react. The material used in this study to model the diffusion of the diamine was m-xylene. This probe molecule was assumed to have the same diffusion

volume as the diamine. The structure of this material is shown in Figure 6.4. The difference between the curing agent and m-xylene is that the amine groups are replaced by methyl groups. Therefore, no reaction will occur with the m-xylene, but it is approximately the same size and structure as the curing agent. As noted previously, the diffusivities of the secondary and tertiary amines (D_{A2} and D_{A3}) are lower than that of the primary amine, due to the larger size of these molecules. D_{A2} and D_{A3} were estimated by multiplying the diffusivity of the primary amine by molecular weight ratios of the primary amine to the secondary or tertiary amine. Since diffusivity is known to be dependent upon molecular weight, this is a good assumption.

To determine the diffusivity of m-xylene in the epoxy, an electrobalance was used, which measured the weight gain with time with a chart recorder. The epoxy was placed in a small aluminum pan so that only one side was exposed to the atmosphere. A schematic of the experimental setup is shown in Figure 6.5. Nitrogen was blown over the epoxy sample and the electrobalance measured the weight loss due to volatiles removed by the nitrogen. Once the epoxy sample reached a constant weight, it was ready for exposure to m-xylene. M-xylene was converted to the vapor phase by bubbling nitrogen through the liquid m-xylene. The epoxy sample was then exposed to the vapor mixture of nitrogen and m-xylene

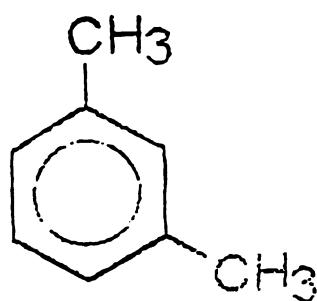


Figure 6.4 - Structure of m-xylene

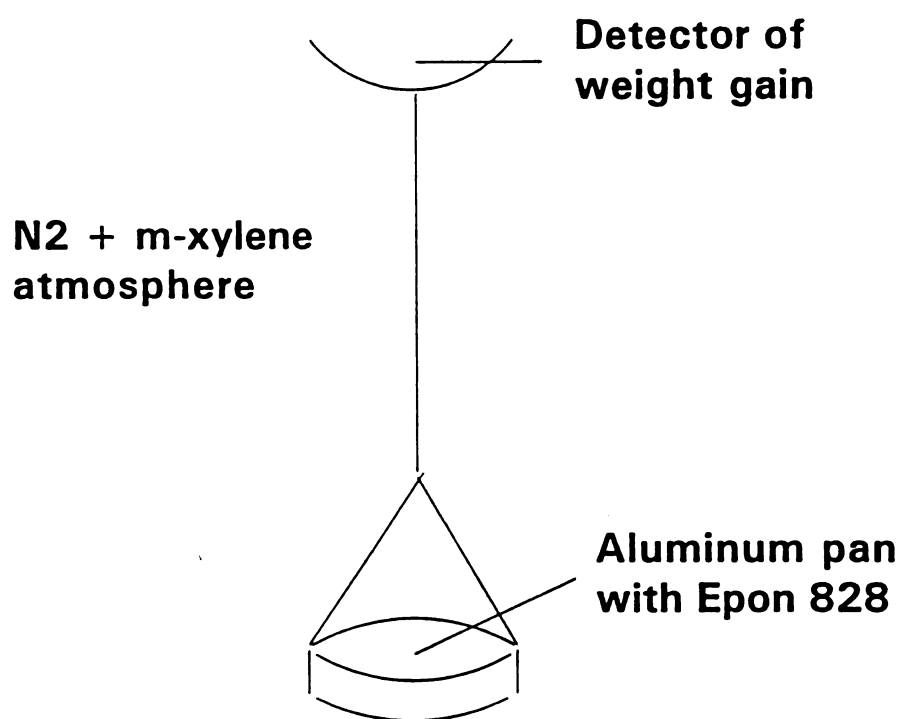


Figure 6.5 - Schematic of electrobalance experiment

and the weight gain with time was measured. The concentration of xylene at the gas-solid interphase was determined using the steady state weight gain in the epoxy sample. This experimentally determined concentration was checked by determination of the concentration through the use of solubility parameters. It is noted that these experiments were conducted at room temperature only and at this point a temperature dependent diffusion coefficient was not determined.

The solubility of xylene in the epoxy was theoretically determined using the Flory-Huggins theory, which describes the entropy of mixing of polymer solutions. The entropy change of mixing of polymer molecules with small solvent molecules is;

$$\Delta S_m = -R(x_1 \ln \phi_1 + x_2 \ln \phi_2) \quad \text{Eqn. 6.9}$$

Combining the entropy change on mixing with the non-ideal heat of mixing, the free energy change on mixing can be found.

$$\frac{\Delta G_m}{RT} = (x_1 \ln \phi_1 + x_2 \ln \phi_2 + x_1 g \phi_2) \quad \text{Eqn. 6.10}$$

In equation 6.10, g is the polymer-solvent interaction parameter. By differentiating equation 6.10 by n_1 , the number of moles of solvent, the reduced partial molar Gibbs

free energy of mixing for the solvent can be obtained, which then produces the solvent activity.³⁷

$$\frac{\Delta G_m}{RT} = \ln a_1 = \ln \phi_1 + \phi_2 + \chi \phi_2^2 \quad \text{Eqn. 6.11}$$

In equation 6.11, χ is the interaction parameter and the ϕ 's represent the volume fractions. Once the solvent activity is determined, the solubility of xylene can be easily determined.

To solve for the solvent activity, the interaction parameter must first be found. A useful equation to determine the interaction parameter is;

$$\chi = 0.34 + \frac{V_1}{RT} (\delta_1 - \delta_2)^2 \quad \text{Eqn. 6.12}$$

From the literature, it is known that the solubility parameter of m-xylene is $8.8 \text{ (cal/cm}^3\text{)}^{0.5}$ and its molar volume is 0.1229 L/mol .²⁸ The solubility parameter of Epon 828 epoxy is approximately $8.5 \text{ (cal/cm}^3\text{)}^{0.5}$.³⁸ Therefore, based upon equation 6.12, the interaction parameter is 0.3587. The volume fractions are determined from the molar volumes of each of the components and are;

$$\begin{aligned} \theta_1 &= 0.2717 \\ \theta_2 &= 0.7283 \end{aligned}$$

Therefore, the solvent activity was determined to be 0.6808.

The solvent activity can be considered an effective mole fraction, such that;

$$a_1 = n(\text{xylene})/n(\text{epoxy})$$

Since the mass of the epoxy was known to be approximately 0.085 g, the moles of epoxy were determined to be 2.219×10^{-4} moles. Multiplying this number by the solvent activity gives 1.511×10^{-4} moles of xylene. The volume of the epoxy was found to be 7.398×10^{-5} L, so the solubility of xylene in the epoxy was 2.0424 moles/L. This is the theoretical solubility of xylene in the epoxy.

The electrobalance experiment was run until the weight gain reached steady state, which means that there was no more weight gain with exposure to the vapor. Figures 6.6a, b, and c show the results of three electrobalance experiments. Runs #1 and #2 were done at the same conditions, showing that the experiment was reproducible. Run #3 was done at a lower concentration of xylene vapor in the system.

The concentration of xylene in the system could be checked with the theoretical value of 2.0424 mol/L by using the steady state weight gain found using the electrobalance. The concentration is the weight gain of xylene at steady state, divided by the molecular weight of xylene, divided by the volume of the epoxy sample. Since the volume of the epoxy sample was greater after exposure to xylene, due to

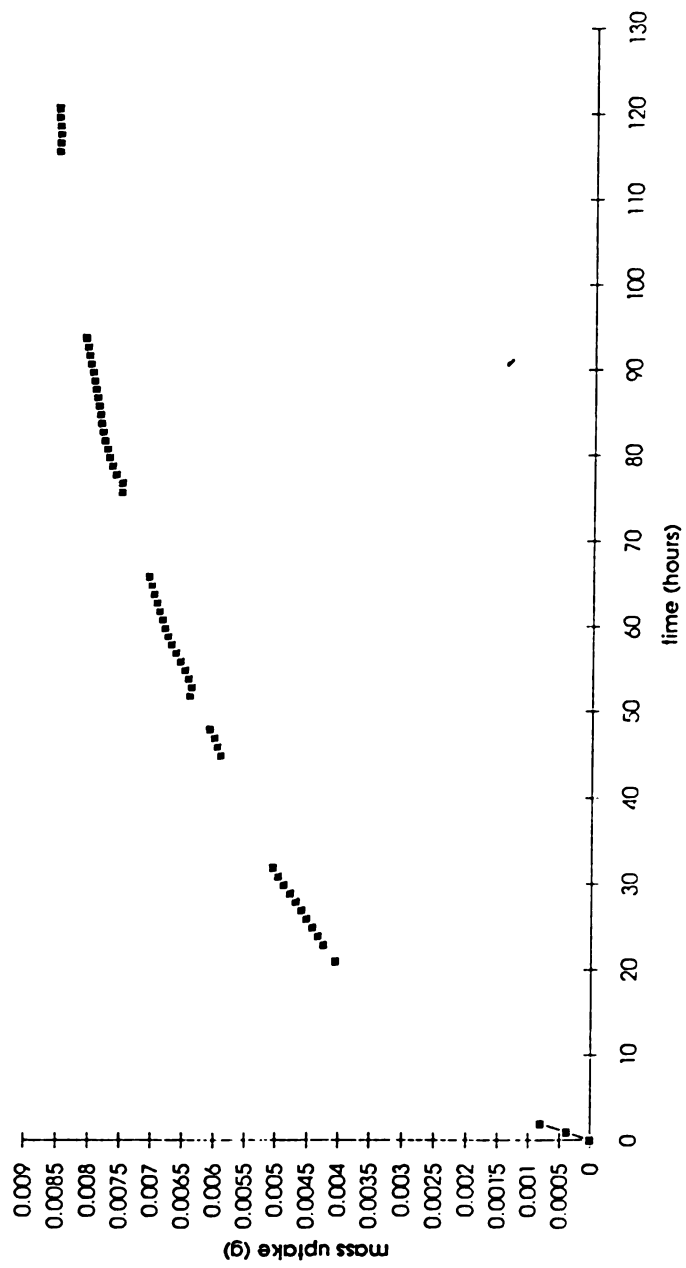


Figure 6.6a - Weight gain with time for run #1
using the electrobalance

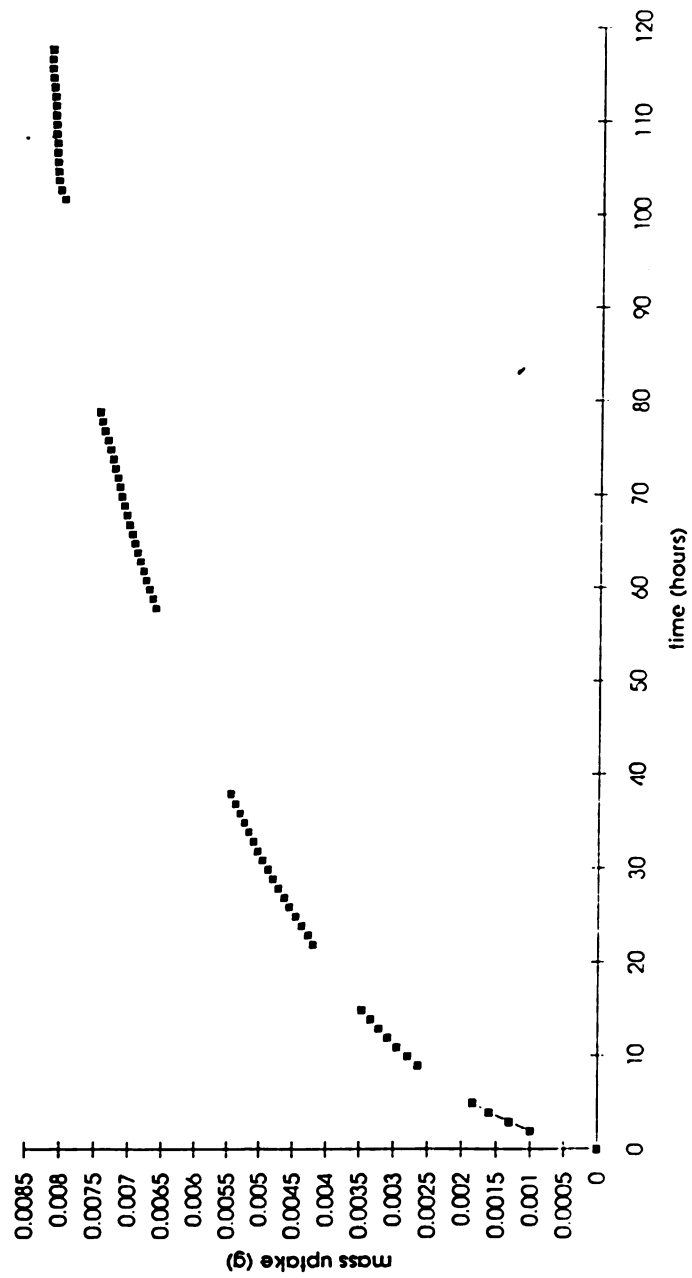


Figure 6.6b - Weight gain with time for run #2
using the electrobalance

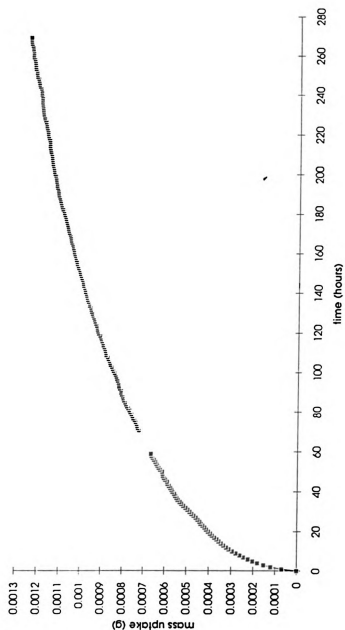


Figure 6.6c - Weight gain with time for run #3 using the electrobalance

the added xylene within the epoxy, the epoxy sample volume was;

$$V \text{ (epoxy)} = \frac{\text{mass epoxy}}{\text{density epoxy}} + \frac{\text{mass xylene}}{\text{density xylene}}$$

The initial mass of the epoxy sample was 0.085 g, the density of the epoxy was 1.1625 g/cm³, and the density of m-xylene was 0.8642 g/cm³. The mass of xylene was taken as the maximum weight gain as indicated by the electrobalance. Experimentally determined concentrations of xylene are given in Table 6.1.

Run #	Maximum weight gain of xylene (g)	Concentration of xylene (mol/L)
1	0.008502	0.9653
2	0.008150	0.9298
3	0.001235	0.1593

Table 6.1: Experimental solubility of xylene in epoxy

The concentrations reported in Table 6.1 are actually the experimental solubilities of xylene in the epoxy. These values are less than the theoretical solubility of 2.0424 mol/L. Theoretical solubilities typically have errors of 30-50% of the actual solubility, and therefore, are not very reliable. Thus, in modelling this system, the experimentally determined solubilities were used as the boundary condition at $x = 0$ to determine the diffusion coefficient of m-xylene in the epoxy, due to the greater confidence in these values.

Determination of the Diffusion Coefficient:

The shape of these curves shown in Figures 6.6a, b, and c are typical for a system which is diffusion controlled. To determine the form of the diffusion coefficient of m-xylene into the epoxy, the following partial differential equation was solved numerically;

$$\frac{\partial C_x}{\partial t} = \frac{\partial}{\partial x} D_{C_x} \frac{\partial C_x}{\partial x} \quad \text{Eqn. 6.13}$$

where C_x is the concentration of xylene. The method used to solve this equation is the same as that used to solve Equation 6.3, except that no reaction occurs in this process. The output of the model was concentration of xylene along length increments of the cross section of the film. To determine the mass uptake from the model results, the concentrations of xylene across the depth of the sample were averaged and multiplied by the volume of the epoxy sample and the molecular weight of m-xylene. The volume of the epoxy sample was the sum of the volume of epoxy and the m-xylene which has diffused into the epoxy.

Initially, a constant diffusion coefficient was used to fit the experimental data. Although a constant diffusion coefficient would fit the experimental curves at low times, the difference was too great at long times. Also, the constant diffusion coefficient which fit the data at low times for run #3 was $2 \times 10^{-12} \text{ m}^2/\text{sec}$, while the diffusivity

for run #2 was $6.3 \times 10^{-12} \text{ m}^2/\text{sec}$. Comparisons of the constant diffusivity to the experimental results are shown in Figure 6.7a and b, which show how the constant diffusion coefficients fit the data well until high times. Since the diffusivities were different for runs with different concentrations, however, it was concluded that diffusion coefficient was dependent upon concentration.

A common form of the concentration-dependent diffusivity has an exponential dependency upon concentration. This form of this diffusivity is;

$$D = D_0 e^{ac} \quad \text{Eqn. 6.14}$$

where D_0 is the diffusion coefficient in the limit of zero concentration and a is an arbitrary constant. Since the constant diffusion coefficients which fit the data at low concentrations were known, it was necessary to determine the constants of the above equation which gave approximately the same diffusion coefficients at low xylene concentrations. After several attempts to fit the data, it was found that the best fit for both runs were found with;

$$D_0 = 1.5 \times 10^{-12} \text{ m}^2/\text{sec} \pm 0.4 \times 10^{-12}$$

$$a = 1.69 \pm 0.2$$

A comparison of the exponential diffusion coefficient with the constant diffusivity and the experimental results are shown in Figure 6.7a and b. These figures shows that the

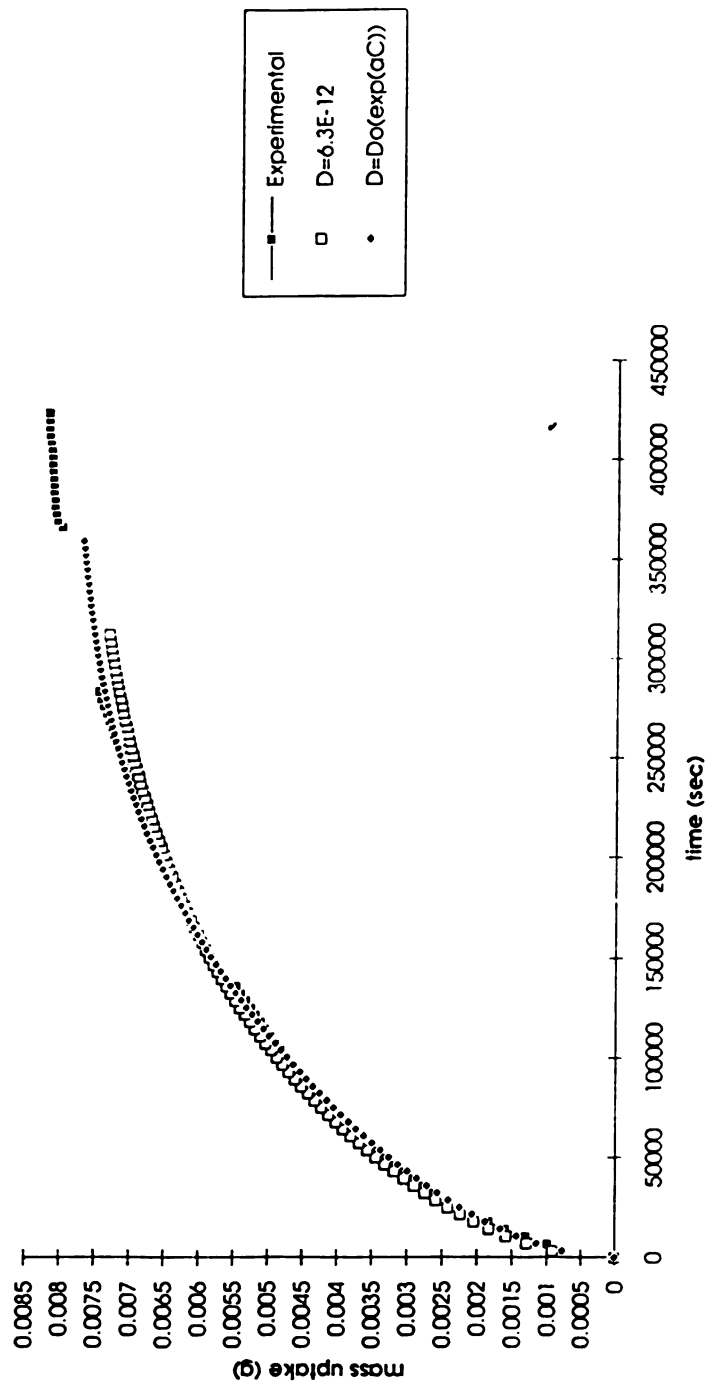


Figure 6.7a - Comparison of experimental results to model results for run #1

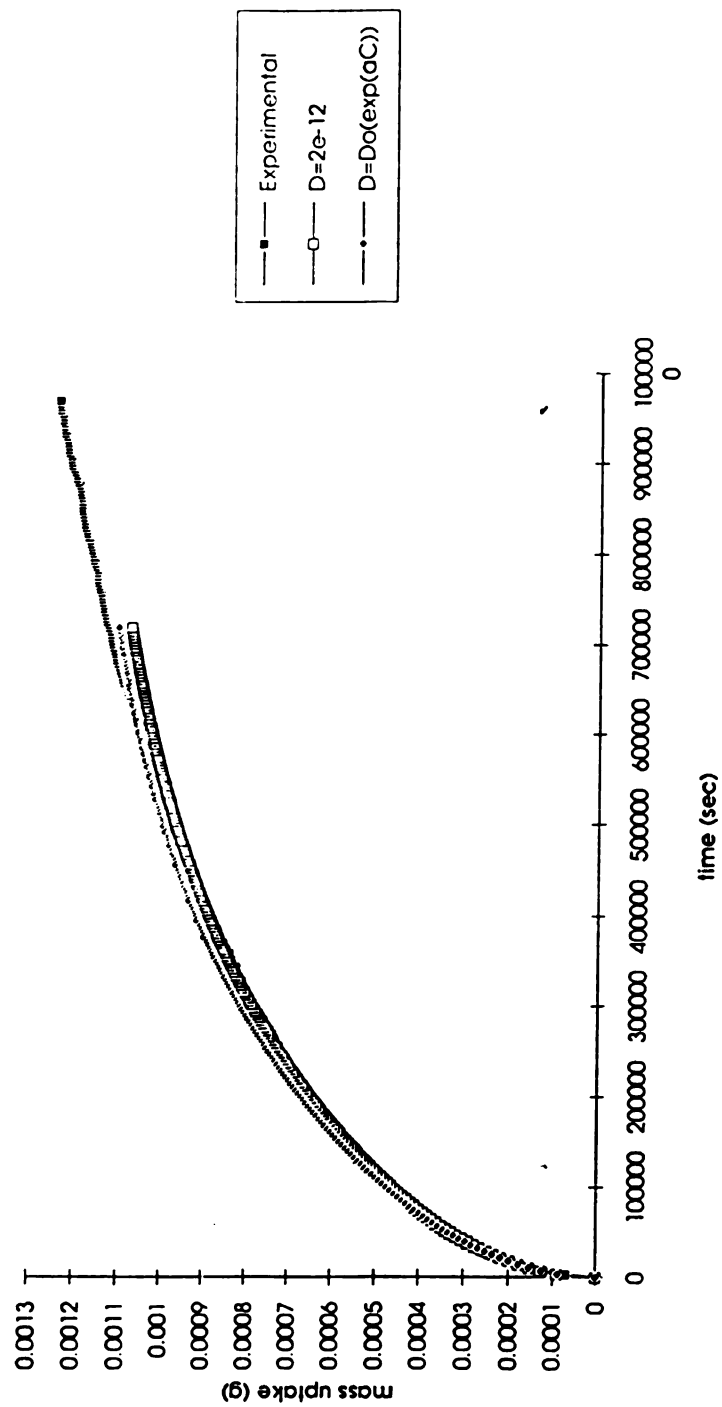


Figure 6.7b - Comparison of experimental results to model results for run #3

exponential dependency on concentration provides a good fit to the experimental data, except at very high times. Since the fit to the experimental data is good over a majority of the time range, it was taken as a good approximation to the concentration-dependent diffusion coefficient, particularly for use in the mathematical model of this thesis.

A least squares error analysis was done on both the constant diffusion coefficient results and the exponential dependency results. For run #2, the least squares error for the constant diffusivity was 1.33×10^{-6} , while the least squares error for the exponentially concentration dependent diffusivity was 1.9×10^{-7} , almost an order of magnitude less, indicating a better fit to the experimental data. For run #3, the least squares error for the constant diffusivity was 7.44×10^{-8} , while the error for the exponentially concentration dependent diffusivity was 1.12×10^{-7} . Table 6.2 summarizes the results of the least squares analysis. Although the error for the exponential form of the diffusivity is slightly higher for run #3, it is still quite low and the form of the diffusion coefficients, with the values of D_0 and a given above, provide a good approximation to the diffusion coefficient of the curing agent into the epoxy at low temperatures.

Run #	Least Squares Error for Constant D	Least Squares Error for Exponential D
2	1.33×10^{-6}	1.90×10^{-7}
3	7.44×10^{-8}	1.12×10^{-7}

Table 6.2 - Comparison of Least Squares Error for Constant and Exponentially-Dependent Diffusivities

In the above determination of the diffusion coefficient, the temperature dependence of the diffusion coefficient was not addressed. In reality, the diffusion coefficient has the form;

$$D = D_{oA} \exp(aC) \exp\left(-\frac{E_a}{RT}\right) \quad \text{Eqn. 6.15}$$

Since the experiments described above were run at room temperature (25° C), D_{oA} can be determined by solving the following equation;

$$D_o = 1.5 \times 10^{-12} \frac{m^2}{sec} = D_{oA} \exp\left(-\frac{E_a}{RT}\right) \quad \text{Eqn. 6.16}$$

The resulting value for D_{oA} is 3.24×10^{-5} .

Determination of reaction rate constants:

The next step in the modelling of the diffusion and reaction problem was the determination of the kinetic rate constants for the two primary reactions which occur. Rate constants have been reported for high temperature cures,

where the reaction is not diffusion-controlled³⁰, but there is not much information about rate constants for low temperature cures (less than 80° C). However, Finzel³⁵ reported that the rate constant for the second reaction was one-half that of the rate constant for the first reaction. Therefore, the rate constants can be determined by fitting the model to experimental data. It is assumed in the model that the rate constants have an Arrhenius dependence upon temperature, or;

$$k = k_0 \exp \frac{-E_a}{RT} \quad \text{Eqn. 6.17}$$

where E_a is the activation energy, R is the gas constant, and T is the temperature in Kelvin. To solve the problem, k was varied until a good fit with the experimental data was obtained. It was assumed that E_a was a constant value.

Before the model can be used to find the rate constants, the initial and boundary conditions of the system were specified. The molecular weight of the epoxy resin was 383 g/gmol and the density of the resin was 1.1625 g/cm³. The molecular weight of mPDA was 108 g/gmol and its density was 1.0686 g/cm³. At $t = 0$, only the epoxy surrounded the fiber, so the concentration of epoxy groups was;

$$E_o = 1000 \frac{\rho_E}{2MW_E} = 1.5176 \frac{gmol}{L} \quad \text{Eqn. 6.18}$$

where the 2 takes into account the fact that there are two epoxide groups within each resin chain and the 1000 is a conversion factor so that the concentration is in units of gmol/L. In the matrix surrounding the epoxy layer there was a 1:1 stoichiometric ratio of amine to epoxy and 14.5 parts by weight amine to 100 parts by weight of epoxy resin at $t > 0$. The volume of this matrix was;

$$V = 1000 \left(\frac{14.5}{\rho_A} + \frac{100}{\rho_E} \right) = 0.0996L \quad \text{Eqn. 6.19}$$

Therefore, the concentration of primary amine groups at $x = 0$ was;

$$A_{11} = \left(\frac{14.5}{MW_A} \right) \frac{1}{0.0996L} = 1.3464 \frac{gmol}{L} \quad \text{Eqn. 6.20}$$

As noted earlier in this chapter, the curing cycle was modified to allow reaction at room temperature to slow the diffusion of diamine through the epoxy. To account for this in the model, both E_o and A_{11} are multiplied by $1-X$, where X is the extent of reaction during the room temperature portion of the cure. If this is not accounted for in the model, diffusion will be too fast and the mathematical model

will overflow. This would be an indication that the equations describing the system above are invalid and the process is not diffusion-controlled. However, the system has been shown to be diffusion-controlled below 80° C, so inclusion of the extent of reaction during room temperature cure is important. In this model, X was estimated to be 0.30.

The experimental data that the model attempts to fit was determined by Rao³⁰ and is the extent of reaction versus time. A plot of this data is given in Figure 6.8. Since two reactions occur in the process, the best method of determining the extent of cure is by monitoring the epoxide concentration. Therefore, the extent of reaction is;

$$X = \frac{C_{E0} - C_E}{C_{E0}} \quad \text{Eqn. 6.21}$$

where C_{E0} is the concentration of epoxide groups at $t = 0$ and C_E is the concentration of epoxide groups at $x = 0$ and time t . The gel point can be determined by;

$$p_c = \frac{1}{(1 + \rho(f-2))^{\frac{1}{2}}} \quad \text{Eqn. 6.19}$$

where f is the functionality of the branch unit and ρ is the ratio of all A groups, reacted and unreacted, that are part of the branch units, to the total number of A groups in

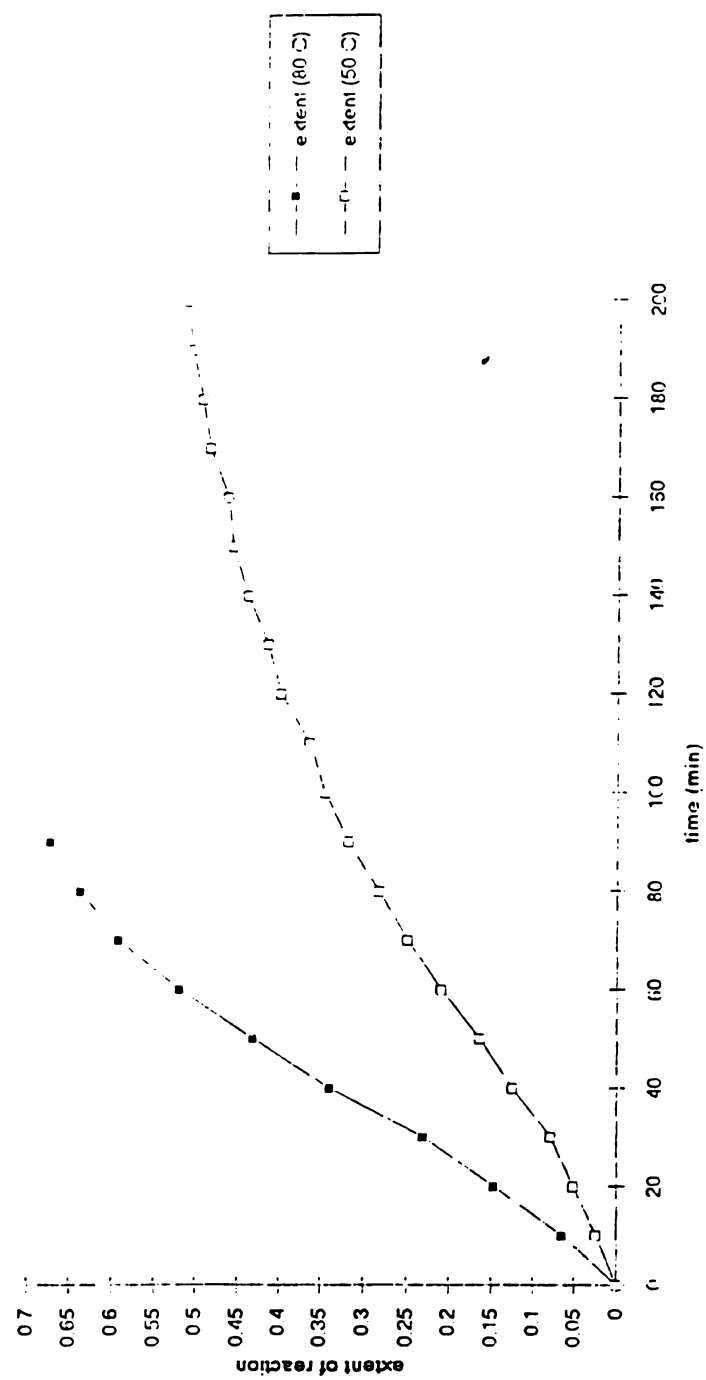


Figure 6.8 - Experimental extent of reaction

the mixture.⁴¹ In this case the diamine is the branch unit and is tetrafunctional. Therefore, $f = 4$. If A is the epoxide group, then there are 2 epoxide groups involved in the branch and 4 which are in the mixture. Therefore, ρ is 0.5. Thus, the critical extent of reaction, which occurs at the gel point, is 0.7071. The model is able to predict the gelation time using this critical extent of reaction. From the data by Rao, a critical extent of reaction of 0.7071 is not obtained during the low temperature portion of the cure cycle. Temperatures higher than 80° C are required to reach gelation.

To obtain the curves for the calculated extents of reaction shown in Figure 6.8, the reaction rate constants were estimated to obtain an approximate fit to the experimental data. At 80° C the best fit rate constant was 0.000178 L/mol, while at 50° C the rate constant was 0.000076 L/mol. A fit of the model results to the experimental extents of reaction is shown in Figure 6.9. To determine the temperature dependency of the rate constant, $\ln k_0$ versus $1/T$ was plotted, as in Figure 6.10. The slope of the plot was $-2347.18 = -E_a/R$. Therefore, the activation energy for the reaction was 4.664 kcal/mol. The y-intercept of the line was $-2.1325 = \ln k_0$. Therefore, k_0 was found to be 0.1185 ± 0.005 .

Finally, the concentration gradients for the primary amine, secondary amine, and tertiary amine within the epoxy

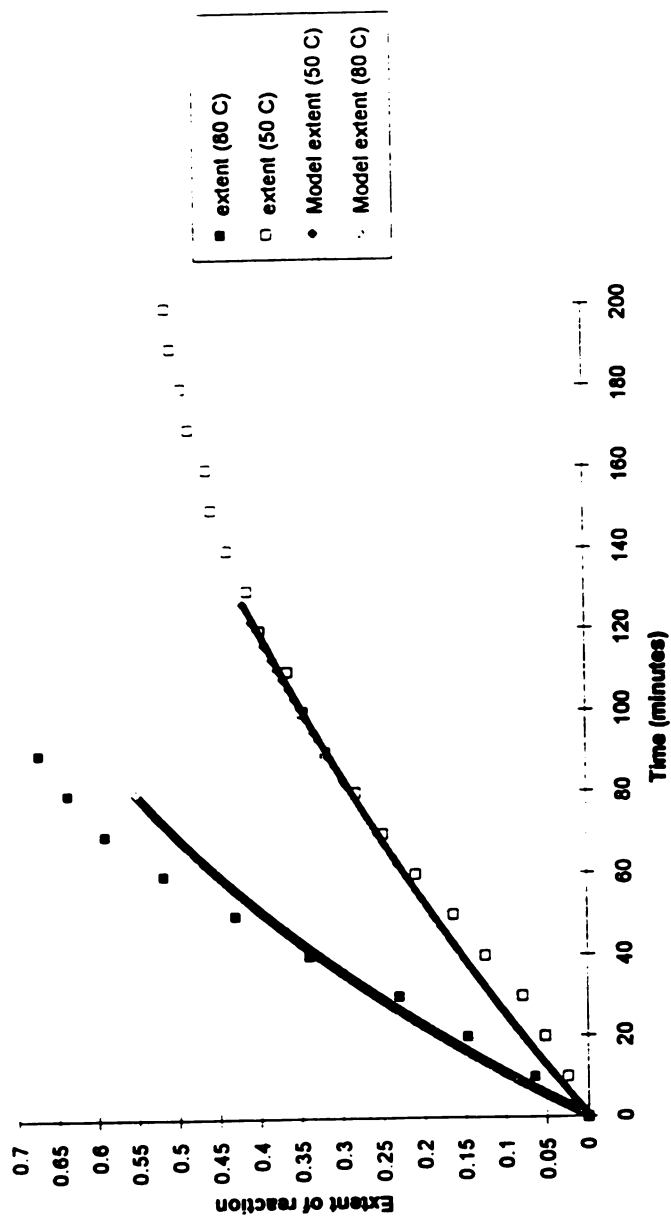


Figure 6.9 - Comparison of model to experimental extent of reaction

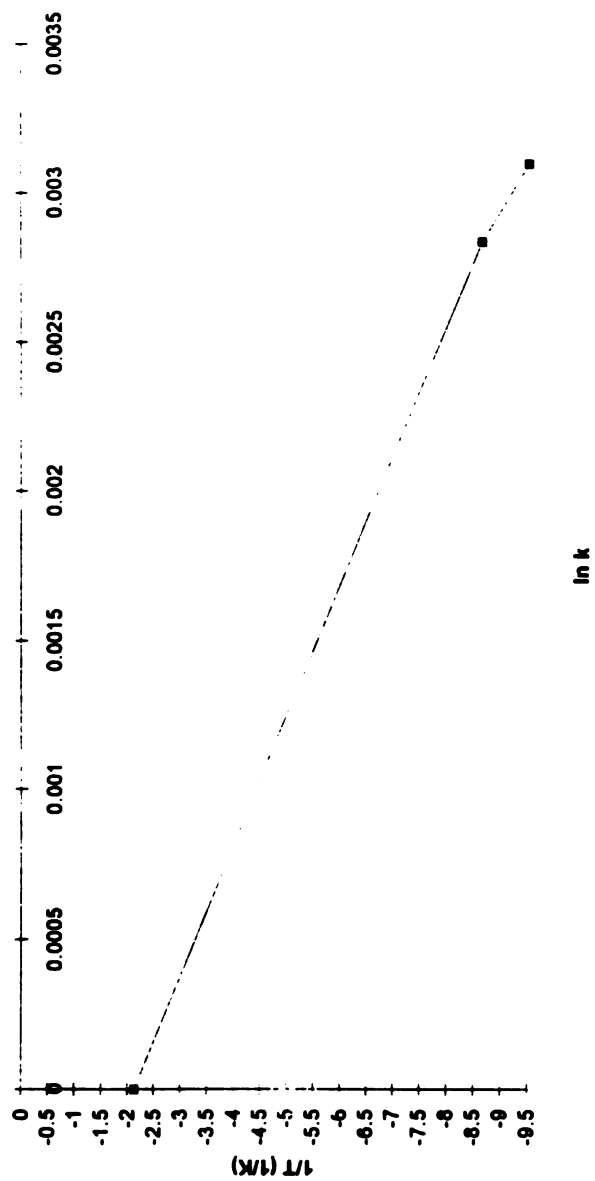


Figure 6.10 - Plot to determine k_0 and E_a

layer after two hours of exposure at 75° C are shown in Figures 6.11, 6.12, and 6.13. The concentration of the primary amine decreases with position into the epoxy as expected. However, the concentration of both the secondary and tertiary amine species increases with position into the epoxy. A possible explanation for this phenomenon may be that the diffusion of the primary amine is faster than the reaction mechanism, so the diffusing species does not react until it reaches layers farther from the interface. This correlates well with the earlier statement that this is a diffusion controlled process at temperature less than 80° C.

Further Studies

To provide a more accurate determination of the diffusion coefficient and the kinetic rate constants at temperatures less than 80° C, further experimental data is required. In this research, experimental data was only available at 50° C, 80° C, and higher temperatures. To further determine the characteristics of the diffusion controlled region, two or more sets of data less than 80° C are required.

The model used in this thesis did not consider the import of the secondary reactions, and further studies of these reaction mechanisms are required.

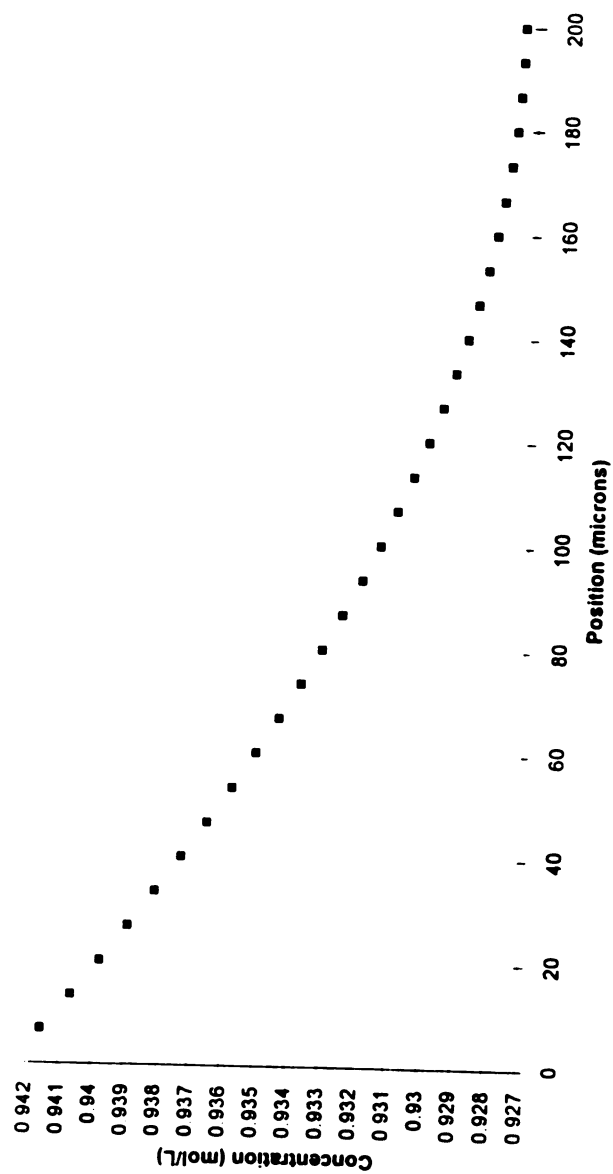


Figure 6.11 - Predicted concentration gradient of primary amine after two hours at 75° C

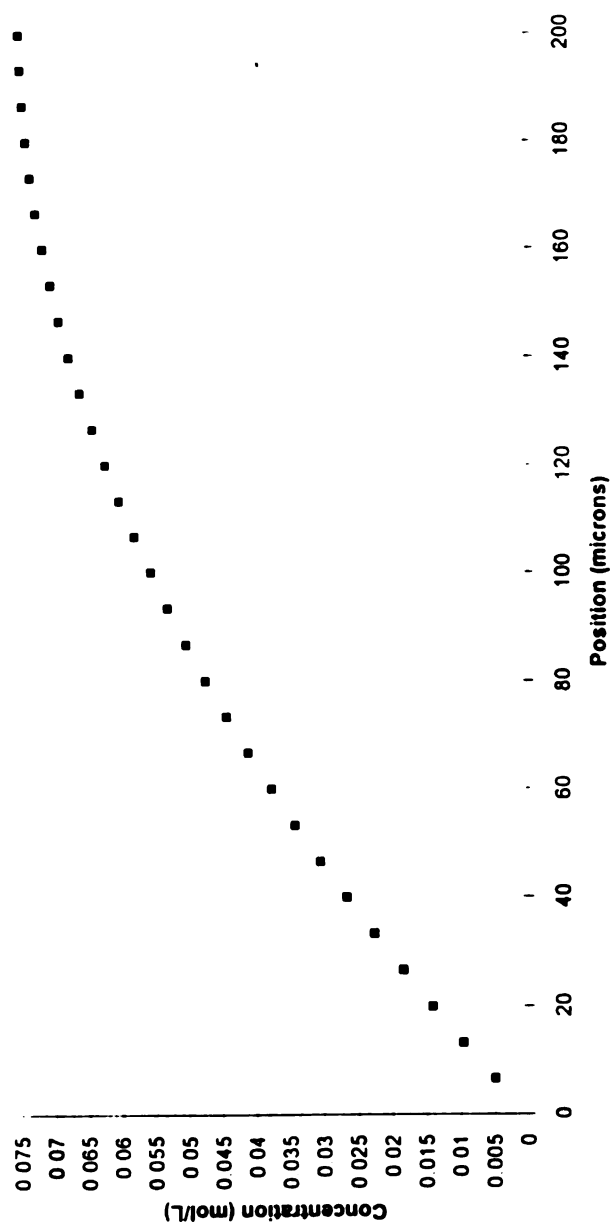


Figure 6.12 - Predicted concentration of secondary amine after two hours at 75° C

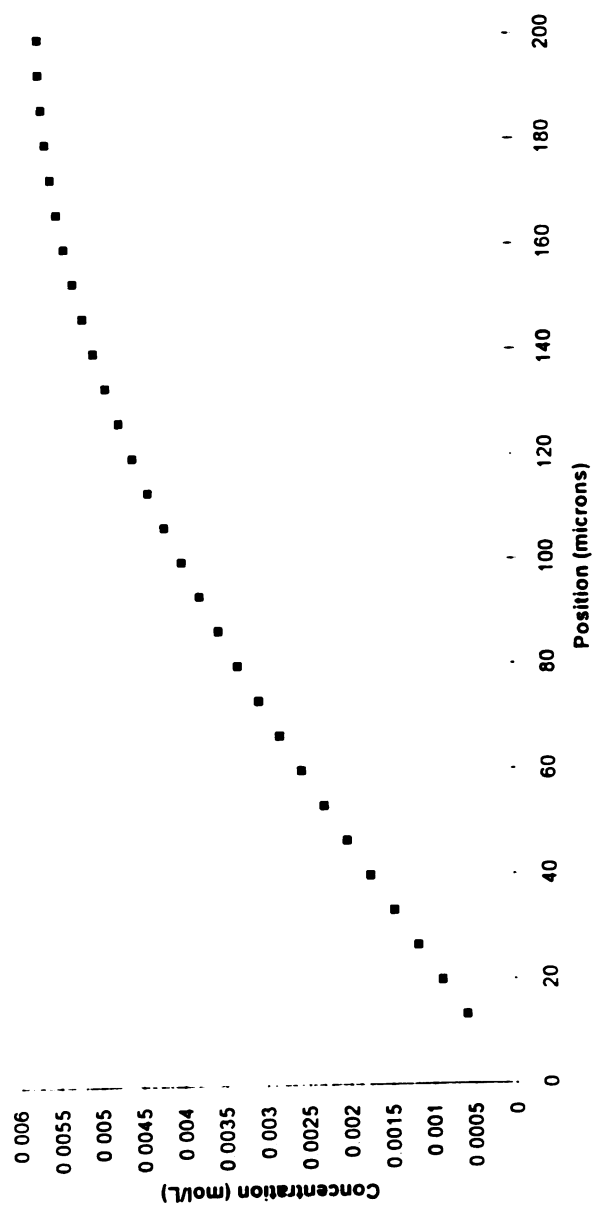


Figure 6.13 - Predicted concentration gradient of tertiary amine after two hours at 75° C

APPENDICES

APPENDIX A - Basic Program for Modelling Diffusion

The following basic program was written to model the diffusion of a vapor species into a solid, polymeric material. It is assumed that the diffusion coefficient is constant and the solid-vapor boundary does not swell with time. To model this system an explicit finite difference method was used, the Saul'yev method.

The differential equations describing the system can be solved using Laplace transforms and the result is an error function equation. The output from this model was compared to the error function to determine the accuracy of the model.

```
'Test of model to compare to error function
OPEN "GMM.DAT" FOR OUTPUT AS #1

'QUESTIONS OF THE USER
  PRINT "WHAT IS THE POSITION INCREMENT IN METERS?": INPUT
    DELX#
  PRINT "WHAT IS THE DIFFUSIVITY OF THE GAS IN M^2/SEC?":
    INPUT D#
  PRINT "WHAT IS THE TIME STEP IN SECONDS?": INPUT DELT#
  PRINT "WHAT IS THE MAXIMUM PENETRATION DEPTH IN
    MICRONS?": INPUT INDEX
  PRINT "AT WHAT POSITIONS WOULD YOU LIKE A PRINTOUT?":
    INPUT A: INPUT B: INPUT C: INPUT D: INPUT E

'SET ARRAY SIZE
  MARK = 10
  REPS = 10
  LET SIZE = INDEX + 1
  DIM V#(INDEX, INDEX)
  DIM P#(INDEX, INDEX)
  DIM Q#(INDEX, INDEX)
  COUNT = 0

'INITIAL CONDITIONS
  FOR I = 0 TO INDEX
```

```

P#(I, 0) = 0
Q#(I, 0) = 0
V#(I, 0) = 0
NEXT I

```

'BOUNDARY CONDITIONS

```

FOR N = 1 TO MARK
P#(0, N) = 3
Q#(0, N) = 3
Q#(INDEX, N) = 0
V#(0, N) = 3
NEXT N

```

```

LET B# = (D# * DELT#) / ((DELX#) ^ 2)
FOR J = 1 TO REPS
FOR N = 0 TO MARK - 1

```

'CALCULATION FOR GAS CONCENTRATION

```

FOR I = 1 TO INDEX - 1
P#(I, N + 1) = (B# * (P#(I - 1, N + 1) - V#(I, N) + V#(I
+ 1, N)) + V#(I, N)) / (1 + B#)
NEXT I
FOR I = 1 TO INDEX - 1
Q#(INDEX - I, N + 1) = (B# * (V#(INDEX - I - 1, N) -
V#(INDEX - I, N) + Q#(INDEX - I + 1, N + 1))
+ V#(INDEX - I, N)) / (1 + B#)
NEXT I
FOR I = 1 TO INDEX
V#(I, N + 1) = .5 * (P#(I, N + 1) + Q#(I, N + 1))
NEXT I
NEXT N

```

'OUTPUT INSTRUCTIONS

```

COUNT = COUNT + 1
PRINT A * DELX#; "METER", B * DELX#; "METER", C * DELX#;
"METER", D * DELX#; "METER", E * DELX#; "METER"
FOR N = 1 TO MARK
PRINT V#(A, N); V#(B, N); V#(C, N); V#(D, N); V#(E, N)
WRITE #1, V#(A, N), V#(B, N), V#(C, N), V#(D, N), V#(E, N)
NEXT N
GOSUB 900
PRINT "COUNT= "; COUNT * DELT# * 10; "SEC"
NEXT J
CLOSE #1
END

```

```

900 FOR I = 0 TO INDEX
V#(I, 0) = V#(I, MARK)
P#(I, 0) = P#(I, MARK)
Q#(I, 0) = Q#(I, MARK)
NEXT I
RETURN

```

APPENDIX B - Basic Program to Model Sulfonation

The following Basic computer program is a modification of the program in appendix A, which includes the concentration-dependent diffusion coefficient for sulfur trioxide vapor and the kinetic rate constant. In the program, V# denotes the concentration of sulfur trioxide vapor, Z# is the concentration of unsulfonated polymer, S# is the concentration of the sulfonated polymer, and MT# is the mass uptake of sulfur trioxide vapor in the polymer.

```
'Diffusion of sulfur trioxide gas into polymer samples
OPEN "SO32.CSV" FOR OUTPUT AS #1

'QUESTIONS OF THE USER
  PRINT "WHAT IS THE POSITION INCREMENT IN METERS?": INPUT
    DELX#
  PRINT "WHAT IS THE TIME STEP IN SECONDS?": INPUT DELT#
  PRINT "WHAT IS THE MAXIMUM PENETRATION DEPTH IN
    MICRONS?": INPUT INDEX
  PRINT "WHAT IS THE TEMPERATURE OF THE SYSTEM? (IN
    DEGREES CELSIUS)": INPUT T#
  PRINT "WHAT IS THE WEIGHT OF THE POLYMER SAMPLE? (IN
    GRAMS)": INPUT WT#
  PRINT "WHAT IS THE MOLECULAR WEIGHT OF THE POLYMER
    FILM?": INPUT MW#
  PRINT "WHAT IS THE VOLUME OF THE POLYMER SAMPLE? (IN
    LITERS)": INPUT VOL#
  PRINT "AT WHAT POSITIONS WOULD YOU LIKE A PRINTOUT?":
    INPUT A: INPUT B

'SET ARRAY SIZE
  TP# = T# + 273.15
  MARK = 10
  REPS = 60
  DIM V#(INDEX, INDEX)
  DIM P#(INDEX, INDEX)
  DIM Q#(INDEX, INDEX)
  DIM Z#(INDEX, INDEX)
  DIM Z1#(INDEX, INDEX)
  DIM S#(INDEX, INDEX)
  DIM S1#(INDEX, INDEX)
```

```

DIM MT1#(INDEX, INDEX)
DIM MT2#(INDEX, INDEX)
DIM MT#(INDEX, INDEX)
COUNT = 0
LET TO = 0
LET M = 0

```

'INITIAL CONDITIONS

```

FOR I = 0 TO INDEX
  Z#(I, 0) = DEN# * 1000 / MW#
  Z1#(I, 0) = DEN# * 1000 / MW#
  S#(I, 0) = 0
  S1#(I, 0) = 0
  P#(I, 0) = 0
  Q#(I, 0) = 0
  V#(I, 0) = 0
NEXT I

```

'BOUNDARY CONDITIONS

```

FOR N = 1 TO MARK
  Z#(INDEX, N) = DEN# * 1000 / MW#
  S#(INDEX, N) = 0
  P#(0, N) = 2.6022
  P#(INDEX, N) = 0
  Q#(0, N) = 2.6022
  Q#(INDEX, N) = 0
  V#(0, N) = 2.6022
  V#(INDEX, N) = 0
NEXT N

```

```

DO# = 1.37E-14
A = .41
K0# = 2.22
EA# = 10000
R = 8.314 * .239
K# = K0# * EXP(-EA# / (R * TP#))
B# = (DO# * DELT#) / ((DELX#) ^ 2)
FOR J = 1 TO REPS
  FOR N = 0 TO MARK - 1

```

'CALCULATION FOR GAS CONCENTRATION

```

FOR I = 1 TO INDEX - 1
  P#(I, N + 1) = (V#(I, N) + B# * EXP(A * V#(I, N)) *
    (P#(I - 1, N + 1) - V#(I, N) + V#(I + 1, N)) + B# *
    A * EXP(A * V#(I, N)) * (V#(I, N) * V#(I, N) - 2 *
    V#(I + 1, N) * V#(I, N) + V#(I + 1, N) * V#(I + 1,
    N)) - K# * DELT# * V#(I, N) * Z#(I, N)) / (1 + B# *
    EXP(A * V#(I, N)))
NEXT I
P#(INDEX, N + 1) = (V#(INDEX, N) + B# * EXP(A *
  V#(INDEX, N)) * (P#(INDEX - 1, N + 1) - V#(INDEX,
  N) + V#(INDEX - 1, N)) + B# * A * EXP(A * V#(INDEX,

```

```

N)) * (V#(INDEX, N) * V#(INDEX, N) - 2 * V#(INDEX -
1, N) * V#(INDEX, N) + V#(INDEX - 1, N) * V#(INDEX
- 1, N)) - K# * DELT# * V#(INDEX, N) * Z#(INDEX,
N)) / (1 + B# * EXP(A * V#(INDEX, N)))
Q#(INDEX, N + 1) = (V#(INDEX, N) + B# * EXP(A *
V#(INDEX, N)) * (V#(INDEX - 1, N) - V#(INDEX, N) +
Q#(INDEX - 1, N)) + B# * A * EXP(A * V#(INDEX, N))
* (V#(INDEX, N) * V#(INDEX, N) - 2 * V#(INDEX - 1,
N) * V#(INDEX, N) + V#(INDEX - 1, N) * V#(INDEX -
1, N)) - K# * DELT# * V#(INDEX, N) * Z#(INDEX, N))
/ (1 + B# * EXP(A * V#(INDEX, N)))
FOR I = 1 TO INDEX - 1
Q#(INDEX - I, N + 1) = (V#(INDEX - I, N) + B# * EXP(A *
V#(INDEX - I, N)) * (V#(INDEX - I - 1, N) -
V#(INDEX - I, N) + Q#(INDEX - I + 1, N + 1)) + B# *
A * EXP(A * V#(INDEX - I, N)) * (V#(INDEX - I, N) *
V#(INDEX - I, N) - 2 * V#(INDEX - I + 1, N) *
V#(INDEX - I, N) + V#(INDEX - I + 1, N) * V#(INDEX
- I + 1, N)) - K# * DELT# * V#(INDEX - I, N) *
Z#(INDEX - I, N)) / (1 + B# * EXP(A * V#(INDEX - I,
N)))
NEXT I
M = M + 1
T = TO + M * DELT#
FOR I = 1 TO INDEX
V#(I, N + 1) = .5 * (P#(I, N + 1) + Q#(I, N + 1))
NEXT I

'CALCULATION OF UNSULFONATED POLYMER CONCENTRATION
FOR I = 1 TO INDEX
Z#(I, N + 1) = Z1#(I, 0) - K# * DELT# * Z#(I, N) * V#(I,
N)
NEXT I

'CALCULATION OF SULFONATED POLYMER CONCENTRATION
FOR I = 1 TO INDEX
S#(I, N + 1) = S1#(I, 0) + K# * DELT# * Z#(I, N) * V#(I,
N)
NEXT I
MT1#(0, N + 1) = (2 * (.5 * V#(0, N + 1) + V#(1, N + 1)
+ V#(2, N + 1) + V#(3, N + 1) + V#(4, N + 1) +
V#(5, N + 1) + V#(6, N + 1) + V#(7, N + 1) + V#(8,
N + 1) + V#(9, N + 1) + V#(10, N + 1) + V#(11, N +
1) + V#(12, N + 1) + V#(13, N + 1) + V#(14, N + 1)
+ V#(15, N + 1) + V#(16, N + 1) + V#(17, N + 1) +
V#(18, N + 1) + V#(19, N + 1) + V#(20, N + 1) +
V#(21, N + 1) + V#(22, N + 1) + V#(23, N + 1) +
V#(24, N + 1) + V#(25, N + 1) + V#(26, N + 1) +
V#(27, N + 1) + V#(28, N + 1) + V#(29, N + 1) + .5
* V#(29, N + 1)) / 31) * (VOL# + MT#(0, N) / (1000
* 1.97)) * 80.06

```

```

MT2#(0, N + 1) = (2 * (.5 * S#(0, N + 1) + S#(1, N + 1)
+ S#(2, N + 1) + S#(3, N + 1) + S#(4, N + 1) +
S#(5, N + 1) + S#(6, N + 1) + S#(7, N + 1) + S#(8,
N + 1) + S#(9, N + 1) + S#(10, N + 1) + S#(11, N +
1) + S#(12, N + 1) + S#(13, N + 1) + S#(14, N + 1)
+ S#(15, N + 1) + S#(16, N + 1) + S#(17, N + 1) +
S#(18, N + 1) + S#(19, N + 1) + S#(20, N + 1) +
S#(21, N + 1) + S#(22, N + 1) + S#(23, N + 1) +
S#(24, N + 1) + S#(25, N + 1) + S#(26, N + 1) +
S#(27, N + 1) + S#(28, N + 1) + S#(29, N + 1) + .5
* S#(29, N + 1)) / 31) * (VOL# + MT#(0, N) / (1000
* 1.97)) * 80.06
MT#(0, N + 1) = MT1#(0, N + 1) + MT2#(0, N + 1)
NEXT N

```

'OUTPUT INSTRUCTIONS

```

COUNT = COUNT + 1
PRINT A * DELX#; "METER", B * DELX#; "METER"
FOR N = 1 TO MARK
PRINT V#(B, N), Z#(B, N), S#(B, N), MT#(0, N)
WRITE #1, MT#(0, N)
NEXT N
GOSUB 900
PRINT "COUNT= "; COUNT * DELT# * 10; "SEC"
NEXT J
CLOSE #1
END

```

```

900 FOR I = 0 TO INDEX
V#(I, 0) = V#(I, MARK)
P#(I, 0) = P#(I, MARK)
Q#(I, 0) = Q#(I, MARK)
Z#(I, 0) = Z#(I, MARK)
S#(I, 0) = S#(I, MARK)
MT#(I, 0) = MT#(I, MARK)
NEXT I
RETURN

```

APPENDIX C - Weight Gain from Sulfonation

	A	B	C	D	E	F	G	H
1	Weight gain in polystyrene and polypropylene due to sulfonation with sulfur trioxide							
2								
3	Run #1 - PS			Run #1 - PP			Run #2 - PS	
4								
5	Reactor T	90		Reactor T	90		Reactor T	90
6	Bath T	11		Bath T	11		Bath T	20
7	Wt	0.0463 g		Wt=	0.0501 g		Wt	0.0464 g
8								
9								
10	Time (sec)	Wt gain (g)		Time (sec)	Wt gain (g)		Time (sec)	Wt gain
11	0	0		0	0		0	0
12	30	0.0004		30			30	0
13	60	0.00073		60	0.0003333		60	0
14	90	0.000867		90	0.0028		90	0.000867
15	120	0.000933		120	0.0028667		120	0.001
16	150	0.000933		150	0.0048667		150	0.001267
17	180	0.001067		180	0.005		180	0.001
18	210	0.001067		210	0.0074667		210	0.001133
19	240	0.001267		240	0.0092		240	0.001133
20	270	0.000933		270	0.0106667		270	0.001133
21	300	0.001067		300	0.0118667		300	0.001133
22	330	0.001		330	0.0128667		360	0.0014
23	360	0.001133		360	0.0137333		420	0.00133
24	390	0.001267		390	0.0152		450	0.001533
25	420	0.001333		420	0.0161333			
26	450	0.001267		450	0.0168667			
27	480	0.001133		480	0.0175333			
28	510	0.001333						
29	540	0.001067						
30	570	0.001067						
31	630	0.001467						
32	690	0.001067						
33								
34								
35								
36								
37								
38								
39								
40								
41								

	I	J	K	L	M	N	O	P
1								
2								
3	Run #2 - PP			Run #3 - PS			Run #3 - PP	
4								
5	Reactor T	90		Reactor T	110		Reactor T	110
6	Bath T	20		Bath T	11		Bath T	11
7	Wt=	0.0499 g		Wt=	0.0456 g		Wt=	0.051 g
8								
9								
10	Time (sec)	Wt gain (g)		Time (sec)	Wt gain (g)		Time (sec)	Wt gain (g)
11	0	0		0	0		0	0
12	30			30			30	0.0008
13	60			60			60	0.0055333
14	90			90			90	0.0091333
15	120	0.001		120	0.0002		120	0.0126
16	150	0.0023333		150	0.0002667		150	0.0158
17	180	0.0036667		180	0.0002667		180	0.0188667
18	210	0.0047333		210			210	0.0218
19	240	0.0060667		240	0.0002667		240	0.0238
20	270	0.0076		270	0.0002667		270	0.0268
21	300	0.0088667		300	0.0002		300	0.0282
22	330	0.0106		330	0.0002		330	0.0307333
23	360	0.0115333		360	0.0004		360	0.0329333
24	390	0.0128		390	0.0004		390	0.0347333
25	420	0.0142667		420	0.0005333		420	0.0370667
26	450			450	0.0005333		450	0.0384667
27	480	0.0167333		480	0.0006		480	0.0404667
28	510	0.018		510	0.0006		510	0.042
29	540	0.0192		540	0.0006		540	0.0446
30	570	0.0203333		570	0.0008		570	0.0471333
31	600	0.0215333		600	0.0007333		600	0.0485333
32	630	0.0228		660	0.0007333			
33	660	0.024		720	0.0011333			
34	690	0.0256		780	0.0012			
35	720	0.0266		840	0.0013333			
36				900	0.0014667			
37				960	0.0015333			
38				1020	0.0016			
39				1080	0.0015333			
40				1140	0.0017333			
41				1200	0.0018667			

	Q	R	S	T	U	V
1						
2						
3	Run #4 - PS			Run #4 - PP		
4						
5	Reactor T	110		Reactor T	110	
6	Bath T	20		Bath T	20	
7	Wt=	0.0445 g		Wt=	0.049 g	
8						
9						
10	Time (sec)	Wt gain (g)		Time (sec)	Wt gain (g)	
11	0	0		0	0	
12	30	0.0004		30		
13	60	0.000867		60	0.0028	
14	90	0.000933		90	0.006533	
15	120	0.001		120	0.0112	
16	150	0.001067		150	0.014667	
17	180	0.0012		180	0.017067	
18	210	0.0012		210	0.0204	
19	240	0.001333		240	0.023	
20	270	0.001533		270	0.025667	
21	300	0.0014		300	0.0284	
22	330	0.001533		330	0.030667	
23	360	0.001733		360	0.033133	
24	390	0.001933		390	0.0354	
25	420	0.001933		420	0.037667	
26	450	0.001867		450	0.039733	
27	480	0.002		480	0.0418	
28	510	0.0018		510	0.043333	
29	540	0.0018		540	0.045133	
30	570	0.001867		570	0.046867	
31	600	0.001933		600	0.048667	
32	660	0.001933				
33	720	0.001933				
34	780	0.002				
35	840	0.0022				
36	900	0.002267				
37	960	0.002333				
38	1020	0.0024				
39	1080	0.002467				
40	1140	0.0026				
41	1200	0.002867				

APPENDIX D - Basic Program to Model Curing of an Epoxy

This program is also a modification of the program in Appendix A to model the diffusion and reaction of a diamine into an epoxy system. In this program, V# is the concentration of the primary amine, E# is the concentration of the uncured epoxy, DM# is the concentration of the secondary amine, and MDM# is the concentration of the tertiary amine.

'Model for the curing of an epoxy resin system

OPEN "AMI.CSV" FOR OUTPUT AS #1

'QUESTIONS OF THE USER

```
PRINT "WHAT IS THE POSITION INCREMENT IN METERS?": INPUT DELX#
PRINT "WHAT IS THE TIME STEP IN SECONDS?": INPUT DELT#
PRINT "WHAT IS THE MAXIMUM PENETRATION DEPTH IN MICRONS?": INPUT
INDEX
PRINT "WHAT IS THE TEMPERATURE OF THE SYSTEM? (IN DEGREES CELSIUS)":
INPUT T#
PRINT "AT WHAT POSITIONS WOULD YOU LIKE A PRINTOUT?": INPUT A:
INPUT B
```

'SET ARRAY SIZE

```
DELX# = 6.667E-06
DELT# = 10
INDEX = 30
T# = 80
TP# = T# + 273.15
MARK = 10
REPS = 76
DIM V#(INDEX, INDEX)
DIM P#(INDEX, INDEX)
DIM Q#(INDEX, INDEX)
DIM MT#(INDEX, INDEX)
DIM Z#(INDEX, INDEX)
DIM Z1#(INDEX, INDEX)
DIM Z1#(INDEX, INDEX)
DIM DM#(INDEX, INDEX)
DIM DM1#(INDEX, INDEX)
DIM DM2#(INDEX, INDEX)
DIM MTM#(INDEX, INDEX)
DIM MTM1#(INDEX, INDEX)
DIM MTM2#(INDEX, INDEX)
DIM X#(INDEX, INDEX)
DIM X1#(INDEX, INDEX)
COUNT = 0
```

```
LET TO = 0
LET M = 0
```

'INITIAL CONDITIONS

```
FOR I = 0 TO INDEX
  V#(I, 0) = 0
  P#(I, 0) = 0
  Q#(I, 0) = 0
  MT#(0, 0) = 0
  Z#(I, 0) = 0.7 * 1.5176
  Z1#(I, 0) = 0.7 * 1.5176
  DM#(I, 0) = 0
  DM1#(I, 0) = 0
  DM2#(I, 0) = 0
  DM#(I, 0) = 0
  DM1#(I, 0) = 0
  DM2#(I, 0) = 0
  X#(0, 0) = 0
NEXT I
```

'BOUNDARY CONDITIONS

```
FOR N = 1 TO MARK
  V#(0, N) = 0.7 * 1.3464
  P#(0, N) = 0.7 * 1.3464
  Q#(0, N) = 0.7 * 1.3464
NEXT N
```

```
LET ED# = 10000
LET R# = 8.314 * 0.239
DO# = 1.5E-12
DOB# = 0.0000324
DOA# = DOB# * EXP(-ED# / (R# * T1#))
LET B# = (DOA# * DELT#) / (DELX#) ^2
A = 1.69
K1# = 0.000178
K2# = 0.5 * K1#
FOR J = 1 TO REPS
  FOR N = 0 TO MARK - 1
```

'CALCULATION FOR PRIMARY AMINE CONCENTRATION

```
FOR I = 1 TO INDEX - 1
  P#(I, N + 1) = (V#(I, N) + B# * EXP(A * V#(I, N)) * (P#(I - 1, N + 1) - V#(I, N) + V#(I + 1, N)) + B# * A * EXP(A * V#(I, N)) * (V#(I, N) * V#(I, N) - 2 * V#(I + 1, N) * V#(I, N) + V#(I + 1, N) * V#(I + 1, N)) - K1# * DELT# * V#(I, N) * Z#(I, N)) / (1 + B# * EXP(A * V#(I, N)))
NEXT I
P#(INDEX, N + 1) = (V#(INDEX, N) + B# * EXP(A * V#(INDEX, N)) * (P#(INDEX - 1, N + 1) - V#(INDEX, N) + V#(INDEX - 1, N)) + B# * A * EXP(A * V#(INDEX, N)) * (V#(INDEX, N) * V#(INDEX, N) - 2 * V#(INDEX - 1, N) * V#(INDEX, N) + V#(INDEX - 1, N) * V#(INDEX - 1, N)))
```

```

      * V#(INDEX, N) + V#(INDEX - 1, N) * V#(INDEX - 1,
      N)) - K1# * DELT# * V#(INDEX, N) * Z#(INDEX, N)) /
      (1 + B# * EXP(A * V#(INDEX, N)))
Q#(INDEX, N + 1) = (V#(INDEX, N) + B# * EXP(A * V#(INDEX, N)) *
      (V#(INDEX - 1, N) - V#(INDEX, N) + Q#(INDEX - 1,
      N)) + B# * A * EXP(A * V#(INDEX, N)) * (V#(INDEX,
      N) * V#(INDEX, N) - 2 * V#(INDEX - 1, N) *
      V#(INDEX, N) + V#(INDEX - 1, N) * V#(INDEX - 1, N))
      - K1# * DELT# * V#(INDEX, N) * Z#(INDEX, N)) / (1 +
      B# * EXP(A * V#(INDEX, N)))
FOR I = 1 TO INDEX - 1
Q#(INDEX - I, N + 1) = (V#(INDEX - I, N) + B# * EXP(A * V#(INDEX -
      I, N)) * (V#(INDEX - I - 1, N) - V#(INDEX - I, N) +
      Q#(INDEX - I + 1, N + 1)) + B# * A * EXP(A *
      V#(INDEX - I, N)) * (V#(INDEX - I, N) * V#(INDEX -
      I, N) - 2 * V#(INDEX - I + 1, N) * V#(INDEX - I, N)
      + V#(INDEX - I + 1, N) * V#(INDEX - I + 1, N)) -
      K1# * DELT# * V#(INDEX - I, N) * Z#(INDEX - I, N))
      / (1 + B# * EXP(A * V#(INDEX - I, N)))
NEXT I
M = M + 1
T = T0 + M * DELT#
FOR I = 1 TO INDEX
V#(I, N + 1) = .5 * (P#(I, N + 1) + Q#(I, N + 1))
NEXT I

'CALCULATION OF EPOXY RESIN CONCENTRATION
FOR I = 1 TO INDEX
Z#(I, N + 1) = Z1#(I, 0) - K1# * DELT# * Z#(I, N) * V#(I, N) - K2# *
      DELT# * Z#(I, N) * DM#(I, N)
X#(0, N) = (Z1#(I, 0) - Z#(1, N+1)) / Z1#(I, 0)
IF X#(0, N+1) < 0.7071 THEN GOTO 400
IF X#(0, N+1) = 0.7071 THEN GOTO 380
IF X#(0, N+1) > 0.7071 THEN GOTO 380
380 PRINT "GELATION"
400 NEXT I

'CALCULATION OF SECONDARY AMINE CONCENTRATION
FOR I = 1 TO INDEX
D01# = DOA# * 108/490
B1# = D01# * DELT# / (DELX# ^ 2)
DM1#(I, N + 1) = (DM#(I, N) + B# * EXP(A * V#(I, N)) * (DM1#(I - 1,
      N + 1) - DM#(I, N) + DM#(I + 1, N)) + B# * A *
      EXP(A * V#(I, N)) * (DM#(I, N) * DM#(I, N) - 2 *
      DM#(I + 1, N) * DM#(I, N) + DM#(I + 1, N) * DM#(I +
      1, N)) + K1# * DELT# * V#(I, N) * Z#(I, N) - K2# *
      DELT# * Z#(I, N) * DM#(I, N)) / (1 + B# * EXP(A *
      V#(I, N)))
NEXT I
DM1#(INDEX, N + 1) = (DM#(INDEX, N) + B# * EXP(A * V#(INDEX, N)) *
      (DM1#(INDEX - 1, N + 1) - DM#(INDEX, N) + DM#(INDEX
      - 1, N)) + B# * A * EXP(A * V#(INDEX, N)) *

```

```

(DM#(INDEX, N) * DM#(INDEX, N) - 2 * DM#(INDEX - 1,
N) * DM#(INDEX, N) + DM#(INDEX - 1, N) * DM#(INDEX
- 1, N)) + K1# * DELT# * V#(INDEX, N) * Z#(INDEX,
N) - K2# * DELT# * Z#(INDEX, N) * DM#(INDEX, N)) /
(1 + B# * EXP(A * V#(INDEX, N)))
DM2#(INDEX, N + 1) = (DM#(INDEX, N) + B# * EXP(A * V#(INDEX, N)) *
(DM#(INDEX - 1, N) - DM#(INDEX, N) + DM2#(INDEX -
1, N)) + B# * A * EXP(A * V#(INDEX, N)) *
(DM#(INDEX, N) * DM#(INDEX, N) - 2 * DM#(INDEX - 1,
N) * DM#(INDEX, N) + DM#(INDEX - 1, N) * DM#(INDEX
- 1, N)) + K1# * DELT# * V#(INDEX, N) * Z#(INDEX,
N) - K2# * DELT# * Z#(INDEX, N) * DM#(INDEX, N)) /
(1 + B# * EXP(A * V#(INDEX, N)))
FOR I = 1 TO INDEX - 1
DM2#(INDEX - I, N + 1) = (DM#(INDEX - I, N) + B# * EXP(A * V#(INDEX
- I, N)) * (DM#(INDEX - I - 1, N) - DM#(INDEX - I,
N) + DM2#(INDEX - I + 1, N + 1)) + B# * A * EXP(A *
V#(INDEX - I, N)) * (DM#(INDEX - I, N) * DM#(INDEX
- I, N) - 2 * DM#(INDEX - I + 1, N) * DM#(INDEX -
I, N) + DM#(INDEX - I + 1, N) * DM#(INDEX - I + 1,
N)) + K1# * DELT# * V#(INDEX - I, N) * Z#(INDEX -
I, N) - K2# * DELT# * Z#(INDEX - I, N) * DM#(INDEX
- I, N)) / (1 + B# * EXP(A * V#(INDEX - I, N)))
NEXT I
FOR I = 1 TO INDEX
DM#(I, N+1) = 0.5 * (DM1#(I, N + 1) + DM2#(I, N + 1))
NEXT I

```

'CALCULATION OF TERTIARY AMINE CONCENTRATION

```

FOR I = 1 TO INDEX
DO2# = DOA# * 108/872
B2# = DO2# * DELT# / (DELX# ^ 2)
MDM1#(I, N + 1) = (MDM#(I, N) + B2# * EXP(A * V#(I, N)) * (MDM1#(I -
1, N + 1) - MDM#(I, N) + MDM#(I + 1, N)) + B2# * A
* EXP(A * V#(I, N)) * (MDM#(I, N) * MDM#(I, N) - 2
* MDM#(I + 1, N) * MDM#(I, N) + MDM#(I + 1, N) *
MDM#(I + 1, N)) + K1# * DELT# * V#(I, N) * Z#(I, N)
+ K2# * DELT# * Z#(I, N) * DM#(I, N)) / (1 + B2# *
EXP(A * V#(I, N)))
NEXT I
MDM1#(INDEX, N + 1) = (MDM#(INDEX, N) + B2# * EXP(A * V#(INDEX, N))
* (MDM1#(INDEX - 1, N + 1) - MDM#(INDEX, N) +
MDM#(INDEX - 1, N)) + B2# * A * EXP(A * V#(INDEX,
N)) * (MDM#(INDEX, N) * MDM#(INDEX, N) - 2 *
MDM#(INDEX - 1, N) * MDM#(INDEX, N) + MDM#(INDEX -
1, N) * MDM#(INDEX - 1, N)) + K1# * DELT# *
V#(INDEX, N) * Z#(INDEX, N) + K2# * DELT# *
Z#(INDEX, N) * DM#(INDEX, N)) / (1 + B2# * EXP(A *
V#(INDEX, N)))
MDM2#(INDEX, N + 1) = (MDM#(INDEX, N) + B2# * EXP(A * V#(INDEX, N))
* (MDM#(INDEX - 1, N) - MDM#(INDEX, N) +
MDM2#(INDEX - 1, N)) + B2# * A * EXP(A * V#(INDEX,

```

```

N)) * (MDM#(INDEX, N) * MDM#(INDEX, N) - 2 *
MDM#(INDEX - 1, N) * MDM#(INDEX, N) + MDM#(INDEX -
1, N) * MDM#(INDEX - 1, N)) + K1# * DELT# *
V#(INDEX, N) * Z#(INDEX, N) + K2# * DELT# *
Z#(INDEX, N) * DM#(INDEX, N)) / (1 + B2# * EXP(A *
V#(INDEX, N)))
FOR I = 1 TO INDEX - 1
MDM2#(INDEX - I, N + 1) = (MDM#(INDEX - I, N) + B2# * EXP(A *
V#(INDEX - I, N)) * (MDM#(INDEX - I - 1, N) -
MDM#(INDEX - I, N) + MDM2#(INDEX - I + 1, N + 1)) +
B2# * A * EXP(A * V#(INDEX - I, N)) * (MDM#(INDEX -
I, N) * MDM#(INDEX - I, N) - 2 * MDM#(INDEX - I +
1, N) * MDM#(INDEX - I, N) + MDM#(INDEX - I + 1, N)
* MDM#(INDEX - I + 1, N)) + K1# * DELT# * V#(INDEX
- I, N) * Z#(INDEX - I, N) + K2# * DELT# * Z#(INDEX
- I, N) * DM#(INDEX - I, N)) / (1 + B2# * EXP(A *
V#(INDEX - I, N)))
NEXT I
FOR I = 1 TO INDEX
MDM#(I, N+1) = 0.5 * (MDM1#(I, N + 1) + MDM2#(I, N + 1))
NEXT I

'OUTPUT INSTRUCTIONS
COUNT = COUNT + 1
PRINT A * DELX#; "METER", B * DELX#; "METER"
FOR N = 1 TO MARK
PRINT V#(B, N), X#(0, N)
WRITE #1, X#(0, N)
NEXT N
GOSUB 900
PRINT "COUNT= "; COUNT * DELT# * 10; "SEC"
NEXT J
CLOSE #1
END

900 FOR I = 0 TO INDEX
V#(I, 0) = V#(I, MARK)
P#(I, 0) = P#(I, MARK)
Q#(I, 0) = Q#(I, MARK)
Z#(I, 0) = Z#(I, MARK)
DM#(I, 0) = DM#(I, MARK)
DM1#(I, 0) = DM1#(I, MARK)
DM2#(I, 0) = DM2#(I, MARK)
MDM#(I, 0) = MDM#(I, MARK)
MDM1#(I, 0) = MDM1#(I, MARK)
MDM2#(I, 0) = MDM2#(I, MARK)
X#(I, 0) = X#(I, MARK)
NEXT I
RETURN

```

REFERENCES

1. U.S. Patent #4,752,428, issued to Air Products and Chemicals Inc., June 21, 1988.
2. U.S. Patent #4,771,110, issued to Air Products and Chemicals Inc., September 13, 1988.
3. Hayes, L.J. and D.D. Dixon, "Journal of Applied Polymer Science", **22**, 1007 (1978).
4. Koros, W.J., V.T. Stannett, and H.B. Hopfenberg, "Polymer Science and Engineering", **22**, 738 (1982).
5. Elman, J.F., L.J. Gerenser, K.E. Goppert-Berarducci, and J.M. Pochan, "Macromolecules", **23**, 3922 (1990).
6. Grimm, H.J. and E.L. Thomas, "Polymer", **26**, 38 (1985).
7. Sikorski, R.T. and E. Czerwinska, "Polymer", **25**, 1371 (1984).
8. Gilbert, Everett, Sulfonation and Related Reactions, Interscience Publishers, New York, 1965.
9. Private communication with Bill Walles.
10. Wade, L.G. Jr., Organic Chemistry, Prentice-Hall, Inc., Englewood Cliffs, N.J., 1987.
11. Walles, W.E. in Barrier Polymers and Structures, American Chemical Society, 1990.
12. Ihata, Jyoji, "Journal of Polymer Science: Part A: Polymer Chemistry", **26**, 167 (1988).
13. Wang, J., A. Khokhlov, D. Peiffer, and B. Chu, "Macromolecules", **25**, 2566 (1992).
14. Hara, M., J. Wu, and A. Lee, "Macromolecules", **21**, 2214 (1988).
15. Lantman, C.W., W.J. MacKnight, J.S. Higgins, D.G. Peiffer, S.K. Sinha, and R.D. Lundberg, "Macromolecules", **21**, 1339 (1988).
16. Weiss, R.A. and X. Lu, ANTEC '92, 1424.

17. Armstrong, G.H., M.R. Dargin, and L. Johnson, ANTEC '92, 1904.
18. Crank, J., The Mathematics of Diffusion, Clarendon Press, Oxford, England, 1975.
19. Geankopolis, Christie, Mass Transport Phenomena, Holt, Rinehart and Winston, New York, 1972.
20. Hornbeck, Robert W., Numerical Methods, Quantum Publishers, New York, 1975.
21. Carnahan, Brice, H.A. Luther, and James O. Wilkes, Applied Numerical Methods, John Wiley and Sons, N.Y., 1969.
22. Coalition Technologies Ltd., Freeland, Michigan.
23. Cerfontain, Hans, Mechanistic Aspects in Aromatic Sulfonation and Desulfonation, Interscience Publishers, New York, 1968.
24. Skoog, Douglas A., Principles of Instrumental Analysis, 3rd edition, Saunders College Publishing, Philadelphia, Pa., 1985.
25. Walls, J.M. (Ed.), Methods of Surface Analysis - Techniques and Applications, Cambridge University Press, New York, 1989.
26. Kalantar, Javad, PhD thesis, Michigan State University, 1991.
27. Klomparens, K.L., S.L. Flegler and G.R. Hooper, "Procedures for Transmission and Scanning Electron Microscopy for Biological and Medical Science", LADD Research Industries, Burlington, VT, 1986.
28. Weast, Robert C. (Ed.), CRC Handbook of Chemistry and Physics, 65th edition, CRC Press, Boca Raton, FL, 1985.
29. Gupta, V.B., L.T. Drzal, C. Y-C. Lee, and M.J. Rich, "Polymer Engineering and Science", 25, 812 (1985).
30. Rao, Venkatesh, PhD thesis, Michigan State University, 1991.
31. Kenny, J.M., A. Apicella, and L. Nicolais, "Polymer Engineering and Science", 29, 973 (1989).

MICHIGAN STATE UNIV. LIBRARIES



31293011093774